APPLICATION OF IMAGING TO STUDY THE EVOLUTION AND DYNAMICS OF LASER PRODUCED PLASMA FROM SOLID AND THIN FILM Li TARGETS

Sony George

Ph D Thesis submitted to Cochin University of Science and Technology in partial fulfillment of the requirements for the award of the Degree of

Doctor of Philosophy

International School of Photonics
Faculty of Technology
Cochin University of Science and Technology
Cochin -6820 22, Kerala, India

September 2011

Application of Imaging to Study the Evolution and Dynamics of Laser Produced Plasma from Solid and Thin Film Li Targets

Ph D thesis in the field of Photonics

Author:
Sony George
Research Fellow
International School of Photonics
Cochin University of Science & Technology
Cochin -682022, Kerala, India
sony@cusat.ac.in, sonytgeorge@gmail.com

Research Advisor:
Dr. V. P. N. Nampoori
Emeritus Professor
International School of Photonics
Cochin University of Science & Technology
Cochin -682022, Kerala, India
vpnnampoori@cusat.ac.in, nampoori@gmail.com

International School of Photonics
Cochin University of Science & Technology
Cochin -682022, Kerala, India
www.photonics.cusat.in
September 2011

Cover image: Plasma ball

INTERNATIONAL SCHOOL OF PHOTONICS
COCHIN UNIVERSITY OF SCIENCE AND TECHNOLOGY
COCHIN -682022, KERALA, INDIA

Dr. V. P. N. Nampoori
Emeritus Professor

Certificate

Certified that the research work presented in this thesis entitled "**APPLICATION OF IMAGING TO STUDY THE EVOLUTION AND DYNAMICS OF LASER PRODUCED PLASMA FROM SOLID AND THIN FILM Li TARGETS**" is an authentic record of the bonafide research work done by **Mr. Sony George** under my guidance at the International School of Photonics, Cochin University of Science and Technology, Cochin, India and has not been included in any other thesis submitted previously for the award of any degree.

Cochin-22
23- 09- 2011

Dr. V. P. N. Nampoori
(Supervising guide)

Phone: +91 484 2575848 Fax: 0091-484-2576714. Email: nampoori@cusat.ac.in
nampoori@gmail.com

Declaration

I hereby declare that the work presented in this thesis entitled '***Application of Imaging to Study the Evolution and Dynamics of Laser Produced Plasma from Solid and Thin Film Li Targets'*** is based on the original research work done by me under the supervision of **Dr. V P N Nampoori**, Emeritus Professor in International School of Photonics, Cochin University of Science and Technology, Cochin, India and has not been included in any other thesis submitted previously for the award of any degree.

Cochin-22 Sony George

23-09-2011

Preface

Laser-induced plasma is a subject of investigations in light matter interaction which will solve many of the unanswered problems related to interaction of radiation with matter. There have been many developments in laser plasma physics since the last few decades. Laser-produced plasma (LPP) is a rich, expanding topic of growing interest in different fields because of its substantial application to inertial confinement fusion (ICF), material processing, plasma diagnostics, space applications and pulsed laser deposition, basic spectroscopy of excited neutrals and ionic species etc.

With the advent of very short duration laser pulses, intensities broaden from the threshold of plasma formation ranging from 10^9 W/cm^2 on the nanosecond time scale up to the highest energy flux densities of several 10^{22} W/cm^2 currently available in the femtosecond lasers. These lasers are capable of supplying large amount of energy in extremely short time duration. Interaction of high power laser radiation with matter causes the vaporization of surface layers which leads to the formation of an expanding atomic plasma. The first salient aspect of the laser-induced plasma is its fast dynamics, and in concomitance, inhomogeneity in density, temperature and flow velocity.

The formation and dynamics of laser-produced plasma (LPP) from solid target has been studied extensively for long time. In LPP, high power laser focused onto a solid material (known as 'target'), leads to rapid ionisation and generated plasma propagates in the opposite direction to the laser beam, i.e., normal to the target surface. In contrast to this, laser-induced forward transfer technique also knows as laser blow off (LBO), consists of the propagation of the ablated material along the direction of the laser beam. In this case the laser pulse is irradiated through a transparent substrate onto a thin film target and the energy of the pulse will be absorbed in the layer and an expanding plasma cloud is formed along the laser beam direction.

The present thesis report the results obtained from the studies carried out on the laser blow off plasma (LBO) from LiF-C (Lithium Fluoride with Carbon) thin film target, which is of particular importance in Tokamak plasma diagnostics. Keeping in view of its significance, plasma generated by the irradiation of thin film target by nanosecond laser pulses from an Nd:YAG laser over the thin film target has been characterized by fast photography using intensified CCD. In comparison to other diagnostic techniques, imaging studies provide better understanding of plasma geometry (size, shape, divergence etc) and structural formations inside the plume during different stages of expansion. The thesis has been divided into seven chapters:

Chapter 1 aim to give a brief introduction to laser induced plasmas with particular focus to laser-induced forward transfer or laser blow off (LBO) technique. A short description on the plasma formation and dynamics is discussed. Some of the theoretical considerations in connection with laser matter interaction are also discussed in this section. The motivation of choosing lithium (Li) target for this study has been explained on the basis of diagnostic applications in Tokamak plasma. This chapter also gives an overview of the various diagnostic techniques used for characterisation of the laser-induced plasma.

Chapter 2 discusses the design and development of the experimental setup to study the expansion dynamics of laser-induced plasma plume from both thin film as well as solid target under various experimental conditions. The details of different diagnostic techniques, which are used in this research, have been explained in this chapter. This includes ICCD imaging, emission spectroscopy and probe diagnostics. One of the main topics presented in this chapter is the study of the influence of magnetic field over the expanding plasma. In order to carry out these studies, magnetic field setup is designed, fabricated and calibrated. A timing sequencing control module has also been developed for time synchronization of diagnostics with laser pulse, ICCD and magnetic field.

The main emphasis of **Chapter 3** is to present the study carried out to understand the effect of different ambient gases on the plume expansion dynamics of laser blow off plume from LiF-C target. First part of the chapter discusses the plume propagation in vacuum and various argon pressure levels. In the later part, the investigation has been extended to study the influence of helium ambient on the LBO plasma. Helium is chosen for this due to the large difference in atomic mass and ionisation potential. Images of the plume recorded with intensified CCD at different time intervals after the plasma formation reveal several interesting observations. This includes enhancement of the plume intensity, change in size and shape of plume focusing, plume stopping etc. Details of which are included in this chapter. The geometrical data extracted from the images have been examined by means of appropriate theoretical models and are found to be in good agreement with the observations.

Chapter 4 has divided into two sections: First part sketches the results of the influence of intensity profile of the ablating laser on the dynamics of LBO plume. This work mainly emphasizes the geometrical aspect of the plume generated with lasers having gaussian and flat-top laser intensity profiles. Results from the studies demonstrate that laser beam with gaussian profile produces a well-collimated, low divergence plasma plume as compared to the plume formed by laser beam with top-hat profile. The sequence of film removal processes is invoked to explain the role of energy density profile of the ablating laser in LBO mechanism. This study has also been carried out with three different ambient gases and results of which are described in the second section of this chapter. Further investigations reveal the possibility of the phenomenological development of shock waves when high velocity plasma plume propagates in an ambient gas and sweeps the background medium. Shock strength and other shock parameters have been extracted from the plume images recorded. These data clearly show the dependency of shock wave formation over the ambient medium and is highly influenced by the mass of ambient gas.

Chapter 5 is to describe the effect of magnetic field on the dynamics of plasma generated from solid Li and thin film LiF-C targets. This study has been of particular relevance in the context of Tokamak application of Li neutral beams and plasma confinement. In addition to this, there are several interesting phenomena induced by magnetic field, like plume splitting and intensity enhancement over the plasma upon applying magnetic field. Image analysis shows the enhancement in the overall emission intensity as well as appearance of distinct structures (lobes) in the plasma plume in the presence of magnetic field. By introducing a variable magnetic field, the influence of Lorentz force (J × B) in expanding plasma plume across the transverse magnetic field has been explored. In the second part, influence of magnetic field on the plasma plume formed from LiF-C thin film target in LBO scheme has been discussed. In the presence of magnetic field, the temporal profiles of Li neutral lines show distinct features with an enhancement in their intensities.

Chapter 6 discusses the comparative study between the plasma formed by two different schemes viz., the laser-blow off (LBO) of multicomponent LiF-C thin film and conventional laser-produced plasma (LPP) from solid lithium have been studied. On comparing their evolution geometry, apart from similarities, some interesting differences are also noticed in propagation dynamics of the plumes generated by LPP and LBO both in vacuum as well as in the presence of the ambient gases. The differences of LBO and LPP plumes with regard to plume splitting, plume confinement and plume expansion are discussed using fast imaging technique.

General conclusions drawn from the present studies and some of the directions for future work form the subject matter of **Chapter 7**

List of Publications

I. International Journals

- Fast imaging of laser blow off plume: lateral confinement in ambient environment. **Sony George**, Ajai Kumar, R. K. Singh, V. P. N. Nampoori, *Applied Physics Letters 94, 141501 (2009).*
- Effect of ambient gas on the expansion dynamics of plasma plume formed by laser blow off of thin film. **Sony George**, Ajai Kumar, R. K. Singh, V. P. N. Nampoori, *Applied Physics A, 1432-0630 (2009).*
- An experimental setup to study the expansion dynamics of laser blow-off plasma plume in variable transverse magnetic field. Ajai Kumar, Vishnu Chaudhari, Kiran Patel, **Sony George**, S. Sunil, R. K. Singh, and Ranjeet Singh, *Review of Scientific Instruments **80**, 033503 (2009).*
- Influence of laser beam intensity profile on propagation dynamics of laser-blow- off plasma plume. Ajai Kumar, **Sony George**, R. K. Singh, V. P. N. Nampoori, *Laser and Particle Beams, 28:387-392 (2010).*
- Image analysis of expanding laser-produced lithium plasma plume in variable transverse magnetic field., Ajai Kumar, **Sony George**, R. K. Singh, V. P. N. Nampoori, *Laser and Particle Beams, 29:241-247 (2011).*
- Fast imaging of the laser-blow-off plume driven shock wave: Dependence on the mass and density of the ambient gas. **Sony George**, R. K. Singh, V. P. N. Nampoori, Ajai Kumar, *Journal of Physics:D, Applied Physics (Under review, 2011).*
- Comparison of plasma generated from solid and thin film targets: An imaging study., **Sony George**, R. K. Singh, V. P. N. Nampoori, Ajai Kumar (Under preparation).

II. Conference Proceedings

- Study of laser induced forward plasma dynamics under helium ambient using fast photography. **Sony George**, Ajai Kumar, R. K. Singh, V. P. N. Nampoori, *Proceedings of National Laser Symposium (2008).*
- Comparitive study using fast imaging of plasma plume generated from solid target and thin film. **Sony George**, Ajai Kumar, R. K. Singh, V. P. N. Nampoori, *Proceedings of National Laser Symposium (2009).*
- Study of mode structures and their dynamics in expanding laser blow off plume. Ajai Kumar, D Raju, **Sony George**, R. K. Singh, *International Conf on Waves, Coherent structures and Turbulence in Plasmas (2010).*
- Study of laser profile dependance on LiF-C film ablation using ICCD imaging technique. **Sony George**, Ajai Kumar, R.K.Singh, P Rashakrishnan, V. P. N.Nampoori, *International Conference on Fiber Optics and Photonics-Photonics 2010* .
- Comparative study using Gaussian and Top hat intensity profile laser beam on the dynamics of LBO plasma plume., **Sony George**, Ajai Kumar, R. K. Singh, V. P. N. Nampoori, *Proceedings of National Laser Symposium (2010).*
- Fast imaging of laser blow off plume: Dynamics in an oxygen atmosphere., **Sony George**, Ajai Kumar, R. K. Singh, V. P. N. Nampoori, *Proceedings of National Laser Symposium (2010).*
- Shadowgraphic imaging studies of laser produced aluminium plasma. Sreeja Thampi, **Sony George**, Nampoori V P N and P Radhakrishnan. International *Conference on Contemporary trends in Optics and Optoelectronics, XXXV- Optical Society of India Symposium, Thiruvananthapuram, India, 17-19, Jan 2011.*

Acknowledgements

"When you really want something, all the universe conspires in helping you to achieve it"
Paulo Coelho

I never imagined that I could come so far without the generous and endless assistance of many people. I believe I was blessed by God who placed all these people close to me and I thank each of them from the bottom of my heart.

Firstly, I would like to thank my PhD supervisor **Prof. V.P. N. Nampoori**. His energy, enthusiasm, and supports always encouraged and inspired me during my research studies. Furthermore, I really appreciate that he has shown me a great vision in science. I believe that it will be great nutrients for my future scientific carrier.

I am grateful to **Prof. Ajai Kumar** of Institute for Plasma Research (IPR) for all his guidance and for extending the enormous facilities of IPR for my research. His passionate and persistent attitude towards the experimental research had inspired and motivated me in my work and helped me through many bottlenecks.

My sincere thanks to **Prof. P. Radhakrishnan**, Director, ISP for all his support throughout my research period. The suggestions and motivation from him always made my research period more productive.

I thank **Prof. P. K. Kaw**, Director, IPR for allowing me to do my experiments during the research period. All the administrative staff of IPR was so co-operative and helpful every time I visit IPR.

I want to thank **Dr. Rajesh K. Singh** (IPR), with whom I spent the most time in the lab and from whom I learned the most. His knowledge of experimental techniques, data analysis and technical writing is encyclopaedic.

My special and sincere acknowledgement goes to **Prof. C. P. Girijavallabhan** for his valuable suggestions and constant encouragements to improve my research.

I thank **Prof. Nandakumaran, Dr. Kailasnath and Dr. Sheenu Thomas, Dr. Reethama** for their support, advice and co-operation rented during these years.

I got a lot of inspiration and support from **Prof. Jon Yngve Hardeberg** (Director, Colorlab, Norway) during these years. Technical discussions with Prof. Jon was really helped me to frame out my carrier in imaging.

IPR was just like my home department. All the people, both inmates of lab and other friends were so helpful for me. All the members of Laser Diagnostic Group- **Vishnu Chaudhari, Renjith Singh, Kiran Patel, Jinto Thomas, Dr. Manoj Gupta, Kaushal Pandey** were ready to assist me at any time to any extend. My interactions with members of this lab have certainly made me a better professional. I extend my sincere thanks to **Dr. Joshi, Dr. Prahlad and Dr. A.V Ravikumar** for their scientific support to review journal drafts and fruitful comments.

I thank the **PSSI** for their support through visiting student fellowship. **Dr. A. V Ravikumar** (IPR) and **Dr. Ranjana (**IPR**)** were extremely helpful to arrange this in time.

I would like to thank **Dr. V. J Dann, Dr. Tina** and **Neo** for their support from the beginning and more than just a junior, the brotherly love was unforgettable.

I thank all my **dear friends of ISP** for their affection and timely help. I feel very fortunate and happy to have such a great company and colorful experience.

Many friends helped me to get journals and other research materials from abroad. I thank **Praveen, Prabhathan, Vineeth, Sithara** for their help and support.

I would also like to express gratitude to all the office members of ISP for their administrative assistance.

I whole-heartedly thank **Tomson f**or his constant support and encouragement, which played a major role for me to start my research studies.

I wish to thank University Grants Commission (**UGC**) for the financial assistance in the form of Research Fellowship for Meritorious Students (**RFSMS**)

I wish to place on record my gratitude to my **teachers, mentors and my friends** at all stages of my education.

I would like to dedicate this thesis to my **grandmother** who always wanted me to get the best. I am sure she is now smiling at me from heaven.

Lastly, and most importantly, I wish to thank my **loving parents and dearest brother**. They bore me, raised me, supported me, taught me, and loved me. To them I dedicate this thesis.

SONY GEORGE

Contents

Chapter 1

Introduction

Abstract

This chapter gives an introduction to laser induced plasma. Formation and dynamics of plasma from a solid as well as thin film target has been explained. More emphasis of this chapter has been given to plasma formed from thin film targets and its applications in various fields. Finally, different techniques used for the diagnostics of plasma has been presented.

1.1. Laser induced plasma

Laser-induced plasmas represent a comparatively new field of study related to electromagnetic interaction with macroscopic matter. There have been many developments in laser plasma physics since the last few decades both in terms of theoretical and experimental studies. Laser-produced plasmas (LPP) is a rich, burgeoning topic of growing interest in different fields because of its substantial applications to areas like inertial confinement fusion (ICF), X-ray lasers, extreme ultra-violet (EUV) lithography, material processing, plasma diagnostics, Tokamaks, space applications and pulsed laser deposition {1-11}. High power lasers are proving to be remarkable tools for the creation and study of high energy density phenomena in the laboratory. With the advent of very short duration laser systems, intensities broaden from the threshold of plasma formation (around 10^9 W/cm^2) on the nanosecond time scale up to the highest power densities of 10^{22} W/cm^2 currently available in femtosecond lasers.

Interaction of high power laser with matter causes heating and melting of the irradiated volume. This followed by the vaporization of surface layers, which leads to the formation of an expanding plasma. The basic properties of these plasmas are critically controlled by the laser power density. Generated plasma also depends on other laser parameters like, pulse width, intensity profile etc and the material characteristics. After the initial ionisation, it is basically the field strength and the quiver motion of free electrons that enables further ionisation of matter, forming a dense 'free' electron cloud. If the electron density is high enough in the Debye-sphere, the plasma behaves in a collective manner. The first salient aspect of the laser-induced plasma is its fast dynamics, along with its inhomogeneity in density, temperature and flow velocity. The laser interaction itself is characterized by a limiting electron density beyond which no electromagnetic propagation is possible i.e., beyond critical density where laser is efficiently absorbed by the electron population through collisional inverse bremsstrahlung {12-14}. This

property is the main reason for laser plasmas to be very hot and more or less close to ideality, and is responsible for sharp density variations in the transition zone from under-dense to over-dense plasma.

At super-high intensities when the effect of collisions and absorption are almost absent, the laser acts progressively as an exceedingly efficient accelerator of energetic electrons by anharmonic resonance. Over-dense samples of matter are indirectly heated only by electron heat conduction, fast electron jets, electron plasma waves, plasma radiation and plasma shock waves. On the slow time scale of the ions, electrons are bound to them by quasi-neutrality, which is one of the fundamental properties of any plasma state. The dynamics of the laser plasma on the ion time scale is governed by the thermal pressure of the electrons and to certain extent, by that of the ions. Under several aspects, the laser plasma represents an extreme state of matter far from thermodynamic equilibrium, both on large scale e.g., spatial gradients of density, temperature, pressure, ionization and on local scale e.g., electron and ion temperatures differing from each other, non-equilibrium velocity distribution. At resonance, the electron plasma waves are driven into non-linearities to the extent of breaking leading to filmentation of the plasma. The dynamics of atoms in strong laser fields have become a rich and fascinating field of modern atomic and plasma physics. Different stages of laser-matter interaction and plasma formation mechanisms are explained in the coming sections of this chapter.

1.2. Dynamics of laser ablation

Laser ablation of solids with nanosecond/femtosecond pulses of high intensity leads to complicated interactions of the laser beam with both the solid and the ablated material. There exist a number of processing parameters, which determine the dynamics of ablation and properties of the generated plasma {15-19}. Some of the fundamental physical features such as the nature of the laser absorption in the vaporized material and acceleration mechanism for the ions are not yet fully

understood. Nevertheless, the processing of solids by intense laser light and the generated plasma is used in various applications {8-10}.

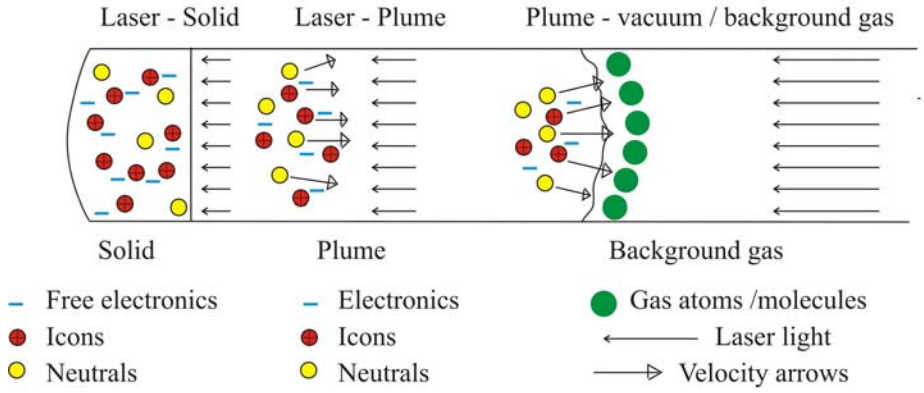

Figure 1.1 *A schematic view of the processes that take place during ablation by a ns laser pulse. Light absorption in the solid (stage 1), ejection of the ablated material in a plasma plume and the interaction of the light with the plume (stage 2), and the expansion in a background gas (stage 3)*

Interaction of a nanosecond laser pulse on a solid surface causes the rapid rise in temperature, which leads to intense evaporation of atoms and molecules from the solid surface. Even at relatively low intensities near the threshold for ablation, it is observed that the ablated material is significantly ionized and the ions in the plasma plume have energies ranging upto several hundred electron volts (eV). Near the ablation threshold, the ablation cloud consists of neutrals, ions and electrons. At the end of the nanosecond laser pulse, the ablated material exists as a thin layer of plasma on the target surface. Initially the expansion of the plume is primarily driven by the plasma pressure gradients {20}, but there may be an additional contribution from coulomb repulsion between the ions if there is significant net loss of the more mobile electrons. In any case, when the plume has propagated more than a few hundred millimeter from the target surface, major part of the initial thermal energy in the plasma is converted to the directed kinetic energy of the ions, which are much more massive than the electrons.

The adiabatic expansion models of Anisimov et al.{15} and Singh and Narayan {16} have proved to be very useful for the understanding and interpretation of the laser ablation experiments. The ablation process using lasers with pulses of nanosecond or longer duration can be thought of as occurring in three different stages, which are explained in the subsequent sections, though these stages do overlap each other to some extent in time.

1.2.1. Interaction of laser beam with the target

In the initial stages, the intense laser beam strikes the target surface, which is either in solid or in thin film forms. Part of the energy is reflected back and the remaining part is absorbed by the electrons in the target. The primary heating of the target leads to strong evaporative ejection of material. Since the heating is extremely fast, surface temperatures close to the thermodynamic critical temperature can be reached. After a period of tens of picoseconds, the electrons and atoms in the solid equilibrate which leads to a strong heating of the irradiated volume. The removal of the material from the target by laser irradiation depends on the coupling of the beam with the solid. Intense heating of the surface layers by high-powered nanosecond laser pulses occurs, resulting in melting and/or evaporation of the surface layers, depending on its energy density. The thermal history i.e., heating rate, melting, evaporation during pulsed-laser irradiation are influenced by the laser parameters (pulse energy density *E,* pulse duration *T,* intensity profile and wavelength), and the temperature-dependent optical (reflectivity, absorption coefficient) and thermophysical (heat capacity, density, thermal conductivity, etc.) properties of the material. In addition to this, the behaviour of the plasma expansion also depends on the initial plume dimensions and background gas pressure.

1.2.2. Interaction of laser beam with evaporated material

In the second stage, the material from the heated volume is ejected from the target but continues to absorb energy from the laser beam, resulting in the formation

of a thin layer ionised of vapour on the surface of the target. The high surface temperature induced by laser irradiation leads to emission of positive ions and electrons from free surface. The flux of ions and electrons as a function of temperature can be predicted by the Richardson and Langmuir-Saha equations {21-23} respectively. Both of these equations show an exponential increase in the fraction of ionized species with temperature. Different mechanisms may play an important part in the ionization of the laser-generated species. Impact ionization and other mechanisms, especially photoionization, thermal ionization of photon-activated species and electronic excitation may affect the concentration of the excited species. The absorption of photons by free-free transitions involving neutral atoms, although much less effective than free-free transitions involving ions, may be the dominant mechanism as a result of high neutral atom concentrations. In this stage, laser-gas or laser-plasma interactions prevail. For femtosecond lasers the duration of the pulse is so short that any significant movement of the atoms from the lattice happens after the pulse has terminated.

1.2.3. After the termination of laser pulse

The third stage begins after the termination of the laser pulse. During this phase, the plume expands adiabatically in three dimensions. In this stage, no particles are evaporated or injected into the inner edge of the plasma. Also, an adiabatic expansion of the plasma occurs where the temperature can be related to the dimensions of the plasma. Further, plume dynamics depends very much on the medium to which the plasma expands.

1.2.3.1. Plume expansion in vacuum

If the expansion takes place in vacuum, the shape and velocity distribution in the plume will reach asymptotically constant values. The thermal energy is rapidly converted into kinetic energy with plasma attaining extremely high expansion velocities.

The rapid expansion of the plasma in vacuum results from large density gradients. The plasma which absorbs the laser energy can be simulated as a high temperature-high pressure (HT-HP) gas which is initially confined in small dimensions and is suddenly allowed to expand in vacuum. Because of the large pressure gradients initially present near the outer edge i.e., in vacuum, very high expansion velocities are induced at the edges. Study of plume expansion after the termination of laser pulse has of great importance for various applications especially laser deposition. Different aspects of expansion in vacuum have already been studied both theoretically and experimentally by various groups. A review on this topic has been presented in chapter 3.

1.2.3.2. Plume expansion in background gases

The use of an ambient gas is a well-established method employed in plasma applications controlling plume species since the gas acts as a moderator for the plasma plume during the flight from target to substrate. The observed differences in plume dynamics when ablation occurs with and without background gases is of crucial importance and this has originated a great amount of experimental and theoretical work.

If the ablation takes place in a background gas, the high plume pressure initially drives the expansion as if it were occurring in vacuum. After several microseconds, the plume expansion is entirely driven by the interaction of the plume atoms with the atoms and molecules of the background gas. The expansion of a laser induced plasma in an ambient gas atmosphere is comparatively more complex phenomenon due to the presence of several physical processes involved in the interaction of the plume with the background gas, such as plume deceleration, splitting, plume stopping, shock-wave formation, thermalization, etc. In all instances, the background gas acts as a regulator of ablated plumes energetics and strongly determines the composition and dynamical behavior of the plume material ablated. The knowledge of the interaction processes between the ablated materials

and the ambient gas seems to be essential for improving/optimizing the various plasma parameters and to control the plume geometry.

Though there exists a large number of research works in this area, many aspects of the expansion are still not fully understood. Keeping its importance in various applications we have investigated behaviour of plasma generated from solid and thin film targets in various ambient gases and has been presented in this thesis {Chapter 3, 4 and 6}.

1.2.4. Plasma expansion in magnetic field

Plasma dynamics can be efficiently controlled by applying magnetic field in various ways. This has of particular relevance in inertial fusion confinement where magnetic field offers a potential means to slow high-energy particles before they implant in surrounding structures. The presence of a magnetic field during the expansion of laser-induced plasma may initiate several interesting physical phenomena including conversion of the plasma thermal energy into kinetic energy, plume confinement, plume splitting, ion acceleration, emission enhancement, plasma instabilities, etc. There are many groups already involved in research in this area. It has been observed that most of the studies were concentrated to investigate plasma expansion in a uniform constant applied field and not with varying magnetic field. To get more understanding we have conducted research using magnetic field over a range of 0 G to 4000 G and has been reported in this thesis {Chapter 5}. Due to the relevance in Tokamaks, we have studied plasma from lithium solid target and laser blow off plasma from LiF-C thin film targets.

The laser ablation of solids/films involves a number of complex physical processes in both condensed and vapour phases. Many processes such as laser properties like wavelength, energy density, pulse duration, and pulse shape temperature-dependent optical properties absorption, reflection, and thermo-physical properties thermal conductivity, heat capacity and density together determine the ablation properties of the material and the thermal history of the

ablated plumes. Hence, a detailed understanding of the spatial and temporal behaviour of the ejected species constituting the ablated plume is essential for using these techniques in applied research.

1.3. Types of laser ablation: LPP and LBO

The formation and dynamics of laser produced plasma (LPP) from solid target has been studied extensively for a long time {24-26}. In LPP, high power laser focused into a solid material, known as 'target', lead to rapid ionisation and the generated plasma propagates in the opposite direction to the laser beam, i.e. normal to the target surface. In contrast to this, in the case of laser induced forward transfer technique, also known as laser blow off (LBO), laser pulse interact with a thin film target and the plume propagates in the forward direction i.e., same direction of laser. LBO scheme consists of a laser and a substrate, which is transparent to the laser wavelength {27}. The substrate is pre-coated with a layer that contains the material which one wants to inject and which must absorb the laser beam. The coating can be either single species or multilayer of several thousand angstrom thickness. In this case the ablated material propagates along the direction of the incident laser beam. LiF-C (Lithium Fluoride with Carbon), target has been used in the present study due to its relevance in Tokamak research {Sec.1.5}. As the laser pulse is irradiated through the transparent substrate onto the coating, the energy of the pulse will be absorbed in the layer and an expanding plasma cloud is formed.

The mechanism for the formation of LBO is impulsive heating of the film, until the vapour pressure at the film support interface becomes large enough to expel the film. Miotello and Kelly {28} discussed the thermal models for ablation process by considering superheating near the spinodal line. According to this model, the superheated liquid undergoes a phase explosion. Further, the expansion dynamics in LBO depends on the thickness of the thin film. If the thickness is less than the skin depth, defined as the penetration depth of the laser in solid target, then

it would result in the explosive expansion of the plume with less number of thermalizing collisions.

Because of the reflection of the atoms on the surface of the thin film target, the atoms acquire a velocity component directed normal to the surface. In the simplest case, the velocity distribution of the atoms can be described as a constant velocity with a superposed thermal distribution in the frame of the centre of mass {14}. The exact velocity distribution depends on the thickness of the coating and the energy density of the laser pulse, and can contain several components such as atoms, clusters etc {29-31}.

The LBO plume is expected to exhibit differences in plume composition and its dynamics in comparison with conventional LPP plumes. LBO plumes are used in thin film deposition, thin film reflectance studies and trace element ejection in plasma environments. The main advantage of the plume generated by the thin film over the bulk target is its use in the generation of neutral atom beams. LBO scheme offers as one of the diagnostic tools for neutral beam injection studies in Tokamak {32-38}. It was found that the neutral atom flux obtained with LBO scheme exceeds that from a solid target by about a factor of 10. The energy of the beam (1-5 eV) is sufficient to penetrate into the edge plasma to the last closed flux surface (LCFS) {39}. Sensitivity of measurement is good because of the relatively high neutral beam density (10^9-10^{10} cm/m^3). More details on neutral beam injection studies are discussed in the coming sections of this chapter.

Further, in LBO scheme nearly 100% material is ejected from an area equal to the laser spot size for every laser shot. This helps in the estimation of the amount of material injected per shot, which renders interpretation of results easier. Not much theoretical studies have yet been carried out related to the formation and dynamics of LBO. Some of the basic characterisation studies including plasma in ambient gas, magnetic field and under different laser profiles are explained in the proceeding chapters of this thesis {Chapter 3, 4, 5 and 6}.

1.4. Importance of LiF-C target

Laser blow off (LBO) technique finds vast number of applications especially in neutral beam injection studies in fusion research and pulsed laser deposition. We have selected the LiF-C target because the fast neutral lithium beam is extensively used as a diagnostic tool for the Tokamak plasmas {32-38}. Lithium is favored due to its low mass, low ionization potential (5.4 eV) and therefore are easily ionized in the plasma. The emission spectra of lithium atoms and ions are simple with strong emission lines in the visible spectral range. The important plasma parameters, such as ion temperature, impurity transport and plasma electron density and temperature at the edge of Tokamak plasma can be measured by analyzing the optical radiation resulting from the collisions of lithium atoms with plasma particles {40, 41}. The active lithium beam is a very important diagnostic tool in Tokamak plasma experiments. The most attractive one is the time resolved measurements of the electron density, temperature and the current distribution of the Tokamak plasma. The lithium beam diagnostic is proved to be a powerful tool to investigate edge plasma parameters in Tokamaks.

1.5. LPP/LBO applications

Plasma enjoys an important role in a wide variety of industrial processes, including material processing; environmental control; electronic chip manufacturing; light sources; bio-medicine; and space propulsion. It is also central to understanding most of the universe outside the Earth {42, 43}.

As the semiconductor industry continues to push toward increasing circuit density, development of extreme-ultraviolet (EUV) lithography sources continues at accelerated rates. One of the recent developments in this area is the application of laser-induced plasma as one of the most viable technologies to achieve high-volume-manufacturing requirements for EUV lithography {44, 45}. Studies are reported on the use of different target material such as xenon, lithium and tin, different target geometry and composition solid, liquid, cluster grains, etc under

various experimental conditions. EUV sources generated by LPP permits to perform processes at the 32 nm node and beyond. Another major application of laser ablation is in pulsed laser deposition (PLD) to deposit high quality films of materials {Sec.1.5.2}. This technique uses high power laser pulses to melt, evaporate and ionize material from the surface of a target.

Laser ablation in rare gas ambiences have been used for nanoparticle preparation, multi-component thin film deposition and carbon nanotube syntheses. Frequent collisions of ablated particles with gas atoms, the particles cool down and form nanoparticles. These nanoparticles are of interest for various fields of device applications, for example, silicon and gallium nitride nanoparticles for luminescent devices {46, 47}. Proton beams accelerated during laser-plasma interaction are very promising for applications in inertial confinement fusion, plasma diagnostics, isochoric heating of matter or medical applications {48}. These energetic protons, which can go a few cm deep, can be utilized for the treatment of cancerous tumors.

The encouraging research in space nuclear power and ultrafast laser technology can make the development of space propulsion systems quite feasible in near future. One such system is 'LAPPS', laser accelerated plasma propulsion system, which is currently at a critical juncture in its development at various laboratories. The interaction of the laser radiation with the pre-formed plasma has already been reported investigated especially in connection with the conditions for self-focusing; a condition deemed to be critical for propulsion applications.

Although there are many promising areas of application, we present here, some of the major applications of plasma generated using LBO scheme.

1.5.1. Neutral beam injection studies

Space and time-resolved measurements of plasma edge parameters are important for the investigation of edge plasma phenomena in magnetic fusion devices: for example, heat flux to the first wall or divertor plate in relation to impurity generation, confinement improvement of edge plasma control, and

transport of fuel and impurities. Probes or laser scattering techniques are often used for these purposes. However, these techniques have some serious restrictions such as sensitivity, spatial resolution, and/or interference with the boundary plasma. To overcome these difficulties, a new technique was developed a few years ago on TEXTOR Tokamak {49}. It consists of the use of a several eV neutral Li-C beam, produced by laser ablation, to diagnose the plasma edge. This diagnostic allows the measurement of electron density ne(r) and electron temperature Te(r) in the scrape-off layer (SOL) and in the plasma edge.

The active lithium beams have proven to be a powerful tool in SOL and edge plasma diagnostic in Tokamak experiments. The most attractive one is the time-space resolved measurements of the electron density, electron temperature, and the current density distribution in Tokamak plasma. The other diagnostic technique like thermal Li beams restricts its use to the SOL and lower densities due to the small velocity of the atoms and high energy beam has a spatial resolution which, for certain plasma conditions, is larger than the correlation lengths of the electron density fluctuations.

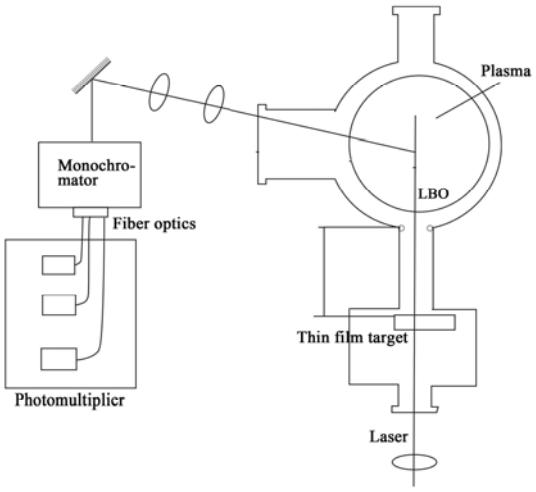

Figure 1.2 *Schematic experimental arrangement for the LBO as diagnostics tool in Tokamak*

The underlying technique is as follows. Focused beam from the laser is directed to the pre-coated (500 nm thick C-layer and 50 nm thick LiF layer) quartz/glass substrate. Laser blow off beam is formed on the rear side of the substrate facing towards the plasma. Once the beam is injected into fusion plasma $n_e(r)$, the atoms are excited and finally ionized by the plasma electrons. Figure 1.2 shows a typical LBO system for Tokamak applications. The temporal and radial distribution of intensity of the resonance line emitted by the injected atoms of these atoms excited by the plasma particles are observed using monochromator. A photomultiplier set was mounted onto one of them, which allow to collect the light emitted from different radial positions. The intensity distribution I(r,t) proportional to the $n_a(r, t)$ $n_e(r)$ and are measured. The various laser blow-off methods differ from each other in the way in which, determine the atom density, measure the intensity distribution and evaluate the profile from the intensity distributions {50-53}.

Therefore, it is possible to determine the profile of the absolute electron density by measuring the relative emission profile up to the point of complete ionization.

1.5.2. Pulsed laser deposition

Pulsed laser deposition (PLD) has emerged as one of the most popular and intrinsically simple techniques for depositing a wide range of materials and are being explored for next-generation applications. Though, the first PLD was demonstrated by Smith and Turner in 1965, the potential of PLD has been recognized well only after the success of high temperature superconductor film deposition by Dijkkamp and Venkatesan et. al. in 1987 {54}. PLD is a physical vapour deposition process, carried out in a vacuum system that shares some process characteristics common with molecular beam epitaxy and some with sputter deposition.

The PLD technique is conceptionally simple. In PLD, a pulsed laser is focused onto a target surface of the material to be deposited. For sufficiently high

laser energy density, each laser pulse vaporizes or ablates a small amount of the material creating a highly forward-directed plasma plume which expands and then is deposited on the substrate usually a few cm away from the target. Properties of laser beam are essential factors in laser material interactions. The energy and intensity directly determine amount of material ablated and the dynamics of the plasma plume. The ablated plasma plume provides the material flux for film growth {8}.

The kinetic motion of the fast expanding plume is highly directional, and considerable fraction of the ablated material is ionised. Therefore, the growth of crystalline film is possible at a relatively low substrate temperature (<100 C) in PLD. The deposition could be performed either in vacuum or in ambient gas. Moreover, the energy source of PLD, i.e., the laser system, is located outside the deposition chamber so the operation is more convenient. It could also be cost-efficient, because a single laser source could serve several systems in the same lab. These advantages of PLD are important since a relatively simple and cost efficient setup is usually desired in industrial applications.

Many studies were already been conducted to characterize plasma to understand the deposition process of PLD in different experimental conditions. A number of experimental parameters including laser energy, wavelength, ambient conditions etc, influence the plume propagation. For instance, plume expansion into an inert gas lends itself as a powerful means to control and optimize the film-growth process. Keeping this in view, we have conducted characterisation of laser induce plasma plume under different experimental conditions. Since the laser deposition process is always forward directed, these results can be extended for the characterisation of LBO plasma and vice versa.

1.6. Diagnostic techniques for laser induced plasma

Plasma can be considered as a gaseous assembly of electrons, ions, and neutral molecules residing in electric and magnetic fields. In order to gain insight

into various physical/chemical processes taking place inside plasma, it is necessary to measure plasma parameters such as density, temperature etc, which characterise the plasma. The way of evaluating these parameters is known as plasma diagnostics. There exist a number of techniques to perform plasma diagnostics, each of them have different degree of accuracy and adaptable to different types of plasmas. Diagnostics of the plasma give details regarding the plasma formation mechanism and its evolution, translational temperature and density of different plasma species, behaviour of plasma under various experimental conditions etc. It also aids one to find the distribution of plasma species during different phases of plasma evolution.

Subsequent sections of this chapter will brief some of the most commonly used plasma diagnostic techniques. Among this fast imaging technique is the main tool used for the characterisation studies in this thesis. In addition to this, emission spectroscopy and probe diagnostics are also used to support/confirm the imaging results. Technical details of these methods are discussed in chapter 2.

1.6.1. Optical emission spectroscopy

Optical emission spectroscopy (OES) provides a non-invasive probe to investigate atoms, ions and molecules within plasma. It can provide information about properties such as excited species densities, electron atom, atom-atom and ion-atom collisional effects, energy distribution of species, charge transfer between plasma constituents, and electric and magnetic fields to name a few. The use of OES in the diagnosis of low density, low temperature plasmas have been ubiquitous and have yielded a great deal of information about the properties of materials within the plasma. Its application in plasmas that are appropriate for processing of materials, such as semiconductor etching, is widespread and has been used {56-58}.

OES system consists of a monochromator, wavelength scanner, detectors like photomultiplier tube or multi channel array and a recorder (DSO) {Chapter 2}. Since the transitions between the electronic energy levels which correspond to the emitted light is in the range IR to UV, the monochromator and detector are also

required to have a good sensitivity throughout this region. Emission spectra collected from generated plasma using a one to one optical imaging guided into the PMT through the entrance slit of monochromator (Fig.1.3).

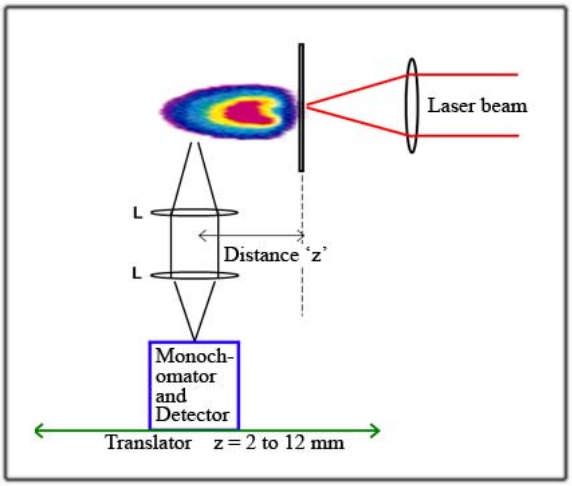

Figure 1.3 *Typical OES experimental setup*

There are different methods to extract different plasma parameters like electron temperature and density from the recorded OES spectrum. Determination of electron temperature from spectroscopic measurements is model dependent {59} and specifically depends upon the equilibrium conditions within the plasma. The simplest method, so called two line radiance ratio method, where the ratios of intensities of two lines is given by

$$\frac{I_1}{I_2} = \frac{g_1 A_1 \lambda_2}{g_2 A_2 \lambda_1} \exp\left(\frac{-E_1 - E_2}{kT}\right) \qquad (1.1)$$

Here E_1 and E_2 are the energy levels corresponding to these two lines, A is the Einstein transition probability and k is the Boltzmann constant. In using the above methods to determine temperatures, it must be carefully considered whether the assumption that the Boltzmann distribution is applicable for the distribution of internal energy states for the gas particles is valid.

1.7.2. Probe diagnostics

Electrostatic probes are incontestably the oldest and one of the most widely used diagnostic tools in plasma physics. The technical and first theoretical explanation of the electrostatic probe was developed by I. Langmuir {60}, and hence it is widely known as Langmuir probe. This method permits to measure the parameters like temperature, density etc by measuring the particle flux variations. Basically a Langmuir probe system consists of a small conducting electrode called probe tip, which is inserted into the plasma at the desired location of measurement and an external control unit (Fig.1.4).

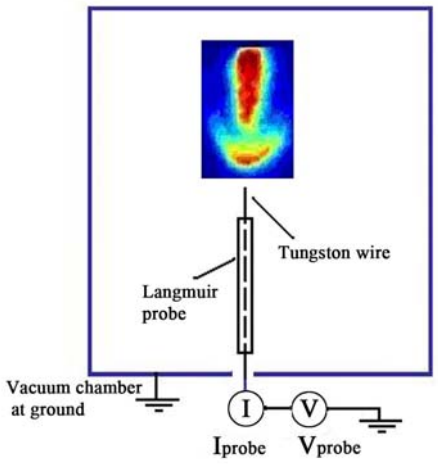

Figure 1.4 *Langmuir probe arrangement: Schematic diagram of the setup*

The probe tip can be of any shape but often planar, spherical or cylindrical shapes. Choice of shape is often limited by the experimental setup and the limitations of theoretical description {61}. The probe tip is kept very close to an electrically insulated floating electrode. Change in particle flux, appears as the variation in biasing current and is detected by external electrical circuit associated with the control unit. Analysis based on probe theory {62, 63} of the probe voltage 'V' with respect to the reference electrode is used to obtain the ion and electron

current. The obtained relation between the probe current and the applied probe voltage, I *vs.* V is called the probe characteristics.

Considering the complexity of diagnostics, probes are easy to construct and are very flexible with the dimension but the simplicity in the technical part has to compromise a lot with extremely complicated theories involved. In other words, very easily obtained data can be badly interpreted in the absence of implementation of an appropriate theory. Another hurdle associated with probe measurements is due to its physical presence in the discharge.

The plasma has a basic nature of shielding any external perturbation within some Debye length, but in reality, this shielding effect is never so localized and can be far worse in magnetized plasmas. So to say, physical presence of probe eventually affects a lot the surrounding discharge condition. On the other hand, advantages over diagnostic tools like Thomson scattering, microwave interferometer and optical emission spectroscopy are their low cost and their ability to do local measurements. The simplicity of this technique makes it as one of the most widely used diagnostic tool in plasma research.

1.7.3. Fast imaging technique

Some of the above-mentioned diagnostic techniques are useful to provide information about various local parameters and characteristics of plasma with different degree of accuracy. On the other hand, in many cases it is unsatisfactory to use material probes to determine the internal plasma parameters, so we require non-perturbing methods for diagnostics. The solution to this problem is to use electromagnetic waves as a probe into plasma. If their intensity is not too great, such waves cause negligible perturbation to the plasma, but can give information about the internal plasma properties with quite good spatial resolution. Sometimes even the non-perturbing techniques like OES or interferometry fail to give correct information regarding the plasma geometry like size, shape, structural formations etc. Direct imaging of plasma plume gives exact information about the plume

geometry and formation of various structures inside the plasma. Fast imaging is one of the most commonly used techniques to understand the propagation dynamics of plasma. In most of the cases, plasma, which is generated using pulsed laser, have a lifetime of only few microseconds and hence has to be imaged using a very fast camera. It is also proved that each part of the generated plasma undergoes drastic changes inside the plasma plume. This in fact demands an imaging system, which has a shutter speed or integration time of the order or nano/picoseconds and has a switching delay of few nano/microseconds. The above criteria can be achieved by employing an Integrated Charge Coupled Device (ICCD). The fast imaging of expanding overall visible plume emission, using a nanosecond gated intensified charged coupled device (ICCD), can provides information on the 'local' structure, dynamics of the constituent particles and geometrical aspects of the plume. This diagnostics provide the two-dimensional snap shots of the three-dimensional plume propagation for hydrodynamic understanding of the plume propagation and reactive scattering. Working principle and details of ICCD camera are explained in the next chapter {Sec 2.3.2}.

1.7.4. Shadowgraphy

Shadowgraphy is another non-perturbing diagnostic tool, which comes under the category of imaging. In a plasma, refractive index is primarily a function of the electron density, which is the main plasma parameter determined by refractive-index measurements.

An optical shadowgraphy technique can be used for temporal and spatial evolution of the plasma with high degree of accuracy. In this technique, a beam of light from an intense source, typically low power (5- 10 mW) probe laser is allowed to pass through the plasma and fall directly upon a camera/photographic plate (Fig.1.5).

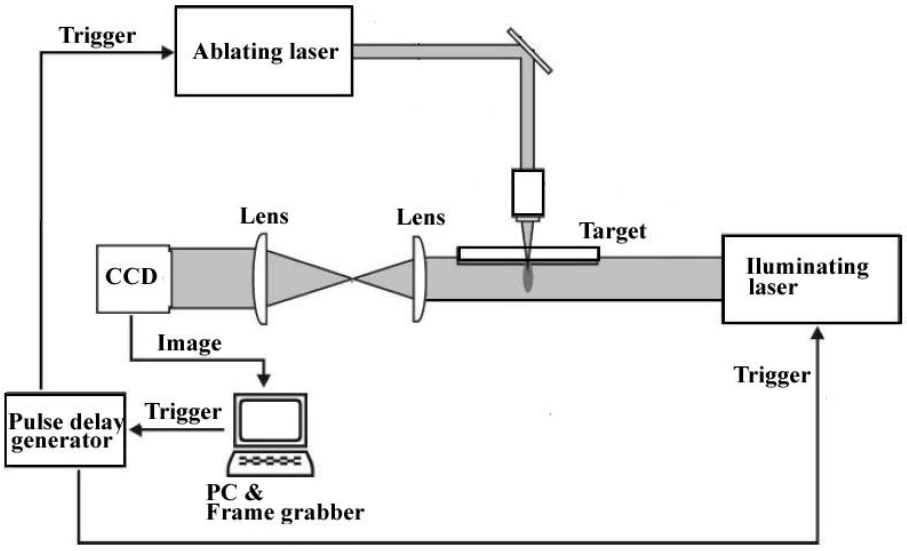

Figure 1.5 *Typical shadowgraphic experimental setup.*

If the refractive index 'n' in the test medium is uniform, the screen will be in effect uniformly illuminated. If, however, the gradient of n varies in space, as one may expect in high density (10^{14}-10^{18}/cm^3) plasma, i.e., if there is a variation in second derivative of the refractive index - the same will be reverberated on the detection plane. Regions where the second derivative is negative will act like converging lenses. The simplest of all optical flow diagnostics, shadowgraphy is also the best for imaging shock waves. It reveals shock waves clearly while de-emphasizing other, less- precipitous flow features {64, 65}.

1.7.5. Microwave and laser interferometry

As we have seen in the above section, the refractive index property of the plasma can provide a better understanding of the dynamics in various aspects. In addition to shadowgraphy and fast imaging, there exists a number of other non-perturbing techniques to extract information from the spatial variation of refractive index. Interferometry is such a method in which two or more waves are allowed to interfere by coherent addition of electric fields. The intensity observed is then

modulated according to whether the fields interfere constructively or destructively, that is, in phase or out of phase.

1.7.5.1. Microwave interferometer

The basic principle of plasma diagnostics using microwave interferometry is to measure the phase shift of a microwave signal, transmitted through the plasma. The phase shift is proportional to the average electron density N, along the path length of the microwave signal through the plasma. The measurement of the phase shift is realized by a coherent microwave receiver where the signal transmitted through the plasma is phase compared with a signal of the same source, passing a section of defined electrical length to provide a phase reference. Conventional microwave transmission interferometers comprise a homodyne phase bridge, requiring a cumbersome reference waveguide when operating at mm- wave frequencies {66}.

1.7.5.2. Optical interferometry

Optical interferometry is another non-perturbing diagnostic technique used to measure plasma density. The use of time-resolved laser-plasma interferometry has been a very important step to resolve plasma evolution in the rapidly evolving, denser regions of laser-produced plasma. There are different types of interferometers like Michelson interferometer and Mach-Zehnder interferometers {67-71}.

Irrespective of the interferometer configuration, the basic principle is to detect the changes in the interference pattern when plasma is introduced into one arm of the interferometer path. The probe beam is split into two components of equal amplitude using a beam splitter (R= 50 %). Once it passes through the plasma, these two components are folded back and overlap on to each other using two mirrors. The only path difference between the two components of the beam is the difference created by the plasma Narrowband filters are usually employed to block unused wavelengths from the plasma. Interference images are usually

recorded using streak cameras/CCDs and digital images are later used for further analysis {71}. The plasma density can be calculated from the fringe images using the formula given below

$$n = \frac{(2pmc^2)}{L\lambda e^2}[\frac{d}{\Delta x}] \qquad (1.2)$$

where Δx , δ and λ are the fringe width, fringe shift and wavelength of the probe radiation respectively, and L is the length of the plasma column along the probe beam propagation. The spatial resolution in the experiment is governed by the width of the interference fringes and the magnification used for imaging the plasma onto the slit. Multi-frame interferometers permits to record sequence of interferograms by generating multiple probe beams in a pre-determined temporal sequence and passing them through the plasma in a single shot.

1.7.6. Laser-induced fluorescence

There are several attractive possibilities for diagnostics in which active perturbation of the excited state populations is used to improve on the usefulness of emitted line radiation {72}.

The basis of this approach is to irradiate some portion of the plasma with intense electromagnetic radiation at some resonant line frequency of an atom in the plasma. Generally, a tunable laser such as dye laser is used to provide appropriate frequency and sufficient intensity. The effect of the radiation is to induce transitions between the atomic levels of the transition chosen. If the radiation is intense enough, these induced transitions will dominate over all other i.e., spontaneous and collisional processes between these levels and the result will be to equalize the occupancy of each quantum state of the two levels. In other words, the effective temperature describing the population difference of the two levels becomes infinite.

The alteration of the state population, generally an enhancement of the upper-level population, causes a change, usually an increase in the observed radiation. When the radiation observed is from the same transition as that excited,

the effect is sometimes called fluorescent scattering, although this terminology may be misleading, since the radiation observed is from spontaneous transitions from the upper level, not those induced by the laser beam. The induced photons are emitted in the direction of the illuminating beam whereas the observed fluorescence is generally in a different direction and consists only of the spontaneous transitions of the enhanced upper-level population. It is desirable and often possible to observe radiation at a different wavelength than the pump laser. This fluorescence is then rather obviously not scattering. The general expression resonance fluorescence or more colloquially "laser induced fluorescence" often denoted "LIF" covers all situations.

1.7. Organisation of the thesis

This thesis explores the physics of laser plasma interactions through fast imaging measurements from plasma produced by laser blow off scheme as well as conventional laser produced plasma from solid targets.

Chapter **Two** provides an overview of the experimental scheme employed for the present studies. Diagnostic techniques used such as fast imaging, emission spectroscopy and probes are well discussed.

Chapter **Three** reports the results of a detailed study conducted using fast imaging to understand the influence of ambient gases (Argon & Helium) on the dynamics of laser blow off plumes of multi-layered LiF-C thin film.

Chapter **Four** is divided into two sections. Part A describes effect of intensity profile of ablating laser on the dynamics of laser-blow-off plume. Part B. presents the formation of shock waves when laser blow off plume formed in an ambient gas.

Chapter **Five** discusses the influence of magnetic field on the dynamics of plasma generated from solid as well as thin film Li targets.

Chapter **Six** presents a comparative study of the plasma formed by two different schemes, LBO and LPP from Li targets.

Chapter **Seven** summarizes the conclusions and proposes future experiments to expand upon the work discussed herein.

1.8. References

1. J. Lindl., *"Development of the indirect-drive approach to inertial confinement fusion and the target physics basis for ignition and gain",* Phys. Plasmas **2**, 3933 (1995).
2. M. F. Becker, J. R. Brock, H. Cai, D. E. Henneke, J. W. Keto, J. Lee, W. T. Nichols, and H. D. Glicksman., *"Metal nanoparticles generated by laser ablation"*, Nanostruct. Mater. **10**, 853 (1998).
3. R. P. Drake, J. J. Carroll, T. B. Smith, et al. *"Laser experiments to simulate supernova remnants"*, Phys. Plasmas **7**, 2142 (2000).
4. "*Inertial Confinement Fusion*", J. D. Lindl, (Springer, New York, 1998).
5. E. M. Campbell, J. T. Hunt, E. S. Bliss, D. R. Speck, and R. P. Drake.,"Nova experimental facility", Rev. Sci. Instrum. **57**, 2101 (1986).
6. "*The Physics of Laser Fusion*", H Motz, London, Academic Press (1979).
7. *"Plasma Physics: Basic Theory with Fusion Applications"*, K. Nishikawa, M. Wakatani., 2nd. ed. Belin: Springer-Verlag (1994).
8. *"Pulsed Laser Deposition of Thin Films: Applications- Led Growth of Functional Materials"*, R.W. Eason., Wiley, New York (2006).
9. P. R. Willmott and J. R. Huber.,*"Pulsed laser vaporization and deposition",* Rev. Mod. Phys. **72**, 315 (2000).
10. "*Pulsed Laser Deposition of Thin Films",* D. B. Chrisey and G. K. Hubler. (Wiley, New York, 1994).
11. S. Bollanti, F. Bonfigli, E. Burattini, P. Di Lazzaro, F. Flora, A. Grilli, T. Letardi, N. Lisi, A. Marinai, L. Mezi, D. Murra, C. Zheng.,*"High-efficiency clean EUV plasma source at 10–30 nm, driven by a long-pulse-width excimer laser*", Appl. Phys. B 76, 277 (2003).
12. "*Physics of Laser Plasmas",* F. F. Chen, in*, A.* Rubenchik, S. Witkowski (eds**.) 3** North Holland, Amsterdam (1991).
13. *"High Power Laser-Matter Interaction"*, Springer Tracts in Modern Physics,, Volume 238/2010, 153-192 (2010).
14. Godwin, R.P., "*Fresnel Absorption, Resonance Absorption, and Bremsstrahlung X-Rays in Laser-Produced Plasmas"*, Los Alamos Report LA- UR 93–1679 (1993).
15. S. I. Anisimov, B. S. Luk'yanchuk, and A. Luches,, *"An analytical model for three-dimensional laser plume expansion into vacuum in hydrodynamic regime"*, Appl. Surf. Sci. **96**, 24 (1996).

16. R. K. Singh and J. Narayan., *"Pulsed-laser evaporation technique for deposition of thin films: Physics and theoretical model"*, Phys. Rev. B **41**, 8843 (1990).

17. Ž Andreić, D Gracin, V Henč-Bartolić, H-J Kunze, F Ruhl, L Aschke., *"Dynamics of laser-produced carbon plasma",* Physica Scripta **53**, 339 (1996).

18. B. Toftmann, J. Schou, and J. G. Lunney.,*"Dynamics of the plume produced by nanosecond ultraviolet laser ablation of metals",* Phys. Rev. B **67**, 104101 (2003).

19. B. Doggett , J. G. Lunney.,*"Expansion dynamics of laser produced plasma"*, J. Appl. Phys. **109**, 093304 (2011)

20. *"Physics of Shock Waves and High-Temperature Hydrodynamic Phenomena"*, Zel'dovich, Ya. R. and Raizer, Yu. P., Dover, Cambridge, Massachusetts (2001).

21. Amoruso, S., *"Modeling of UV pulsed-laser ablation of metallic targets"*, Appl. Phys. A **69**: 323–332 (1999).

22. Lunney, J. G. and Jordan, R., *"Pulsed laser ablation of metals"*, Appl. Surf. Sci., 127-129: 941-946. (1998).

23. *"Lasers and Plasma Applications",* B. C. Tan, New Delhi, Narosa Publishing House, (1992).

24. Geetha K. Varier, Riju C. Issac, S. S. Harilal, C. V. Bindhu, V. P. N. Nampoori, C. P. G. Vallabhan., *"Investigations on nanosecond laser produced plasma in air from the multi-component material* $YBa_2Cu_30_7$*"*, Spectrochimica Act B **52**, 657 (1997).

25. S. S. Harilal, C. V. Bindhu, M. S. Tillack, F. Najmabadi, and A. C. Gaeris., *"Internal structure and expansion dynamics of laser ablation plumes into ambient gases"*, J. Appl. Phys. **93**, 2380 (2003).

26. M. Cirisan, J. M. Jouvard, L. Lavisse, L. Hallo and R. Oltra., "*Laser plasma plume structure and dynamics in the ambient air: The early stage of expansion"*, J. Appl. Phys. **109**, 103301 (2011).

27. J. F. Friichtenilht.,"*Laser-generated pulsed atomic beams"*, Rev. Sci. lustrum. **45**, 51 (1974).

28. Miotello A; Kelly R., "*Critical assessment of thermal models for laser sputtering at high fluences*", Appl Phy Lett **67**, 3535 (1995).

29. Bakos J S, F¨oldes I B, Ign´acz P N, Kocsis G, Szigeti J and Kov´as, J. Opt. Commun. **74,** 374 (1990).

30. Bakos J S, F¨oldes I B, Ign´acz P N and Kocsis G.,*"Investigation of laser blow- off atomic beams by electron impact excitation*", J. Appl. Phys. **69** 1231 (1999).

31. Mattoo S K, Wirtz L, Pospieszczyk A and Schweer B., *"Laboratory studies of metal atomic beams produced by means of UV-laser radiation"*, Nucl. Instrum. Methods Phys. Res. B **124,** 579 (1997).

32. Michaud, D. Ross, G. G. Haddad, E. Mai, H. H. Pospieszczyk, A. St-Germain, J. P.,*"Measurements of ne(r) and Te(r) in TdeV boundary layer by injection of laser ablated Li and C*", Rev. Sci. Instrum. **63**, 5698 (1992).

33. S. Sasaki, Y. Uesugi1, S. Takamura, H. Sanuki, and K. Kadota., *"Temporal behavior of the electron density profile during limiter biasing in the HYBTOK-II tokamak"*, Phys. Plasmas **1**, 1089 (1994).

34. Pospieszczyk and G.G. Ross.,*"Use of laser-ablated fast particle beams for the measurement of n_e and Te profiles in the TEXTOR boundary layer"*, Rev. Sci. Instrum. **59**, 1491 (1988).

35. Sasaki, S. Takamura, S. Uesugi, Y. Ohkouchi, Y. Kadota, K., *"Laser blow-off lithium beam probing with high temporal resolution for edge plasma diagnostics"*, Rev. Sci. Instrum. **64**, 2277 (1993).

36. K. McCormick., *"Measurement of the scrape-off layer density profile on ASDEX via an energetic neutral lithium beam*", Rev. Sci. Instrum. **56**, 1063 (1985).

37. M Bruchhausen, R Burhenn, M Endler, G Kocsis, A Pospieszczyk, S Zoletnik and the W7-AS Team., *"Fluctuation measurements on the Wendelstein 7-AS stellarator by means of repetitive lithium laser blow-off "*, Plasma Phys. Control. Fusion **46**, 489 (2004).

38. E Scavino, J S Bakos, R Dux, H Weisen and TCV Team., *"Effects of plasma shape on laser blow-off injected impurity transport in TCV",* Plasma Phys. Control. Fusion **45**, 1961 (2003).

39. A. Boboc, P. Franz, A. Murari, L. Giudicotti, E. Zilli, P. Zanca, M. O'Gorman and S. Prunty., *"Methods for the estimate of the magnetic axis, the last closed flux surface and the differential shift in an RFP plasma"*, Nucl. Fusion 42, 913 (2002).

    A. Boboc, P. Franz, A. Murari, L. Giudicotti, E. Zilli, P. Zanca, M. O'Gorman and S. Prunty., *"Methods for the estimate of the magnetic axis, the last closed flux surface and the differential shift in an RFP plasma"*, Nucl. Fusion 42, 913 (2002).

40. D. Michaud, G. G. Ross, E. Haddad, H. H. Mai, A. Pospieszczyk and J. P. St-Germaina.,*"Measurements of ne(r) and Te(r) in TdeV boundary layer by injection of laser ablated Li and C"*, Rev. Sci. Instrum. **63**, 5698 (1992)

41. K. McCormick., *"Measurement of the scrape-off layer density profile on ASDEX via an energetic neutral lithium beam"*, Rev. Sci. Instrum. **56**, 1063 (1985).

42. *"Laser Induced Plasmas and Applications"*, L. J. Radziemski, D. A. Cremers, (Marcel Dekker, New York, 1989).

43. *"Laser Ablation and its Applications"*, Phipps Claude., Springer Series in Optical Sciences, Vol. 129 (2007).

44. S. Bollanti, F. Bonfigli, E. Burattini, P. Di Lazzaro, F. Flora, A. Grilli, T. Letardi, N. Lisi, A. Marinai, L. Mezi, D. Murra, C. Zheng., *"High-efficiency clean EUV plasma source at 10–30 nm, driven by a long-pulse-width excimer laser"*, Appl. Phys. B **76**, 277 (2003)

45. J. White, G. O'Sullivan, S. Zakharov, P. Choi, V. Zakharov, H. Nishimura, S. Fujioka, and K. Nishihara.,*"Tin laser-produced plasma source modeling at 13.5 nm for extreme ultraviolet lithography"*,Appl. Phys. Lett. **92**, 151501 (2008).

46. A G Gnedovets, A V Gusarov and I Smurov., *"A model for nanoparticles synthesis by pulsed laser evaporation"*, J. Phys. D: Appl. Phys. **32**, 2162 (1999).

47. S. Amoruso, R. Bruzzese, N. Spinelli, R. Velotta, M. Vitiello, X. Wang, G. Ausanio, V. Iannotti, L. Lanotte.,*"Generation of silicon nanoparticles via femtosecond laser ablation in vacuum"*, Appl. Phys. Lett. **84**, 4502 (2004).

48. A. Maksimchuk, S. Gu, K. Flippo, D. Umstadter nad V. Yu. Bychenkov., *"Forward ion acceleration in thin films driven by a high-intensity laser"*, Phys. Rev. Lett. **84**, 4108 (2000).

49. Pospieszczyk and G. G. Ross., *"Density determination in the TEXTOR boundary layer by laser-ablated fast lithium atoms"*, Rev. Sci. Instrum. 59, 605 (1988).

50. *"Plasma Spectroscopy",* Griem H R, (New York: McGraw-Hill) (1964)

51. Schweinzer J, Brandenburg R, Bray I, Hoekstra R, Aumayr F, Janev R K, Winter H P., *"Database for inelastic collisions of lithium atoms with electrons, protons, and multiply charged ions"*, At. Data Nucl. Data Tables **72**, 239 (1999).

52. Lennon M A, Bell K L, Gilbody H B, Hughes J G, Kingston A E, Murray M J and Smith F J.,*"Recommended data on the electron impact ionization of atoms and ions: fluorine to nickel"*, J. Phys. Chem. Ref. Data **17** 1285(1988).

53. Pospieszczyk A., 1993 Report: Workshop on the Use of Atomic Beams in Plasma Experiments KFKI-19/D Report (1993).

54. D. Dijkkamp and T. Venkatesan, X. D. Wu, S. A. Shareen, N. Jiswari, Y.H. MinLee, W. L. McLean and M.Croft.,*"Preparation of Y-Ba-Cu oxide superconductor thin films using pulsed laser evaporation from high Tc bulk material"*, Appl. Phys. Lett. **51**, 619 (1987).

55. "*Introduction to Plasma Physics and Controlled Fusion"*, Chen, Francis F. Second Edition,(Plenum Press, New York).

56. R.K. Abhilasha, R.K. Abhilasha and R.K. Dwivedi.,*"Optical emission spectroscopy of laser-produced carbon plasma at moderate and low irradiance in an ambient atmosphere* ", Laser and Part. Beams **13**, 481 (1995).

57. Salvatore Amoruso, Riccardo Bruzzese, Nicola Spinelli, Raffaele Velotta, Marco Vitiello, and Xuan Wang.,*"Dynamics of laser-ablated MgB2 plasma expanding in argon probed by optical emission spectroscopy"*, Phys. Rev. B **67**, 224503 (2003).

58. J. J. Camacho, L. Díaz, M. Santos, L. J. Juan and J. M. L. Poyato., "*Time-resolved optical emission spectroscopy of laser-produced air plasma*", J. Appl. Phys **107**, 083306(2010).

59. "*Principles of Laser Plasmas"*, G. Bekefi., John Wiley & Sons, Inc., New York (1976).

60. Langmuir, Irving et al., *"The theory of collectors in gaseous discharges",* Physical Review, (1926).

61. "*Electrical Probes for Plasma Diagnostics*", J. D. Swift and M. J. R. Schwar., American Elsevier, New York (1969).

62. "*Principles of Plasma Diagnostics",* Hutchinson, I.H., Second Edition. (Cambridge Press, 2002).

63. *"Langmuir Probe in Theory and Practice",* Evgeny V. Shun'ko, Universal-Publishers (2009).

64. William Whitty, Jean-Paul Mosnier.,*"Diagnostic of an expanding laser-produced lithium plasma using ICCD frame photography and shadowgraphy*", Appl. Surf. Sci. 127–129, 1035,(1998).

65. K. S. Kaur, R. Fardel, T. C. May-Smith, M. Nagel, D. P. Banks, C. Grivas, T. Lippert, and R. W. Eason., *"Shadowgraphic studies of triazene assisted laser-induced forward transfer of ceramic thin films"*, J. Appl. Phys **105**, 113119 (2009).

66. G. Neumann and U. Banziger, M. Kammeyer.,*"Plasma-density measurements by microwave interferometry and Langmuir probes in an rf discharge"*, Rev. Sci. Instrum. M. Lange. **64**, 19 (1993).

67. R. E. Walkup, J. M. Jasinski, and R. W. Dreyfus., *"Studies of excimer laser ablation of solids using a Michelson interferometer"*, Appl. Phys. Lett. **48**, 1690 (1986).

68. *"Infrared and Milimeter Waves",* D.Veron, Vol. II., edited by K. J. Button (Academic, New York, 1979).

69. Nadja Vogel and Natalie Kochan., "*Interferometric diagnostic of picosecond laser ablation*"., Appl. Surf. Sci. 127-129, 928 (1998).

70. Hongchao Zhang , Jian Lu and Xiaowu N., "*Optical interferometric analysis of colliding laser produced air plasmas*" , J. Appl. Phys. **106**, 063308 (2009).

71. Y. B. S. R. Prasad, P. A. Naik, A. Kumar, and P. D. Gupta., *"Simple interferometer for space and time resolved density measurements of laser produced plasmas"*, Rev. Sci. Instrum. **77**, 093106 (2006).

72. K. Sasaki, S. Matsui, H. Ito, and K. Kadota.,"*Distributions of C_2 and C_3 radical densities in laser-ablation carbon plumes measured by laser-induced fluorescence imaging spectroscopy*", J. Appl. Phys., **92**, 11 (2002).

Chapter 2

Experimental Scheme

Abstract

This chapter deals with different experimental techniques used for the present study. Experimental system has been designed and developed to perform diagnostics of plasma formed from lithium solid as well as multicomponent thin film (LiF-C) targets under various experimental conditions. The experimental procedure for optimizing the setup, such as the production of pulsed field and its synchronization with pulsed plasma and diagnostics systems are also discussed.

2.1. Introduction

Diagnostics of edge plasma parameters in Tokamak using lithium neutral beams are important as they play key role to determine the global plasma confinement {1-6}. The principle of measurement using laser blow off (LBO) technique and the reason for the selection of lithium fluoride-carbon (LiF-C) thin film target has already been discussed in chapter 1. In the previous chapter, we have also discussed quite a few methods to measure plasma parameters. In order to get more insight into these topics, it is necessary to characterize the lithium plasma formed by LBO scheme under various experimental conditions.

Present chapter focuses more into the details of the experimental scheme used for the characterization of LBO plume. Main diagnostic techniques used in plasma characterization are the gated time-resolved imaging using intensified CCD (ICCD), emission spectroscopy and ion probe. Among these, more focus has been given to imaging characterisation using ICCD. Fast imaging using ICCD is one of the commonly used diagnostic techniques and it provides the two dimensional snapshot of the three-dimensional plume {7-9}. Analyses of the recorded images give exact information of the modifications induced in the plume geometry and various other alterations, as a function of time, under different experimental conditions {10-13}. In most of the cases multiple diagnostics are performed simultaneously and this practice offer better understanding of the propagation dynamics {11, 12}.

During the study, we have investigated the influence of various ambient gases, different laser intensity profile and magnetic field over the plasma plume propagation {10, 13}. A comparative study has also been performed on the plasma generated from lithium solid as well as thin film of LiF-C. In the case of LBO, plasma plume (Li) consists of mainly neutral and singly ionized atoms and hence recombination processes could lead to the enhancement of neutral emission lines {14}. This study is important from the point of view of plasma diagnostics in

Tokamak, as the magnitude of magnetic field depends on the location of LBO system with respect to Tokamak. For the study of the effect of variable transverse magnetic field on LBO plume, a system have been developed where, pulsed magnetic field was generated using Helmholtz coil arrangement {15}. Mapping of the field was performed in order to ensure the uniformity over the plume area. As there were many elements involved in each study, it was essential to synchronize all these components. Time synchronization of the various subsystems has been achieved with a synchronization circuit.

2.2. Layout of the experimental setup

This section discusses the different elements involved in the creation of plasma from thin film/solid target. The generated plasma is then diagnosed using fast imaging, emission spectroscopy and probes. Creation of pulsed magnetic field is another important part of the study in this thesis. In order to perform the experiment, it is necessary to synchronize the whole setup and this aspect is discussed in section 2.5

2.2.1. Laser systems

All the experiments in the coming chapters were conducted using the electro-optically Q-switched Nd:YAG laser and utilized its fundamental wavelength 1064 nm. There were two lasers (laser I, laser II), mainly classified based on their laser output intensity profile. Laser I (*QUANTEL, Brio*) produces output pulses with *Gaussian* intensity profile while Laser II (*CONTINUUM*) produces pulses having *top hat* intensity profile.

In the fundamental mode of the Q-Switched Brio laser (laser I), it is possible to obtain a maximum energy of approximately 130 mJ at a pulse width of 6 ns {16}. The average power of the laser depends on the energy per pulse and the repetition rate. This laser can produce an average power of 2.6 W at a frequency of 20 Hz. The beam divergence for laser I is less than 5 mrad. Connector terminals attached to

the laser allows synchronization to the laser flash lamp (and the laser Q-switch, through a positive TTL trigger signal (5 V, 20 mA max, 50 μs duration). All operating parameters and settings for the laser can be controlled through a *remote box*, which is connected to the laser power supply.

Pulses from the laser II (*CONTINUUM*), which operates at a frequency of 30 Hz gives a maximum energy of 1.6 J {17}. This has a pulse width of 8 ns and the beam divergence is less than 6 mrad. Like laser-I, this laser also provides the trigger input-output terminals for the flash lamp and Q-switch. These pulses are utilized to synchronize other subsystems which include beam shutter, PMT, ICCD, magnetic field etc.

2.2.2. Multipurpose chamber and pumping system

The experimental study for laser plasma from solid/thin film target was conducted in a multipurpose chamber made of non-magnetic stainless steel cylinder of 160 cm length and 21 cm inner diameter. This chamber with 28 view ports, each fitted with CF 100 coupling, in an equal-spaced cross geometry. These couplers can be replaced with quartz windows to view the plasma. Chamber was evacuated down to $2x10^{-5}$ mbar using two rotary pumps and an oil diffusion pump (500 liters/second). Gases can be introduced into the chamber at desired pressures through a fine controlled needle valve. Some of the view ports also have the provision for keeping probes without disturbing the vacuum.

2.2.3. Target and its handling system

The thin film target was composed of uniform layers of 0.5 μm thick carbon and 0.05 μm of LiF (Lithium Fluoride-Carbon) film on a 1.2 mm thick quartz plate. In the case of laser blow off (LBO), power density of the laser was adjusted to ablate the entire material from the thin film target on each laser hit. Excess laser power will cause etching of the substrate material.

Figure 2.1 *Photograph of the target plate fixed on a holder. Each circular spot represents the ablated areas.*

For performing LBO plasma studies, it was necessary to change the target position after each laser hit to provide fresh surface for ablation. The targets were placed inside the chamber, on a stainless steel axle with 6 mm diameter through a vacuum compatible Wilson-seal feed through fixed to a motorized X-Y translator system to provide a fresh surface for ablation. The stepper motor driver of the translator and hardware were interfaced to a computer system. By using the software interface of the translator system, position of the target can be adjusted (both X and Y directions) at regular intervals specified by the user. Photograph of the target plate on a target holder is shown in Fig.2.1. To avoid back-reflection into the laser system, the incident laser beam was focused on the target at an angle of 6 degrees.

In the case of LPP studies, multiple laser hit at the same portion of the target may result in the pitting on the surface and thereby change the spot size. In order to eliminate this problem, the target was attached to a motor which rotate continuously and this avoids laser hit in the same target area.

2.3. Diagnostic techniques

This thesis mainly comprises the experimental study of laser blow off (LBO) plasma from thin film targets, using diagnostic techniques such as emission spectroscopy, fast imaging using ICCD and probe diagnostics.

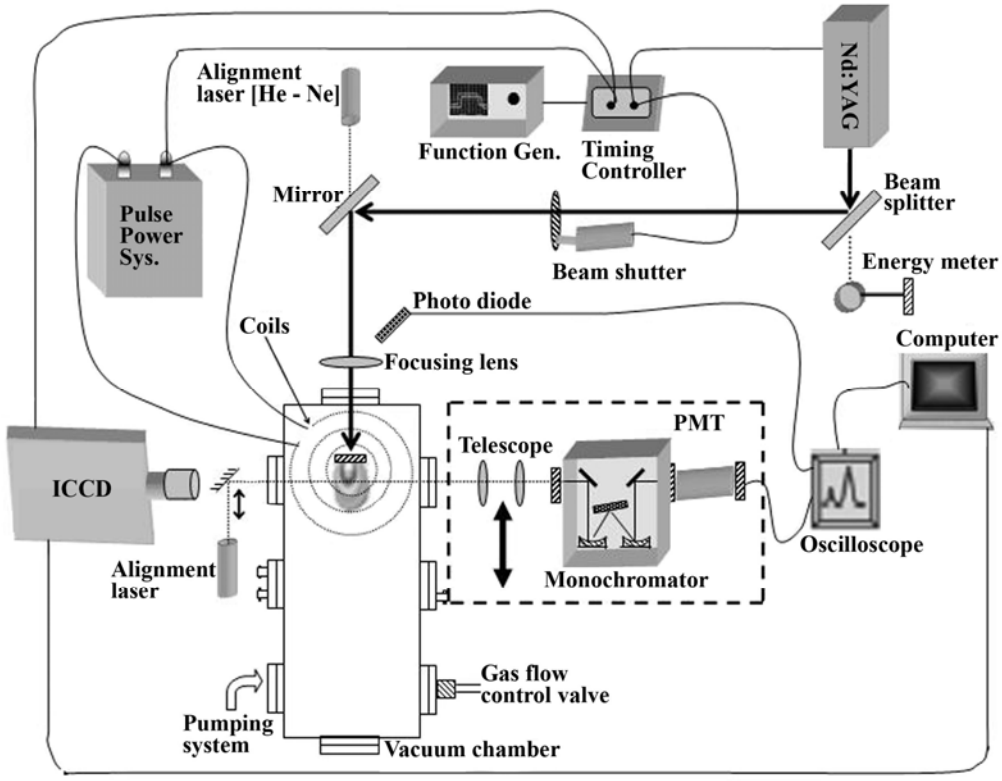

Figure 2.2 *Schematic diagram of the details of experimental setup.*

In subsequent sections of this chapter, we discuss these techniques in detail. The block diagram of experimental scheme used for the study is shown in Fig. 2.2.

2.3.1. Optical emission spectroscopy

Optical emission spectroscopy (OES) is one of the most commonly used non-invasive techniques to investigate dynamics of atoms, ions and molecules within plasma {18-21}. This non-perturbing diagnostic method can provide information about properties, such as excited species densities, electron-atom, atom-

atom and ion-atom collisional effects, energy distribution of species, charge transfer between plasma constituents and electric and magnetic fields etc. Its use as a diagnostic tool for emitting media has led to a greater understanding of very complex phenomena such as the evolution of stellar atmospheres and the study of fusion plasmas. Since the interpretation of OES observations is dependent on the source of emission and the understanding of the physical processes occurring within the source, this technique finds application in plasmas that are suitable for the processing of materials

It is important to define the quantities involved in the use of OES as a diagnostic tool. A portion of this volume emission is focused onto the slit of a spectrometer via a lens or mirror optical system. The calibration of the detected signals are normally done by substituting a surface emitting continuum source of known spectral radiance, like a calibrated tungsten strip lamp in place of the volume emitting source. This calibrated lamp is positioned at the focus of the emission optical system and the amount of its radiation per unit time per unit solid angle per unit wavelength-band per unit area element is precisely known. Thus, the signal from the spectrometer and detection system is calibrated. The spectral radiance of any emitter, L1 , is given in units of radiant energy per unit time per unit area per unit solid angle per unit wavelength-band.

Plasma is created inside the vacuum chamber by irradiating the target (thin film/solid) with the Q-switched nanosecond laser pulse. As we are concentrating on the plasma edge density parameters in this study, lithium emission lines are monitored. For space and time resolved spectroscopy, the expanded plasma is viewed through a quartz window normal to its direction of expansion with appropriate optics. The light emission from the plume is imaged onto the entrance slit of a 0.35 m *Jobin-Yvon* monochromator ($\Delta\lambda$= 12.5 Å) by means of two lens system with unity magnification. For spatially resolved study, monochromator along with the focusing system is mounted on the X-Y translator system, which

facilitate controlled scan of the plume along its expansion axis with spatial resolution ~ 250 μm. The characteristic line selected by the monochromator is detected by a photomultiplier tube (*BURLE C31034*) having 2 ns rise time. For recording the temporal profiles, output of PMT is directly fed to a 1 GHz digital oscilloscope (*Tektronix, TDS 540*) through a 50 Ω termination. The time resolution in the present experiment is about 200 ns. A photodiode is placed just behind the focusing lens of the incident light. A small fraction of scattered light from the lens is detected by the photodiode and this signal is used to trigger the oscilloscope. So we have taken the photodiode signal as a time reference in the present experiment. Data management, analysis and plotting are made possible by directly interfacing the oscilloscope with computer through wave-star software. Interpretation of the spectral data obtained reveals various atomic processes involved during and after the laser irradiation.

2.3.2. Fast imaging using ICCD

Recent developments in imaging technologies provide an effective way to record and analyze ultra fast events. The picosecond gating capability of Intensified CCD (ICCD) cameras are essential for high speed imaging applications in the area of ultrafast phenomena. Fast imaging diagnostics is the main technique employed for most of the investigations in this thesis. We have ICCD used extensively for studies of the LBO plume under various experimental conditions {Chapter 3, 4, 5 and 6}. This section briefly explains the techniques adopted in ICCD (*4 Picos Stanford Computer Optics, Inc.*) for its high speed operation and image amplification.

Fast imaging cameras consist of a high performance CCD camera and an image intensifier that is mounted in front of it {22}. The incoming light is first amplified by the image intensifier. The intensified image is then transmitted from the intensifiers phosphor screen where the multiplied electrons from the micro channel plate convert back into photons. This image is then projected onto the CCD

sensor by means of a coupling lens. Thus, an ICCD camera directly amplifies the incoming light, thereby supplying the CCD sensor with a light intensity far above the thermal noise level of the sensors.

2.3.2.1. The image intensifier

The image intensifier is the key system element of an ICCD high speed camera, besides the CCD sensor itself. The main function of the image intensifier is the amplification of the incoming light signal, i.e. the multiplication of the incoming photons. This permits the ICCD camera to take images at extremely low light conditions and/or at exceedingly short exposure times down to 200 ps, when the integral of the photon flux over the exposure time is very small.

The image intensifier module basically consists of the following three functional units:

- The photocathode that converts the incoming photons to photo electrons,
- The micro channel plate (MCP) that strongly multiplies these photo electrons,
- The phosphor screen that converts the multiplied photo electrons back to photons.

The incoming light first meets the photocathode of the ICCD camera's image intensifier. The photocathode converts the incoming photons to photo electrons by collisional ionization. To obtain a maximum signal to noise ratio in the images the spectral sensitivity of the photocathode should be well suited to the applications light spectrum. A maximum number of photoelectrons per incoming photon are generating in this way. The MCP multiplies the incoming electrons from the photocathode. It can be considered as a matrix of tiny linear channeltrons in which the single channels are arranged by an angle of a few degrees towards the axis of the image intensifier. MCPs are available as single stage, double stage or triple stage. The typical electron multiplication factor of one MCP stage is 1000 secondary electrons per incoming electron. Thus, a two stage MCP will give a

multiplication factor of 1000 x 1000 = 10^6. In the case of a triple stage MCP, the maximum multiplication factor is limited to less than 10^8 due to saturation effects.

2.3.2.2. High speed shutter

It is the image intensifier that provides the so called gating capability of the ICCD camera, i.e. the shutter function.

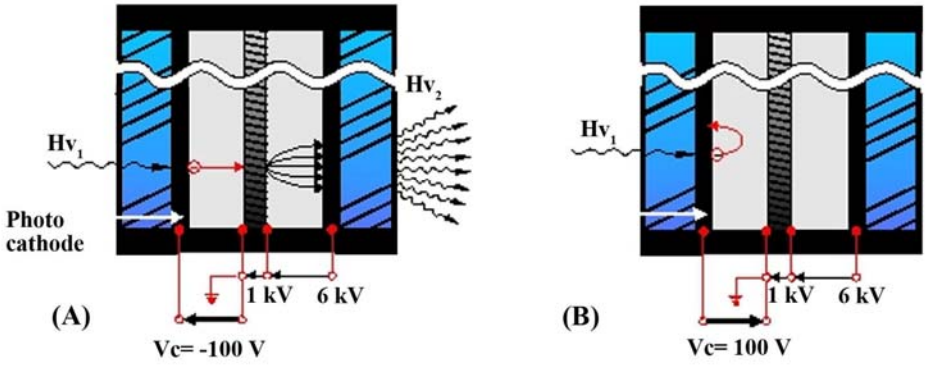

Figure 2.3 *Representation of the ICCD gating operation (A) Shutter open (B) Shutter closed*

A unique advantage of the gateable ICCD camera over all other kinds of cameras is the ability of ultrafast gating. i.e., exposure times in the range of less than 5 ns can be achieved with gateable ICCD cameras. There are three voltages applied to the image intensifier as shown in the Fig.2.3. If the voltage between photocathode and micro channel plate is negative (Fig.2.3(A)), the photoelectrons are accelerated towards the MCP. This means that the ICCD high speed camera is gated, i.e. the shutter is open. If the voltage applied is positive, the photoelectrons are kept at the photocathode which means that the ICCD camera is not gated, i.e. the shutter is closed and no light is transmitted to the CCD sensor (Fig. 2.3(B)). There are triggering options for the ICCD, where the camera can be synchronously triggered to ultrafast events.

2.3.3. Ion probe diagnostics

A movable charge collector (ion probe) is used to study the plume propagation dynamics at longer distances from the target where the optical emission signals are almost undetectable {15}. The length of the probe, which is exposed to the plasma and separation between the probe and target plate are set as 3 mm and 45 mm respectively.

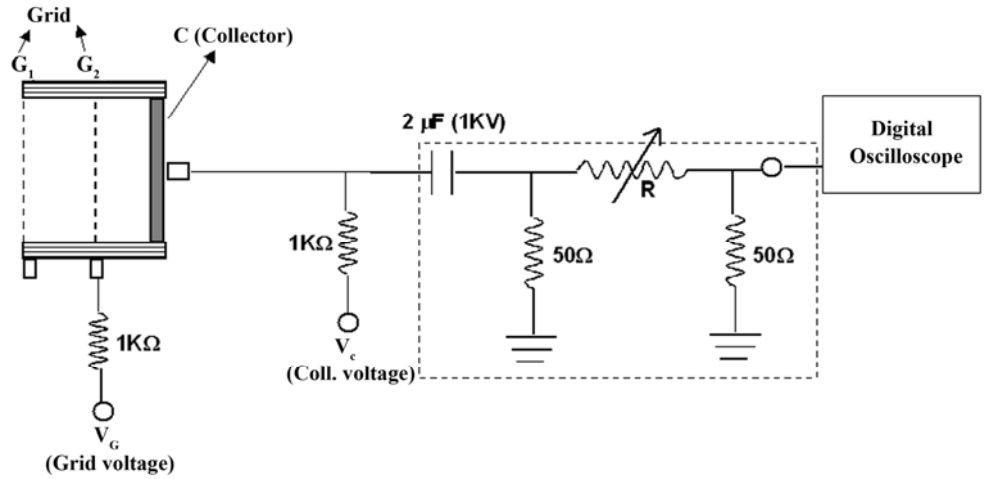

Figure 2.4 *Schematic of the ion probe assembly*

The ion probe consists of a 10 mm diameter stainless steel disk (Fig. 2.4). A pair of high transmission (~80%) stainless steel grids is mounted in front of the collector. The separations between the grids G_1 and G_2 between the second grid (G_2) and collector are 8 and 5 mm, respectively. The whole assembly is mounted on a Wilson feed-through for scanning the beam cross-section. The first grid G_1 is kept at ground potential. To collect the positive ions, negative bias voltages are applied to the second grid G_2 and collector. The potential between G_1 and G_2 prevents the plasma electrons from reaching the collector. A 2 μF capacitor is used to decouple the measuring circuit from the applied bias voltage. The collector signal is terminated on a 50 Ω resistor through a potential divider and signals are recorded on a fast digital oscilloscope.

The applied voltages on the grid G_2 and the collector, and distance between the charge collector to the target plates 'z' require critical optimization to avoid breakdown due to high plasma density. It was found that at distance $z \geq 40$ mm, the bias voltages –70 V and – 40 V to the collector and second grid G_2 respectively give the undistorted time of flight spectrum of the ion current in the saturation region. The potential difference (-30 V) between the collector and G_2 is sufficient to prevent the escape of secondary electrons, emitted by the collector.

2.4. Development of system for pulsed magnetic field

It is well known that the presence of magnetic field during the expansion of laser-produced plasma may induce several interesting physical phenomena, including plume confinement, plume splitting, ion acceleration, emission enhancement and plasma instability {23-26}. The behavior of plasma streams produced by intense laser irradiation of a target made from various materials in an external magnetic field has been the subject of studies at numerous laboratories in the world for many years {27-32}. Taking this into account, we have conducted experiments to investigate the effect of pulsed magnetic field on plasma generated from LiF-C thin film and Li solid targets.

In order to study the effect of uniform magnetic field on laser-induced plasma, a system has been developed. It is required that the magnetic field should be uniform throughout the plume dimension and the field duration longer than the duration of the plasma plume (> few microseconds). The pulsed power system consists of a capacitor bank and wire wound solenoid to produce magnetic field. In this design, the capacitor energy is drained through two identical coils, mounted in parallel resulting in the generation of pulsed magnetic field. The amplitude of the magnetic field depends on the amplitude of time dependent current (flowing through the coil) and the geometrical configuration of the coils.

The schematic diagram of the pulsed power system to produce the magnetic field is shown in Fig. 2.5. A pair of magnetic field coils was constructed using 8

mm diameter multi-stand shielded copper wire. Each coil having 22 turns (two layers of 11 turns each) were wound on the top and bottom port of the vacuum chamber.

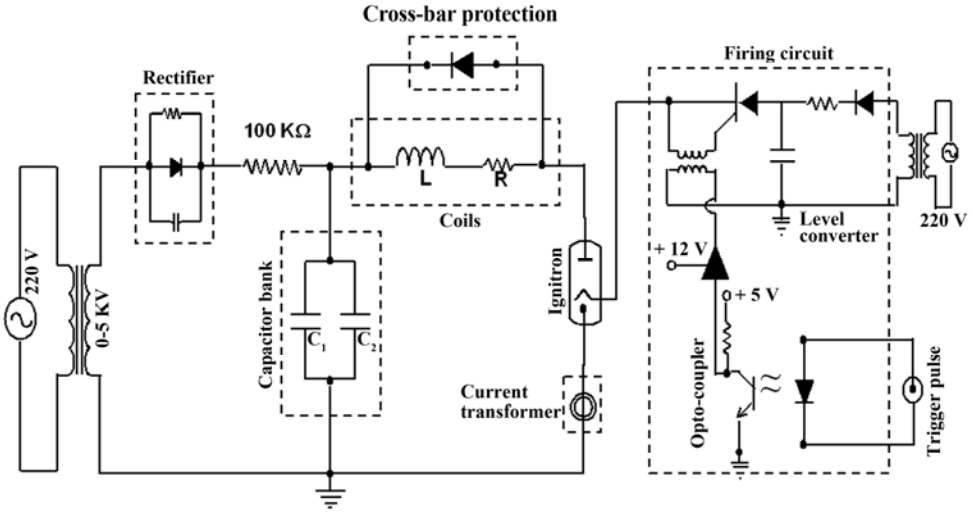

Figure 2.5 *Schematic diagram of the capacitor bank pulsed power system.*

A forma made of hylam was used to hold the coil perfectly parallel to each other. Average diameter of each of the coils is 14 cm and they were 23 cm apart. Figure 2.6 shows the photograph of the coils on the upper and lower part of the chamber. Due to limitations from experimental setup, coils could not be mounted in exact Helmholtz configuration. Both coils were connected in parallel in such a way that the direction of current flow was identical in both the coils. To reduce the input impedance of the discharge circuit, which results in more current through the coil, we have chosen the parallel connection instead of series connection of the coils. The measured inductance and resistance of the coil in parallel configuration were 45 μH and 0.054 Ω respectively.

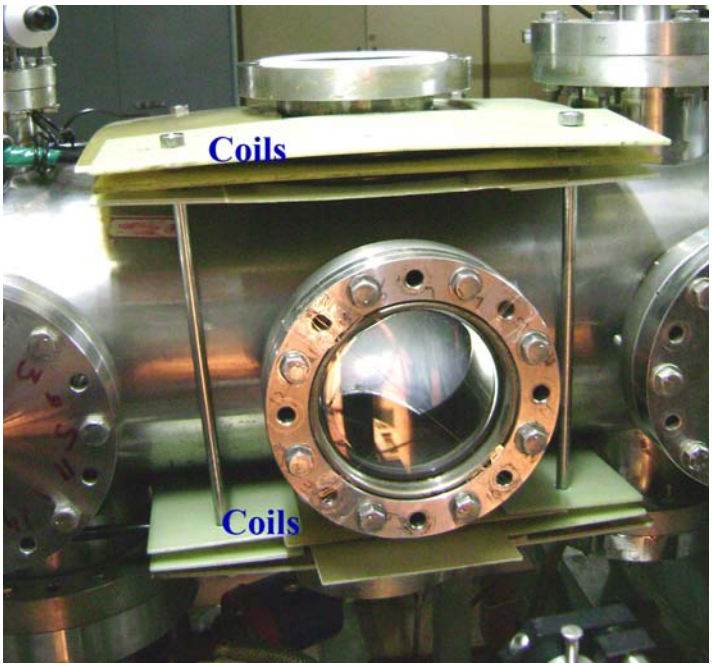

Figure 2.6 *Photograph of the Helmholtz coil arrangement in the vacuum chamber.*

The pulsed power system consists of parallel combination of two capacitors (700 μF and 500 μF, *CSI K-Film, USA*) and can store a maximum energy of 15 kJ at the maximum charging voltage of 5 kV. For charging the capacitor bank, dc voltage up to 5 kV was derived by using a combination of step-up transformer and the rectifier circuit. An ignitron (*BK506*, maximum peak forward anode voltage and current 25 kV and 100 kA, respectively) controls the current flow between the capacitor bank and the coil. During the instant discharge of the capacitor bank, it will recharge in the opposite polarity. To avoid reverse charging of the capacitor bank, a high power fast recovery diode (2.5 kV– 4 kA at 10 ms) was connected across the coil circuit {19}. A current transformer (0.01 V/A) was used to measure the coil current. A thyristor-based triggering circuit was also developed to initiate the switching of ignitron. To fire the thyristor, a +12 V pulse generated from the time synchronization circuit was applied to the gate terminal of thyristor via, a

transformer coupling and an optocoupler. The transformer and optocoupler protect the malfunctioning of time synchronization circuit.

2.4.1. Operation and optimization of field

For the generation of magnetic field, the capacitor bank is charged upto the preset voltage, depending on the required magnetic field strength in the experiment. After ensuring all setup including detectors and laser are ready, a firing pulse from the driving circuitry will apply to the ignitor for discharge the capacitor through the pair of coils wound (Fig.2.6) over the hylum sheet placed on the top and bottom of the vacuum chamber. As a result, a heavy current of few tens of kA flows in coils which was directly proportional to the induced field intensity. The temporal evolutions of the coil current and magnetic field measured by the current transformer and pickup coil, respectively, were used to optimize the design parameters of *LCR* system, magnetic field penetration time, uniformity, and strength of the magnetic field. Characteristics of the generated pulsed magnetic field are discussed as follows.

2.4.2. LCR circuit analysis

The current through the coil in equivalent LCR circuit is governed by the second order differential equation:

$$L\frac{d^2i}{dt^2} + R\frac{di}{dt} + \frac{i}{C} = 0 \qquad (2.1)$$

In our system $L > \frac{1}{4}CR^2$, that is system is under damped.

In this case, the solution of above equation is

$$V(t) = \frac{2\alpha V_0}{\omega_d} e^{-\alpha t} \sin \omega_d t \text{, and}$$

$$I(t) = V(t)/R$$

where, V_0 is the voltage across the charged capacitor,

L and R are the inductance and resistance of the coils, $\alpha = R/2L$ and $\omega_d = [(1/LC) - (R/2L)^2]^{1/2}$.

Simulated temporal evolution of the coil current for the measured parameters, C = 1200 μF, L = 45 μH (@ ~ 500 Hz), R = 0.014 Ω and V_0 = 300 V are shown in Fig.2.7. A typical current profile with crowbar diode is also shown in Fig.2.7.

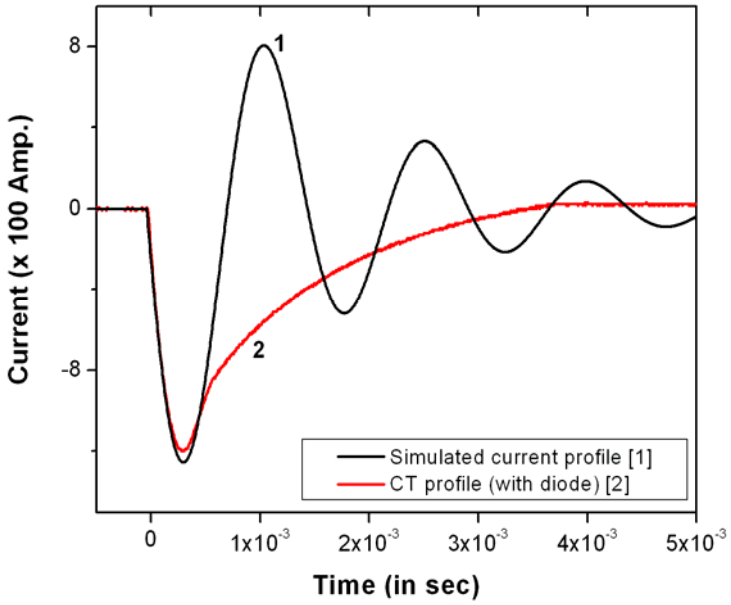

Figure 2.7 *Field profile measurements: Simulated profile and measured profile using current transformer (CT)*

Output current waveform of the LCR circuit shows the damping nature because of the reverse charging of the capacitor. To avoid the reverse charging of the capacitor, we have used high power fast recovery diode (2.5 kV- 4kA @ 10 ms) across the coil circuit {33}. This will overcome the damping of the LCR circuit, where induced reverse voltage across the inductor coil bypasses through the diode. The experimentally observed current profile measured by the current transformer (CT) is also shown in Fig.2.7. The effect of diode across the coil (crow-bar protection) is clearly seen in the current transformer (CT) profile. Due to the

addition of extra resistance of connecting wire, the magnitude of the observed current is slightly lower than the calculated value.

2.4.3. Magnitude and uniformity of the field

A high frequency Gauss-meter (*F. W. Bell, U S A, Model: 9900*) was employed to measure the actual magnetic field profile in the region of interest. For a specific coil current, the calculated and measured magnetic field at the center of the chamber is presented in Table 2.1. The discrepancies (~ 20%) between the calculated and measured field arises mainly due to two reasons. Firstly, field is attenuated by the chamber {34} and secondly errors {35} in measurements of current and geometrical dimensions of coil assembly such as insulation thickness are reflected in field calculation.

Capacitor charging voltage (Volt)	Coil current (Amp)	Calculated magnetic field (Gauss)	Measured magnetic field (Gauss)
300	1180	920	598
600	2400	1872	1216
900	3587	2798	1790
1200	4748	3703	2444
1500	5936	4630	3009

Table 2.1 *Magnetic field calculated theoretically and measured experimentally for a fixed charging voltage of the capacitor*

Further, to ensure the uniformity of the magnetic field, the Gauss meter probe was mounted on *X-Z* translator having a resolution of 5 μm. The transverse components of the magnetic field has been measured as a function of distance along the plume expansion (along z-axis) and radial (perpendicular to the plume expansion., i.e. along y-axis) directions at different positions along the x-axis. It was found that, the magnetic field was almost uniform in the region of slab 30 x 20 x 20 mm. So, the target was placed at a distance where the uniformity start in expansion

direction. This leads to plume expansion in a uniform field at least 30 mm distance along expansion direction.

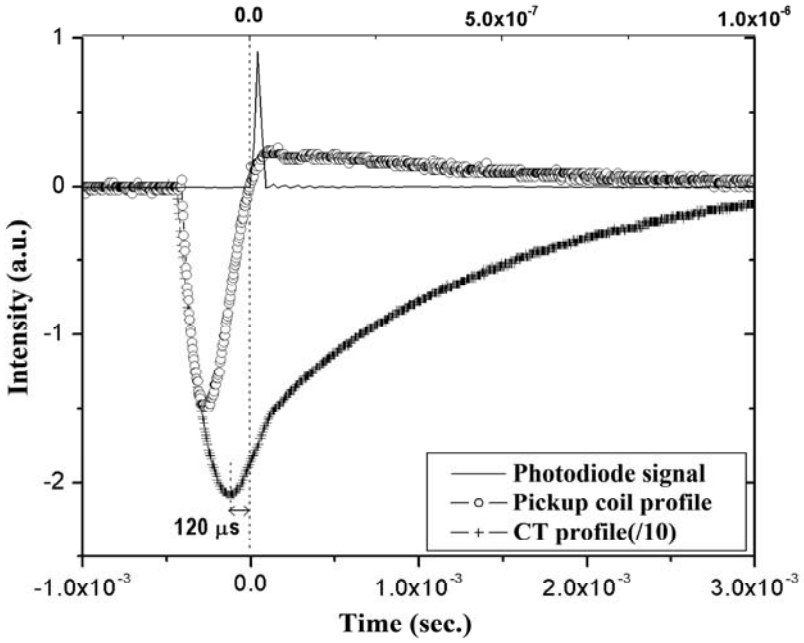

Figure 2.8 *Temporal profiles of induced voltage in pick-up coil and CT current with respect to photodiode signal.*

The typical current and hence the magnetic field profile obtained is shown in Fig.2.8. It is clearly seen that magnetic field is nearly constant for ~ 40 μs duration. The length of flat top portion of the magnetic field is much larger than the laser-plasma lifetime, which is few microseconds. In order to study the dynamics of plume in uniform magnetic fields, it is necessary to ensure that flat top portion of the field and the formation of plume are well synchronized.

Due to induced eddy currents in the SS chamber, a time delay is introduced between the peak in coil current and produced magnetic field. To measure this delay (penetration time of magnetic field), we have used the pick-up coil having 100 turns of insulated copper coil made of 0.04 cm diameter wounded on a 10 mm diameter Teflon rod. Pick-up coil (P-coil) was placed at the center of the chamber, where

laser-material interactions take place. The induced current (voltage) in the P-coil (which is directly proportional to the dB/dt) was monitored on the DSO without using any integration circuit. Temporal profile of pickup coil voltage along with the CT profile of the main coil current is shown in Fig.2.8. The zero-crossing point of the P-coil voltage shows that at this point magnetic field has maximum intensity. Approximately 120 μs delay was observed from the moment of peak coil current to the moment of peak field at the center of the chamber. Therefore, it was concluded that laser pulse should be delayed by 120 μs from the moment of peak coil current for perfect field-plasma synchronization.

2.5. Time synchronization of the integrated system

In the present setup, three independent diagnostic systems viz optical emission spectroscopy, time resolved imaging spectroscopy and fast charge collector technique are used to characterize the laser-induced plasma. Working principle and specialization of each diagnostic tool has already been discussed in previous sections {Sec 2.3} of this chapter.

The simultaneous use of these diagnostics gives complementary information about the plume dynamics in different experimental conditions. Successful operation of the setup requires the synchronization of diagnostics systems, laser pulse and the magnetic field together. The schematic diagram for synchronization of various subsystems and the corresponding timing sequence are shown in Fig.2.9.

A small fraction of scattered laser light from the focusing lens was detected by a photodiode and this signal served as the time reference (Tref = 0) in the whole experiment. The set position of spectrometer and charge collector does not require any time synchronization. To measure temporal profiles from the optical emission spectroscopy and charge collector, the outputs from these diagnostics were connected to 500 MHz oscilloscope (Tektronix TDS 540 A) directly with 50 Ω

terminations. The oscilloscope was triggered at the rising edge of the photodiode output. The ICCD camera has an inbuilt delay of 130 ns, therefore it should be pre-trigger of above delay in order to capture the image at Tref = 0. Similarly, 70 + 120 μs (rise time of the coil current profile + field penetration time) pre-trigger field firing pulse was required to coincide with the peak field inside the chamber with the time reference Tref=0.

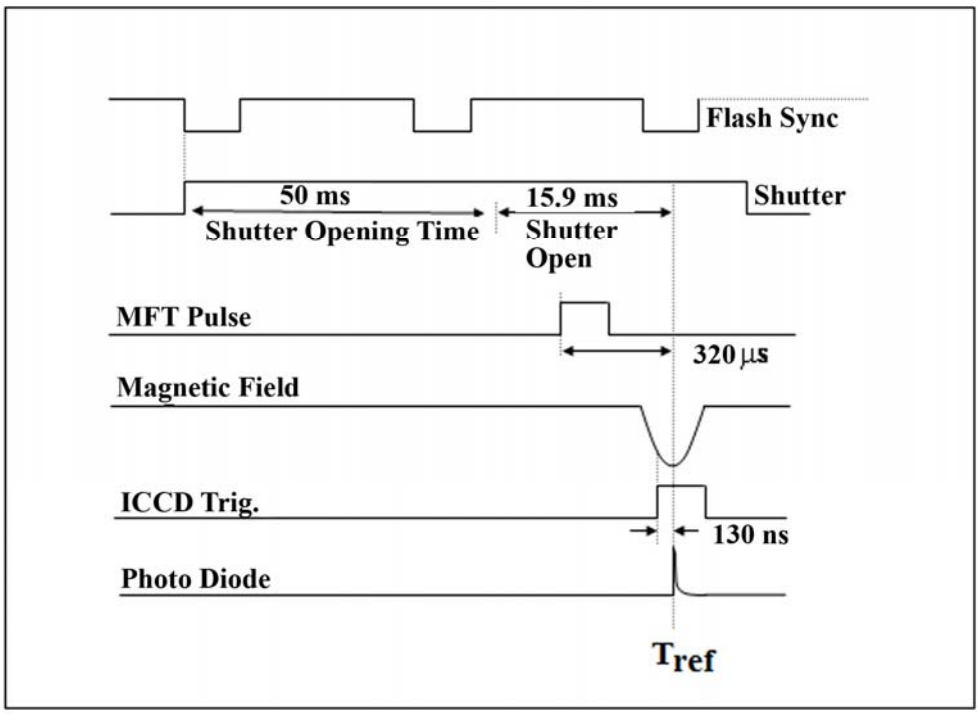

Figure 2.9 *Timing sequence of different sub systems.*

During the experiment, it was observed that the focused flash lamp light (continuously ON with 30 Hz for laser I and 20 Hz for laser II) partially ablated the thin film target. To overcome this problem, an electro-mechanical shutter was introduced in the laser path (Fig.2.2). The trigger pulses for laser and shutter operation (Tref - 65 ms) was gated in such a way that shutter was open for single flash lamp and laser pulse.

Laser is operated at 30 Hz in external mode. In this mode, the flash lamp is triggered with a 10 μs pulse at 30 Hz repetition rate and the *Q*- switch is triggered by a single pulse of same width. Multi-channel function generator provides the continuous flash lamp pulses and master trigger pulse in single burst mode. A programmable microcontroller based timing processor circuit (TPC) is used to control the time sequencing of different systems of the experimental setup. When a master trigger pulse initiated the TPC, sync-out pulse (20/30 Hz) from the laser is locked by the TPC at the negative edge. After locking the sync-out pulse, TPC generate the auxiliary pulse which is the 'time reference' for further time sequencing. With respect to this time reference, TCP generate the different trigger pulses and control the required time-sequencing operation of magnetic field, mechanical shutter, ICCD camera and laser system.

2.6. Conclusions

In conclusion, an experimental facility associated with the setup for characterization of plasma from thin film (LBO) as well as solid (LPP) target has been developed. The various elements in the system including, laser systems, vacuum chamber and associated components and generation of variable pulsed magnetic field were briefly explained in this chapter. Technical specifications of the diagnostics, which used in the present study- OES, fast imaging and probe techniques were also included. Since a number of elements have to be synchronized accurately in order to carry out this experiment, we have developed a timing processor unit, which synchronized all the events and produce necessary trigger pulses for the associated instruments. Technical aspects, optimization and performance tests of the developed setup were briefly described.

2.7. References

1. D. J. Rej, I. Henins, R. J. Fonck, and Y. J. Kim.,*"Intense diagnostic neutral beam development for ITER"*, Rev. Sci. Instrum. **63**, 4934 (1992).

2. A. E. Costley.,*"Large tokamak diagnostics"*, Rev. Sci. Instrum. **66**, 296 (1995).

3. M N Rosenbluth., *"Physics fundamentals for ITER"*, Plasma Phys. Control. Fusion **41,** A99 (1999).

4. E Scavino, J S Bakos, R Dux, H Weisen and TCV Team.,*"Effects of plasma shape on laser blow-off injected impurity transport in TCV"*, Plasma Phys. Control. Fusion **45**, 1961 (2003).

5. A Pospieszczyk., "*Spectroscopic diagnostics of Tokamak edge plasmas*", Physica Scripta **119**, 71 (2005).

6. N. T. Howard, M. Greenwald, and J. E. Rice.,*"Characterization of impurity confinement on Alcator C-Mod using a multi-pulse laser blow-off system"*, Rev. Sci. Instrum. **82**, 033512 (2011).

7. David B. Geohegan., *"Fast intensified-CCD photography of $YBa_2Cu_3O_{7-x}$ laser ablation in vacuum and ambient oxygen"*, Appl. Phys. Lett. **60**, 2732 (1992).

8. S. S. Harilal, C. V. Bindhu, M. S. Tillack, F. Najmabadi, and A. C. Gaeris., "*Internal structure and expansion dynamics of laser ablation plumes into ambient gases"*, J. Appl. Phys. **93**, 2380 (2003).

9. A. Sambri, S. Amoruso, X. Wang, F. Miletto Granozio, and R. Bruzzese.,*"Plume propagation dynamics of complex oxides in oxygen"*, J. Appl. Phys. **104**, 053304 (2008).

10. Sony George, Ajai Kumar, R. K. Singh, V. P. N. Nampoori.,*"Fast imaging of laser blow off plume: lateral confinement in ambient environment*", Appl Phys Lett. **94**, 141501 (2009).

11. Sony George, Ajai Kumar, R. K. Singh, V. P. N. Nampoori.,*"Effect of ambient gas on the expansion dynamics of plasma plume formed by laser blow off of thin film"*, Appl. Phys. A, **98**, 901 (2009).

12. Ajai Kumar, Sony George, R. K. Singh, V. P. N. Nampoori.,*"Influence of laser beam intensity profile on propagation dynamics of laser-blow- off plasma plume"*, Laser and Part. Beams, **28**, 387 (2010).

13. Ajai Kumar, Sony George, R. K. Singh, V. P. N. Nampoori.,*"Image analysis of expanding laser-produced lithium plasma plume in variable transverse magnetic field"*, Laser and Part. Beams, **29,** 241 (2011).

14. R. K. Singh, Ajai Kumar, B. G. Patel, and K. P. Subramanian.,"*Role of ambient gas and laser fluence in governing the dynamics of the plasma plumes produced by laser blow off of LiF–C thin film",* J. Appl. Phys. **101**, 103301 (2007).

15. A. Kumar, V. Chaudhari, K. Patel, S. George, S. Sunil, R. K. Singh and R. Singh., "*An experimental setup to study the expansion dynamics of laser blow-off plasma plume in variable transverse magnetic field"*, Rev. Sci. Instrum. **80**, 033503 (2009).

16. Instruction manual, Quantel Brio laser (www.quantel.com)

17. Instruction manual, Continnum laser (www.continnum.com)

18. R. C. Issac, K. V. Pillai, S. S. Harilal, G. K. Varier, C. V. Bindhu, P. Gopinath, P. Radhakrishnan, V. P. N. Nampoori and C. P. G. Vallabhan., "*Dynamics of laser produced silver plasma under film deposition conditions studied using optical emission spectroscopy*", Appl. Surf. Sci. **125,** 227 (1998).

19. R. K. Singh, Ajai Kumar, V. Prahlad, and H. C. Joshi., *"Generation of fast neutrals in a laser-blow-off of LiF–C film:A formation mechanism"*, Appl. Phys. Lett. **92**, 171502 (2008).

20. S Amoruso, R. Bruzzese, N Spinelli, R Velotta, M Vitiello, and X Wang., "*Dynamics of laser-ablated MgB 2 plasma expanding in argon probed by optical emission spectroscopy"*, Phys. Rev. B **67**, 224503 (2003).

21. S. S. Harilal, Riju C. Issac, C. V. Bindhu, V. P. N. Nampoori, and C. P. G. Vallabhan., "*Emission characteristics and dynamics of C2 from laser produced graphite plasma*", J. Appl. Phys. **81**, 3637 (1997).

22. Instruction manual, ICCD (www.standfordcomputeroptics.com)

23. A. Neogi and R. K. Thareja., *"Laser-produced carbon plasma expanding in vacuum, low pressure ambient gas and nonuniform magnetic field"*, Phys. Plasma **6**, 365 (1999).

24. S. S. Harilal, M. S. Tillack, B. O'Shay, C. V. Bindhu and F. Najmabadi., *"Confinement and dynamics of laser-produced plasma expanding across a transverse magnetic field"*, Phys. Rev. E **69**, 026413 (2004).

25. X. K. Shen, Y. F. Lu, T. Gebre, H. Ling and Y. X. Han., *"Optical emission in magnetically confined laser-induced breakdown spectroscopy"*, J. Appl. Phys. **100**, 053303 (2006).

26. Geohegan, D. B., *"Dynamics of plume propagation and splitting during pulsed-laser ablation"*, Phys. Rev.Lett. **79**, 1571(1997).

27. *"An Introduction to Magnetohydrodynamics",* P. A. Davidson., (Cambridge University Press, Cambridge, 2006).

28. C. Pagano, S. Hafeez and J. G. Lunney., *"Influence of transverse magnetic field on expansion and spectral emission of laser produced plasma*", J. Phys. D: Appl. Phys. **42**, 155205 (2009).

29. H.C. Joshi, Ajai Kumar, R. K. Singh and V. Prahlad.,*"Effect of a transverse magnetic field on the plume emission in laser-produced plasma: An atomic analysis"*, Spectrochimica Acta Part B **65**, 415 (2010).

30. Tae Hyun Kim, Sang Hwan Nam, Hye Sun Park, Jae Kyu Song and Seung Min Park., *"Effects of transverse magnetic field on a laser-produced Zn plasma plume and ZnO films grown by pulsed laser deposition*", Appl. Surf. Sci. **253**, 8054 (2007).

31. S. S. Harilal, B. O'Shay, M. S. Tillack, C. V. Bindhu and F. Najmabadi., *"Fast photography of a laser generated plasma expanding across a transverse magnetic field*", IEEE Transactions on Plasma Science, **33**, 2 (2005).

32. Pramod K. Pandey and R. K. Thareja., "*Plume dynamics and cluster formation in laser-ablated copper plasma in a magnetic field"*, J. Appl. Phys. **109**, 074901 (2011).

33. F. Rothwarf, C. O. Bateman, D. Ford, and P. Milke., "*Silicon-controlled rectifier circuitry for producing pulsed magnetic fields"*, Rev. Sci. Instrum. **38**, 1241 (1967).

34. C.H. Gough., "*Eddy current simulation of a vacuum chamber",* SLS Note 8/97 (1997).

35. H. P. Furth and R. W. Waniek.,"*Production and use of high transient magnetic fields"*, Rev. Sci. Instrum. **27**, 195 (1956).

Chapter 3

Effect of Ambient Gas on the Dynamics of LBO of LiF-C

Abstract

This chapter presents the results of study conducted to understand the influence of ambient gases (Argon & Helium) on the dynamics of laser blow off plumes of multi-layered LiF-C thin film. Plume images at various time intervals are recorded using an intensified CCD camera. Enhancement in the plume intensity and change in size and shape occurs on introducing ambient gases and these changes are found to be highly dependent on the nature and composition of the ambient gas.

3.1. Introduction

The interaction of laser produced plasma plume with ambient gas has been of increased interest in recent years because of its vast applications including laser deposition, nanoparticle formation, cluster production, material science extreme ultraviolet (EUV) lithography etc{1-8}. Further development of these techniques require a better understanding of the mechanisms involved in laser-solid interaction, plasma plume formation and plume expansion in vacuum/gaseous atmospheres. In particular, it is of great concern to examine how the nature of gas and the gas pressure influences the plume propagation.

Compared to the plume expansion in vacuum, the interaction of plume with the background gas is a far more complex dynamical process due to the rise of several physical processes involved such as deceleration, attenuation, thermalization of the ablated species, diffusion, recombination, formation of shock waves, reactive scattering and clustering {9-18}. There exist a vast number of diagnostic techniques to characterize plasma such as optical emission spectroscopy, probe analysis, imaging techniques etc {19-24}. These tools offer a platform to analyze the plume expansion in vacuum and ambient environments. Among this, fast imaging adds another dimension to ablation diagnostics by providing geometrical information of plasma propagation at different time intervals. Imaging data also can be used to understand many physical processes such as deceleration, attenuation/enhancement of emission, hydrodynamic instabilities, formation of shock waves and plume oscillations {16, 18, 25-27}. This information has been of great importance for the modeling of various processes related to space physics and hydrodynamics.

The dynamics of plasma plume formed depends on a number of experimental parameters, like ablation or excitation wavelength, intensity, pulse duration, spatial and temporal energy distribution {28-33} of the laser as well as number of gaseous medium properties, the most important of the later are the nature of the gas and its pressure {10, 34}. Although there have been many investigations already in the

literature in connection with the properties of plasma plume formed under typical laser ablation, the interaction between the ablated plume and ambient gas has yet not been explained satisfactorily. A short review of major studies is included in section 3.2 of this chapter.

This chapter is mainly concerned with the influence of ambient gas (argon and helium) on the dynamics of laser blow off (LBO) plasma from LiF-C thin film target. The formation and expansion dynamics of LBO plume has already been discussed in chapter 1{Sec.1.3}. Recent studies using optical emission spectroscopy of LBO plume {35, 36} have revealed that expansion feature of plume is very much depend on the experimental condition and vary according to the ambient environment and laser fluence. These studies did not provide any information regarding the structure and geometry (shape and size) of the plume. The shape and size of the plume in the presence of ambient gas play crucial roles in thin film deposition {4, 11}, formation of nanoparticles {3, 4}and are important parameters for probing neutral atomic beam {37-39} in plasma environment. Hence, understanding the geometry of ejected plume species and its spatial and temporal variations with different experimental conditions are essential for using these techniques in applied research. It is also worth mentioning here that neutral species are the main constituents of the LBO plumes although it also consists of the ions mostly in singly-ionised state {36, 40}. Hence, it will be worthwhile to study the interaction between background gas and neutral rich plume with regard to the formation of structures in plume due to hydrodynamic instability and reactive scattering.

3.2. Earlier works- A brief summary

Numerous experimental as well as theoretical investigations related to laser produced plasmas formed by solid targets have been reported in the past {15-19, 34, 41-44}. However, only a few measurements have been carried out on the characterization of LBO plasma. Further, the experimental data on lithium plasma

generated by the laser blow off (LBO) of thin films are very rare. This part of the thesis gives an overview of the major works carried out on solid target in ambient gas.

Understanding the complicated interactions between the species within the plume and interaction between the species and incident laser light require a detailed theoretical or computational treatment. To describe the interaction of plasma plume with ambient gas, the expansion is basically classified into three regions based on the background gas pressure viz low pressure, intermediate and high pressure. Most of the studies treat these regions with different theoretical approaches. In low gas pressure, the plume expansion could be described by Monte Carlo simulation {45, 46}. For high pressures, many numerical simulations were performed by considering compressible and non-dissipative conservation equations {47}. Bulgakova et. al has developed {48} gas dynamic model to describe the temporal and spatial evolution of the plume expanding into a gas under a pressure of typically a few tens of pascals. The model is based on the generation of a spherical plasma cloud for which expansion is described in a two-temperature approximation by the Euler equations. The dynamics of laser ablation of YBa_2Cu_30, superconductor in an oxygen environment have been analysed using this model. Atomic nature of the gas plays a major role and this in fact makes the low-medium-high pressure levels to vary for different gases. This research has extended {49} using a two-fluid gas-dynamic model and experimentally with time-of-flight mass spectrometry of laser ablated plume into different ambient gases. In moderate or high pressures, a blast wave model is found to accurately describe the plume propagation distance during the early expansion stages, whereas a shock layer model and an empirical drag model predict the maximum plume length with considerable accuracy {50-52}. It has also been shown that the angular and energy distributions of the ablated material are sensitive to the nature and pressure of the ambient gas{33}. Essentially most of the theoretical and modelling works {53-58} were performed for specific set of

target-background gas combinations and the same cannot be extended to other target-gas combinations.

An extensive literature is available describing the experimental research of plasma-gas interactions {10-13, 16-19, 41-44}. Many of these studies basically discusses the different diagnostic techniques adopted or the experimental conditions employed. For every technique used, the aim was to measure the alterations in plasma parameters including plasma size and shape, spatial distribution of temperature, density etc.

Multiple diagnostics were employed in most of the cases, since it permits better understanding of the propagation dynamics with reduced errors. One of the most commonly used is optical emission spectroscopy (OES) in combination with any of the imaging techniques like fast imaging, shadowgraphy or streak photography. Interpretation of spectral data obtained using OES of selected species allows the estimation of various plasma parameters in both space and time {59, 60}. At the same time, integrated image seems most suitable for studying geometrical details of the plume in ambient gas {34}. Imaging studies provide the advantage of giving indications of the structural modifications in different ambient pressures {61-64}. Many research studies investigated the knowledge of plume expansion from time to time and have advanced tremendously from spectroscopic studies with fast imaging techniques. This in fact is highly helpful to improve control over optimizing the material ablation parameters for applied research.

General observation is that in vacuum, the plume follows linear expansion driven by the pressure gradient. In this regime, the basic features of the plume expansion can be described theoretically in terms of an adiabatic, self-similar expansion of an elliptical gas cloud into vacuum {45}. At low pressure ambient gas, initial expansion of the plume shows similar behaviour as that in vacuum, since the driving pressure of the plume is much higher than that of the background gas {46}. Available experimental results obtained using fast imaging show that, the

plume follows linear expansion in this regime {47}. Subsequently, the plume gradually slows down as a consequence of the adjoint mass due to the background gas molecules at the plume periphery and finally stops as the plume pressure comparable with the ambient gas {48}. Plume confinement occurs during this period and emission enhancement results as an outcome of increased collisions among the elemental species, which contributes to the visible plume {49}. At early time periods, plume appears in spherical shape and later becomes more sharpened. Plume sharpening behaviour suggests that higher kinetic energy particles are emitted closer to the target surface normal. This had been modelled {65-67} by different groups and has also been experimentally {34} observed.

Splitting of the plume or in other words separation of plume into fast and slow components appears during the intermediate pressure levels {53}. Central part of the plume, which represents the high energy components, moves with a higher velocity and undergoes fewer interactions with the background gas. The slower component/circum boundaries of the plume undergo more interaction with the ambient medium and which leads to collisional excitation of the atoms. According to reports, edge instabilities (eg: Rayleigh-Taylor instability) also start appearing during this pressure levels. The intermediate pressure range in which spitting occurs is considered as the transition region where the interaction of the plume species with the gas transits from collisional to collisionless interaction {60}. Geohegan et. al {61} investigated the dynamics of laser-ablated yttrium plume propagation through background argon. During expansion into low-pressure background gases, the ion flux in the laser plasma plume is observed to split into fast and slow components over a limited range of distances. By correlating the data obtained using OES and ICCD, it has been concluded that plume splitting in background gases is consistent with scattering of target constituents by ambient gas atoms.

In addition to splitting, another related observation is the formation of various structures inside the plume and appearance of shock waves with increase in ambient

gas pressure {57}. At high-pressure levels, as the plume moves away from the target, the interpenetration of the gas into the plasma becomes more prominent and structural changes start to appear. The pressure at which these changes begin depends on the background gas pressure and atomic properties of the gas. Dyer et.al {58} performed experiments using streak photography of Y-Ba-Cu-O in an oxygen environment and reported the formation of blast waves with strong mixing at the contact surface of plume and O_2 gas. Occurrence of shock waves at high pressure regime has been reported by many experimental investigations {59}. Shock waves are formed as a result of growing hydrodynamic interaction between the plume and the background gas. At certain distance from the target, part of the plume expands freely, penetrates into the ambient gas like a piston and decrease strongly by the gas pressure {60}.

3.3. Experimental details

A detailed description of experimental setup is given in chapter 2 {74}. The plasma was viewed through a quartz window mounted orthogonal to the direction of plume expansion. The experiment was carried out in a cylindrical stainless steel chamber, which was evacuated to a base pressure better than $2x10^{-5}$ mTorr. Background gas was introduced into the chamber at desired pressures through a fine controlled needle valve. The target was composed of uniform layers of 0.05 μm LiF film and 0.5 μm thick carbon film, deposited on a 1.2 mm thick quartz substrate. The target was mounted on a movable target holder through vacuum compatible feed-through for fresh film positioning after exposure to the laser beam.

Nd: YAG (λ = 1064Å) laser having 8 ns pulse width with maximum pulse energy 1.6 J was used to ablate the thin film target. The laser beam was focused on the target at an incident angle of 6^o with respect to the normal to the surface. The spot size of the laser beam was set to about 1 mm diameter at the target. By adjusting the operating parameters of laser, laser fluence ranging from 2.8 J/cm^2 to 26 J/cm^2 were achieved at the target surface. To ensure that the LBO plume

contained only the species of the multi-layered film, the maximum energy density was set below the ablation threshold of the quartz substrate.

The time resolved images have been recorded by an intensified CCD camera having variable gain, gate time and spectral response in 350-750 nm region. In the present experiment, the gate time was set to 4 ns. Temporal evolution of the LBO plume has been obtained by varying the time delay (from 100 to 2500 ns) between the laser pulse and opening time of the ICCD gate. Five images were recorded under similar experimental conditions. These images were found to be nearly identical in shape and the reproducibility of the emission intensity was better than 5 %. A mesh image of known dimension has been recorded to map the geometrical parameters of the plume. The magnification of the imaging system was found to be 3.5. Dark noise was subtracted from the recorded image using MATLAB. Length and full-width at half maximum of the plume were estimated by segmentation algorithm. For better visibility, gray images have been converted into pseudo-colored images using jet color map *.

To measure the spatio-temporal evolution of spectral lines, the plasma plume was viewed normal to the direction of expansion and imaged at the entrance slit of a monochromator ($\Delta\lambda$= 12.5 Å). The temporal profile of emission signal was detected by a photomultiplier tube (PMT) and output of the PMT was directly fed to a 1 GHz digital oscilloscope. A small fraction of the light reflected from the laser-focusing lens was detected by a photodiode and was used as time reference for both oscilloscope and ICCD.

3.4. Expansion dynamics in argon

Spatio-temporal evolution of optical emission from the electronically excited plume species, driven by collisional processes between electrons, ions and neutrals was imaged by ICCD at different argon (Ar) pressures ranging from 10^{-5} to 3 Torr and is shown below (Fig.3.1). These images are recorded at a laser irradiance of ~ 3 GWcm^{-2}. For comparison, all the images are normalized to its maximum

intensity. Colorbar of the images was changed from arbitrary level 150 for the time delays upto 1000 ns to arbitrary level 100 for t >1500 ns to get better visibility. Following points are noted from the visual observation of the images.

After the termination of the laser pulse, the plume expands in the forward direction. In vacuum, the plume expands adiabatically and has an ellipsoidal shape. During the expansion, electron density reduces rapidly and hence the probability of electron impact excitation is also reduced. This leads to reduction in the emission intensity of the plume. For t > 1000 ns, emission intensity is beyond the detection limit of the ICCD due to lower dynamic range of the camera. It shows a three-line structure parallel to the plume expansion direction and is more intense at the leading edge of the plume closer to the target.

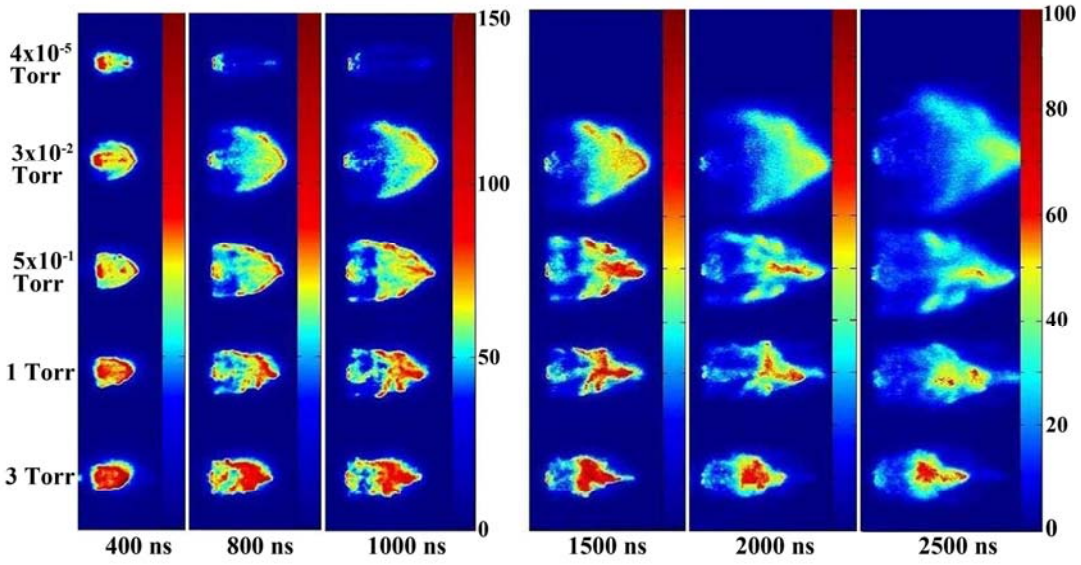

Figure 3.1 *Gated ICCD images of the integrated emission from the expanding plasma plume for different time delays with respect to the plasma initiation. The integration time was fixed as 4 ns. The ambient gas pressure was varied from 10^{-5} to 3 Torr. Colorbar shows the normalized intensity in arbitrary units.*

*Jet colormap- One of the standard false coloring method

The size, shape and intensity of the plasma plume are completely modified with increase in ambient gas pressure. At 10^{-2} Torr of Ar pressure, plasma plume becomes wider and intense in comparison to that observed in vacuum. As shown in Fig.3.1, a bright luminescence on the plume boundary (wake like) is formed between plasma and ambient gas. Lifetime of the plume is also increased and it persists upto t > 2500 ns after the plume initiation. At this pressure, interpenetration of the plasma plume and ambient gas occurs, which causes an increase in collision between the plume species and ambient gas.

Using the Westwood model {75} for the scattering of sputtered atoms by ambient gas, the mean free path of an atom with mass M_s, travelling through a gas consists of atoms of mass M_g is given by Eqn (3.1)

$$\lambda^{-1} = \sqrt{2}\pi N_s \sigma_s^2 + 1/4\pi N_g (\sigma_s + \sigma_g)^2 (1 + M_s/M_g)^{1/2} \qquad (3.1)$$

where N_s, N_g are the numbers per unit volume of sputtered and gas atoms and σ_s, σ_g are the atom diameters. In the present case, mean free path of lithium atoms have been calculated. The estimation shows that at t ~ 400 ns, plume expands in the collisional regime, where the plume dimension (~7 mm) is greater than the mean free path (~ 4.8 mm at $5\text{x}10^{-2}$ Torr) of the ejected species. The increase in collision processes is responsible for the enhancement in the observed emission intensity due to the transfer of kinetic energy from plasma to the background gas via ion–ion Coulomb scattering, ion–neutral collisions, charge exchange interactions, etc. With increase in the time delay, plume becomes more collisional and at t > 2500 ns, plume species diffuses into the background gas. It is worthwhile to mention here that most of the emission comes from the neutral species. This information can be inferred from earlier spectroscopic study of LBO plume {35, 36} that at a distance of 4 mm from the target (corresponding to t > 300 ns), enhancement in emission intensity is more pronounced for Li I in comparison to Li II.

As the background Ar pressure is further increased to $3x10^{-1}$ Torr, the plume appears compressed (lateral direction) as compared to that at 10^{-2} Torr. It can be clearly observed that a sharp boundary is also formed around the expanding plume. At this pressure, interpenetration of the plume species and background gas is relatively weak {21}. The plume material is pushed more against the expansion resulting in the formation of a layer of compressed gas around the plume.

A closer examination of plume structure at pressure > 10^{-1} Torr, reveals that the effect of background gas is more pronounced in the lateral direction than in the direction of expansion. A narrow stream of dense emission is observed along the centerline of the plume, which propagates like free expansion in vacuum. This can be explained on the basis of earlier studies {35, 36}. The results from optical emission spectroscopy have shown that LBO plume consists of fast and slow components formed by two different mechanisms. The fast component corresponding to the leading edge of the plume is the result of direct laser ablation at the target. On the other hand, the remaining material is propelled from the substrate in the form of neutral vapor, moving with much lower translational energy. Due to higher translation energy, energetic fast component of plume penetrates into the ambient gas with little interaction and therefore has same velocity as in vacuum. The slow component of the plume (lateral part) undergoes gas hydrodynamic effect resulting in nonlinear expansion in the ambient environment.

At pressure greater than 10^{-1} Torr, the internal structure (breaking of image at edge) in the plume starts appearing. Center portion of the plasma plume is almost unperturbed whereas internal structure due to turbulence is observed at the edge of the plasma. This edge turbulence is visible right from 400 ns and $3x10^{-1}$ Torr. This effect gets more pronounced with increase in time delay and ambient pressure. For pressure ≥ 1 Torr, the ambient gas penetrates and leads to collisions inside the plume. This results in the generation of complex structures inside the plume.

As stated earlier, for pressure ~10^{-1} Torr, the interpenetration between the plume material and ambient gas is restricted and an interface is formed. This indicates that contact boundary instability begins to appear during plume expansion at this pressure. Therefore, there is a finite probability of development of hydrodynamical instabilities e.g. Rayleigh-Taylor (R-T) instability {76-78} during the expansion. An attempt has been made to investigate the possibility of R-T instability responsible for the above turbulence.

Due to R-T instability, the interface between the expanding plume and ambient gas gets perturbed. We have estimated the background gas density at 400 ns, which produces the R-T instability using the relation (3.2),

$$\rho_b = 3m_{(}4\pi R^3{}_{)} \qquad (3.2)$$

where, m is the mass of the ablated material and R is the plume dimension. As the spot size was fixed as 1 mm throughout the experiments, and laser pulse energy was fixed for the complete material removal in each single shot, in the present case, mass of the ablated material is 0.992 μg. At 400 ns, the measured plume length is 7.3 mm. Using these parameters the estimated density of the background gas comes out to be 0.609 μg/cm^3, which corresponds to a pressure of ~ 2.8x10^{-1} Torr. This is in agreement with the beginning of turbulence at 3x10^{-1} Torr. Based on the above analysis, one can say that R-T instability should be responsible for the observed structure.

In order to explain the plume expansion dynamics in a different gas environment, we studied the plume length *vs*. time (Fig.3.2). The linear dependence of the time with the plume length in vacuum suggests the free expansion of plasma plume as evident from Fig. 3.2.

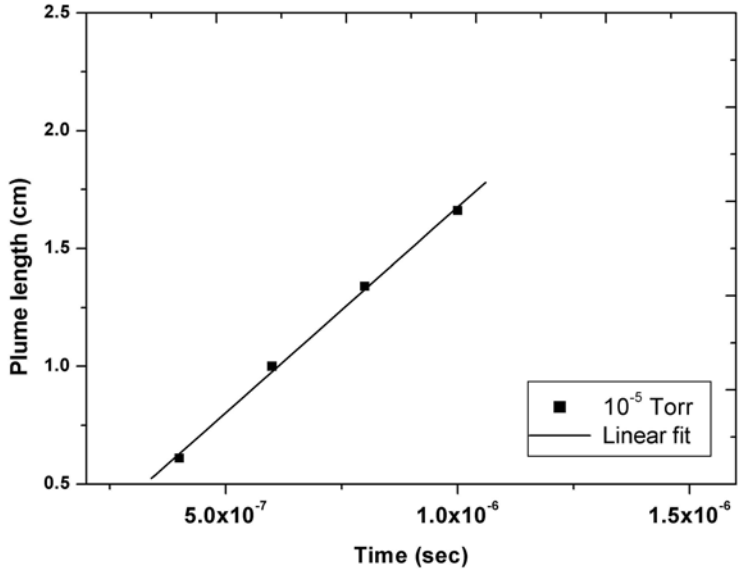

Figure 3.2 *Plume length vs. time plots for the observed images for 10^{-5} Torr. The solid line represents the best fit of the experimental data in accordance with linear fit*

It is observed that initially (<1000 ns), the plume velocity is almost independent of the ambient pressure and follows vacuum-like expansion. After that, it experiences resistive force from the background gas. At lower ambient pressure, slowing down of ejected species can be treated under the classical drag force model {52, 79}. For gas pressure of 10^{-2} Torr, the plume image data fit reasonably well with the drag force model using Eqn (3.3)

$$z = z_f[1 - \exp(-\beta t)] \tag{3.3}$$

where β is the slowing coefficient, z_f is the stopping distance of the plume $(z_f = v_0 / \beta)$ and v_0 is the initial velocity of the ejected species. The best fitting gives β = 3.8 x 10^5/sec and z_f =5.6 cm.

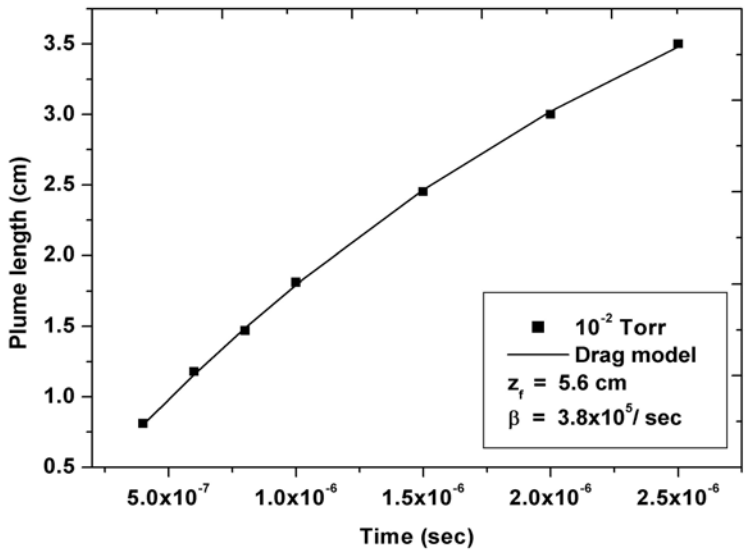

Figure 3.3 *Plume length vs. time plots for the observed images for 10^{-2} Torr Ar gas. The solid line represents the best fit of the experimental data in accordance with drag model*

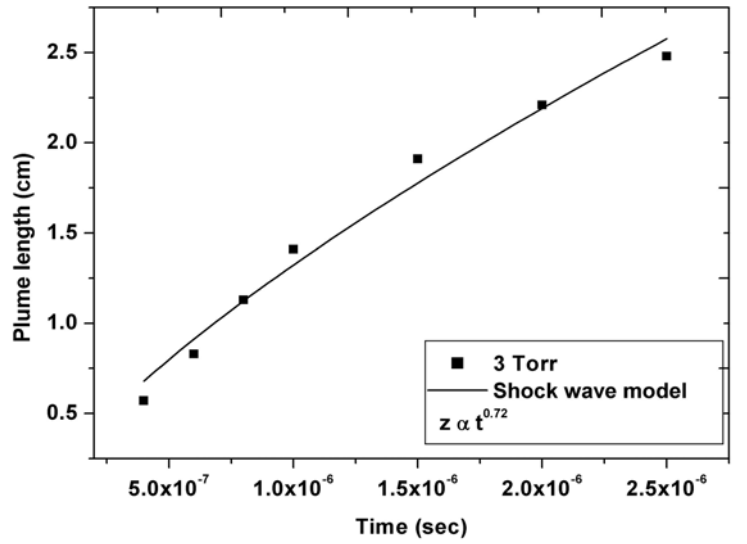

Figure 3.4 *Plume length vs. time plots for the observed images for 3 Torr Ar gas. The solid line represents the best fit of the experimental data in accordance with shockwave model*

On the other hand, at relatively high pressures (≥ 1 Torr), where the ablated mass is small compared to the mass of the background gas in motion, formation of a shock front {80} could be observed. When the shock boundary is formed between the plume and ambient gas, it effectively shields the diffusion of the ambient gas species in the plasma. In the present case with 3 Torr Ar pressure, the plume followed $R \propto t^{0.72}$ agreeing well with the shock model (Fig. 3.4).

Figure 3.5 & 3.6 shows the overall behavior of the plume shape with increasing time delay for different gas pressures. In low-pressure region (up to 10^{-2} Torr), width of the plume increases with time and there is no signature of plume confinement. With increase in the pressure and at delay times, the strong lateral confinement is clearly observed (Fig. 3.5). At 2500 ns, the width of the plume at 3 Torr reduces to half of the width observed in 10^{-2} Torr.

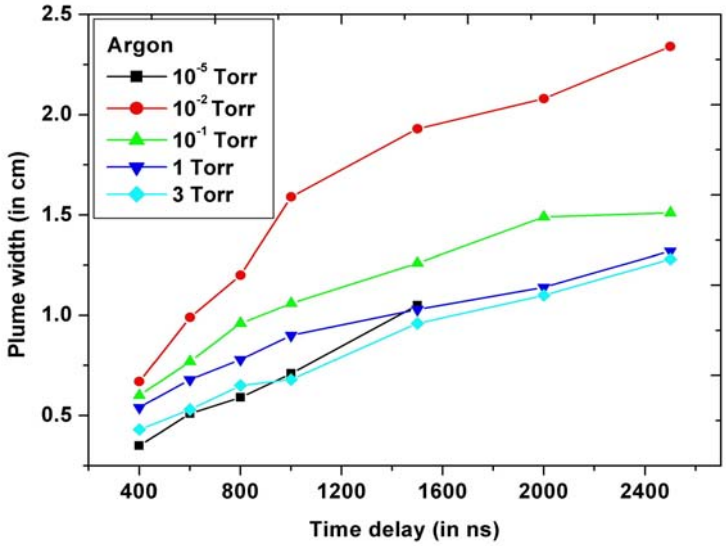

Figure 3.5 *Variation of plume width with the time delay for different gas pressure.*

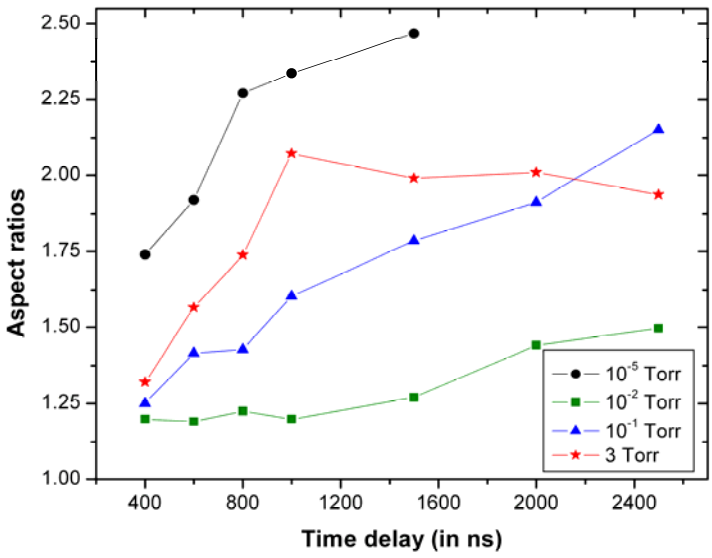

Figure 3.6: *Aspect ratios (width/length) of the plume as a function of time delay and ambient gas pressure*

For better understanding of the effect of ambient environment on the two dimensional shape of the plume, we have plotted the aspect ratio (length/width) as a function of time delay (Fig. 3.6). Up to 1000 ns, plasma plume is nearly hemispherical (width ~ length) for the 10^{-2} Torr. The aspect ratios attain saturation for time $t \geq 1000$ ns at 3 Torr indicating that the gas pressure restricts the lateral as well as forward motion of the plume species in the same proportion

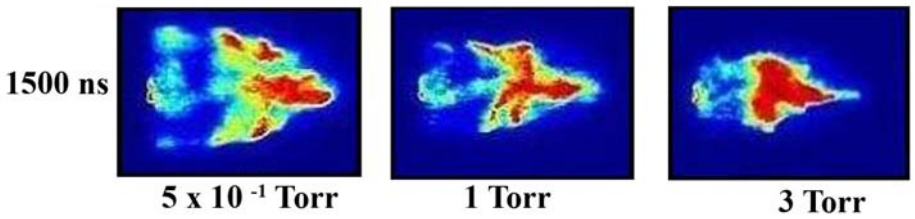

Figure 3.7 *Plume focusing observed at three different pressure levels of Ar gas. All these images are recorded at a time delay of 1500 ns after the plasma formation.*

One of the most important observations of the present experiment is the strong focusing (lateral confinement) of the LBO plume, which persists for longer times (Fig.3.7). We do not observe any divergence of plume up to a time delay of 3.5 μs and 3 Torr pressure. The strength of the focusing depends on the time delay and ambient pressure. These observations are quite different from the earlier reports for the plume confinement/focusing. Similar focusing pattern is also observed in the sequence of images recorded with an interference filter (λ_0 =670.8 nm; FWHM ~ 1nm) corresponding to the neutral lithium line in front of ICCD camera. This also indicates that plume focusing is a gas hydrodynamic phenomenon.

Lichtenwalner et al. {81 }have reported focusing/narrowing of the ablated flux distribution (from a $\cos^{40}\theta$ to $\cos^{260}\theta$) from a PZT target as O_2 pressure increased from 10 to 300 mTorr and further increase in the pressure (~ 900 mTorr) results in plume broadening. At focused position, the size of the ablated plume is ~ ½ in comparison to its maximum size in the lateral direction. The plume focusing is observed over a short spatial distance, which diverges out for longer distance. These plume narrowing or broadening regimes are both explained in terms of gas scattering effects. The most realistic approach to explain the focusing of LPP has been made by Bulgakova et al {56}. They modeled the lateral confinement of the plume using simple gas-dynamic considerations based on the analogy between an ablated plume and a supersonic under-expanded gaseous jet expanding into the background gas. This model provides a basis for the focusing or narrowing of the plume, observed at fairly high laser fluence and ambient pressures and predicts focusing of plume over a short spatial region and thereafter diverging out. On the basis of the above discussion, we conclude that strong LBO plume focusing and its existence at farther spatial positions remain unexplained by earlier proposed models.

3.5. Behavior of LBO plume in helium and argon ambient gases: Comparative study

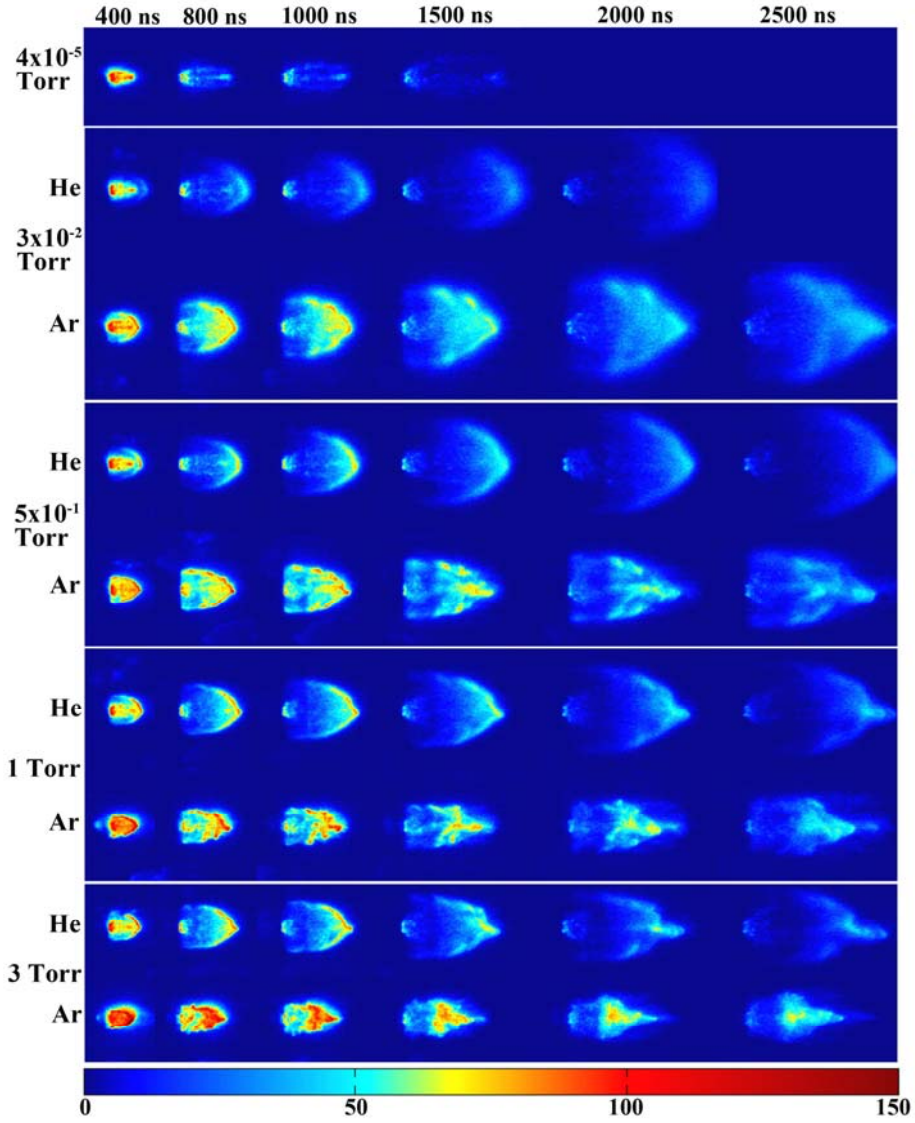

Figure 3.8 *The sequence of images of expanding plasma plume in He and Ar environment at different time delays. The integration time of ICCD was fixed as 4 ns. The ambient gas pressure was varied from 10^{-5} to 3 Torr. Colorbar shows the normalized intensity in arbitrary units.*

This part of the chapter discusses the effect of different ambient gases on LBO plume dynamics.

In order to evaluate the effect of the nature of ambient gas as well as their pressure on the shape and structural dynamics of expanding LBO plume from LiF-C target, we have conducted experiments using helium gas and comparison has been made with the imaging studies of LiF-C plume in Ar gas. LBO plume was imaged by ICCD camera in He and Ar environments under identical experimental conditions. The sequences of images at different time delays, from 400 ns to 2500 ns and at different gas pressures of He and Ar (10^{-5} to 3 Torr) are shown in Fig.3.8. With increasing ambient pressure, the shape, size and emission intensity are highly dependent on the nature of the ambient gas.

Careful examination of plume images at intermediate pressure regime of He (10^{-2} Torr) indicates that the major portion of the shape and size of the plume is nearly identical to that observed in vacuum (up to 1500 ns) except the plume front. A luminous wake-like structure, wider than the plume size in vacuum, is formed at the plume front in the presence of He gas. These images are significantly different as compared to the observed images in 10^{-2} Torr of Ar environment. The emission intensity and lateral expansion of the plume is more prominent in Ar environment than in the He environment. For a fixed time delay, plume generated in He ambient propagates longer distance than in Ar gas (Fig.3.8). In 10^{-2} Torr of He, front end of the plume remains unchanged up to a time period of 2 μs after the plasma formation. On the other hand, there is a strong lateral focusing, which starts after ~1 μs in 10^{-2} Torr Ar environment. The above observations indicate that the nature of the ambient gas, like atomic mass, ionisation energy and thermal conductivity greatly influence the expansion dynamics of LBO plume.

In the first part of this chapter we described the behavior of LiF-C plume in Ar ambient gas at 10^{-2} Torr and time delay $t > 400$ ns, the plume expands in the collisional regime where the plume dimension is greater than the mean free path of

the ejected species {34, 75}. In this regime, interpenetration of the plasma plume into the ambient gas occurs, which causes an increase in collision between the plume species and ambient gas atoms {78}. The increase in collision processes is responsible for the enhancement of observed emission intensity. With increasing time delay, plume becomes more collisional and at t > 2500 ns, plume species diffuse into the background gas. Due to the smaller mass of He, higher diffusion into the plume is expected in comparison to Ar. On the contrary, there is no sign of any significant enhancement in emission intensity in He especially inside the plume in this pressure regime. It is worth to mention here that carbon atoms (major constituents in the plume) change their direction by ~15^0 and ~78^0 in collision with He and Ar atom respectively {75, 79}. Therefore in the collisional regime, divergence of plume species increases with the mass of the background atoms, which is in agreement with observed plume width (larger in Ar environment as compared to He up to the 1500 ns and at 10^{-2} Torr pressure). However, at 2000 ns the size of plume in He is larger than the observed size in Ar. This is because in this regime, the confining effect (discussed later) might be starting to dominate over the scattering processes.

In conventional LPP experiment, Kedreja {82} et al studied the line emission intensity of carbon in He and Ar environment and found that higher emission occurred in He environment. They concluded that the probable mechanism responsible for the increase in emission intensity is the plasma confinement produced by the background gas, resulting in increase in emission. Similar conclusion has also been given by Gonjalo et al. {55} on comparing the line emission intensity in oxygen and argon environment.

In the present study, we observed the large enhancement in emission at 10^{-2} Torr of Ar pressure and could not see any signature of plume confinement as compared to observed images in vacuum. The above observation was supported by the optical emission spectroscopy data recorded in identical experimental

conditions. Figure 3.9 shows the time and space resolved emission profiles for Li I at 670.8 nm line in vacuum and at different pressures of He and Ar.

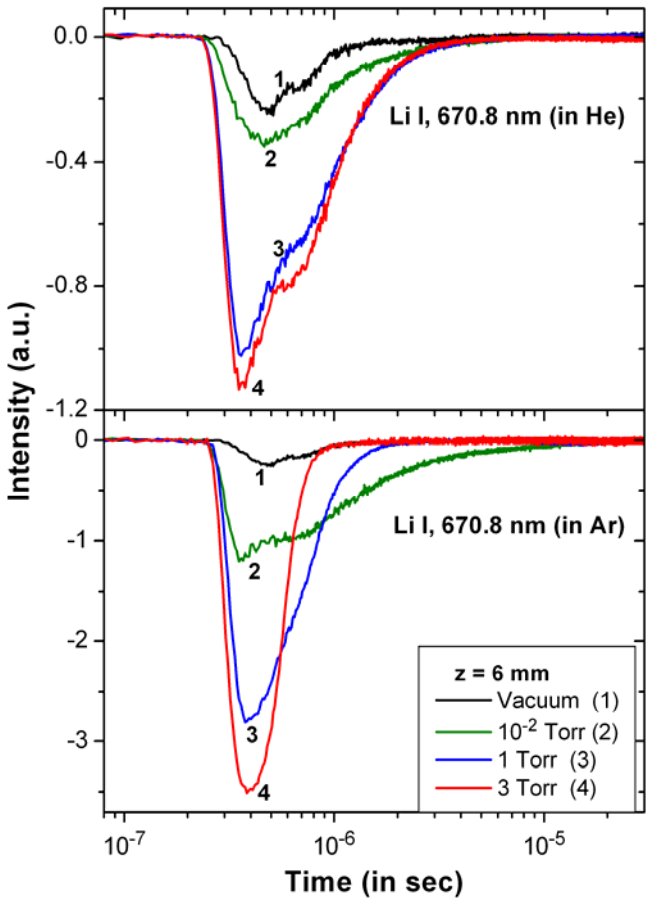

***Figure 3.9**: Temporal evolution of Li I (at 670.8 nm) emission lines in different (a) He as well as (b) Ar pressure. The profiles were recorded at a distance of 6 mm from the target.*

The temporal profiles were recorded at a distance of 6 mm away from the target. With increase in He pressure from vacuum to 1 Torr, the emission intensity increased with pressure. Almost similar intensity was observed at 1 and 3 Torr pressure. However, the emission intensity was enhanced drastically at 10^{-2} Torr of Ar pressure as compared to the observed intensity in vacuum. At this pressure, the

total intensity obtained by integrating area under the curve, was enhanced by a factor of ~2.6 and ~15 in He and Ar environments respectively. At relatively higher Ar pressures (1 & 3 Torr), there was a sharp increase in peak intensity. Interestingly, the integrated yield of emission intensity was nearly equal for 10^{-2}, 1 and 3 Torr of Ar pressure. Moreover, there were no confining effects at 10^{-2} Torr of Ar or in the entire pressure regime of He. It is worthwhile to mention that the spectroscopic measurements predict only the longitudinal confinement, and it is unable to provide information regarding the lateral confinement.

The above observations suggest that the confinement mechanism alone is not adequate to explain the enhancement in overall emission intensity and therefore some other processes are possibly responsible for the observed results.

In the present case, the increase in emission intensity of the expanding plume in background gas can be attributed mainly from (i) excitations due to collisions with background atoms and (ii) electron impact excitation/recombination. Between these two cases, electron impact processes should play the dominant role in excitation, as the cross-sections of atom-atom collision are two orders of magnitude lower than the electron-atom collisions {83}. The interaction between the expanding plume front and the ambient gas can cause the ionisation of ambient gas, which contributes to the increase in electron density. The transfer of kinetic energy from the plume front to the background gas via ion–ion Coulomb scattering, ion–neutral collisions, charge exchange interactions, etc is clearly observed at low-pressure regime of He. Since the ionisation energy of He is greater than that of Ar, more enhancement in electron density is expected in Ar environment. This is supported by the results obtained by comparing the emission intensity in He and Ar environments. In LBO, as neutral atoms are the major constituents of the plume especially at $t > 400$ ns, corresponding to plume length > 7 mm {66}, enhancement due to electron-ion recombination is less likely in this case. Thus, we conclude that an increase in electron density and hence increased electron impact excitation

should be responsible for the enhancement of emission in the presence of background gas.

Another factor, which accounts for the large difference in the emission intensity in He and Ar environments is the cascade growth of the electron number density and absorption coefficient of the plasma in ambient environment {83}. The condition for the cascade growth is expressed as Eqn (3.4)

$$\frac{d\varepsilon}{dt} = \frac{4\pi^2 e^2 I \nu_{eff}}{m_e c \omega^2} - \frac{2 m_e \nu_{eff} E}{M} > 0 \qquad (3.4)$$

where ε is the electron energy; e and m are the charge and mass of the electron; M, the mass of the background gas; E, ionisation energy of the gas; ν_{eff}, the effective frequency of electron-neutral collision; I, the radiation intensity; and ω, the frequency of the radiation. On comparing the atomic data of He and Ar (see, Table 3.1), the condition for cascade growth is more favourable in Ar environment than He. This indicates that electron temperature and density of the plasma plume should be higher in Ar ambient as compared to He {86, 87}. This will result in increase in electron impact excitation, which is largely dependent on electron temperature and density. Of course, this is reflected in the present results, where the emission intensity in Ar is higher as compared to He environment.

	He	Ar
Atomic/Molecular weight	4	40
Ionization energy (eV)	24.6	15.8
Specific heat ratio (γ)	1.67	1.67
Density (at 760 Torr)(g/l)	0.1785	1.784
Thermal conductivity (10^{-1} cal^{-1} deg^{-2} cm^{-1})	360.36	42.57

Table 3.1 *Atomic properties of helium and argon*

Further, the rate of change of electron temperature in the plasma is the sum of three terms viz., elastic collision, electron heating due to collisional de-excitation of metastable ions and recombination of ions. The rate of loss of electron energy at short times is mainly dominated by the elastic collision term $Q_{\Delta t}$, which is inversely proportional to mass of background gas and hence lighter gases are efficient for rapid cooling. Helium, being the lighter gas compared to Ar, gives rise to rapid cooling. Also, due to the higher thermal conductivity of He, plume generated in He cooled very fast as compared to that of Ar. The decrease of electron temperature directly influences the collisional process inside the plume resulting in the reduction of emission intensity in He ambient.

As the background pressure is further increased to $3x10^{-1}$ Torr, the plume appears compressed along the lateral direction in Ar ambient as compared to the observed plume size at 10^{-2} Torr whereas in the case of He, we do not see any lateral confinement in the plume, though the width of the plume further increases at $3x10^{-1}$ Torr pressure. In He ambient, the lateral confinement starts at a later stage of the plume expansion at 1 Torr pressure. On comparing the plume expansion at fixed time delay and pressure > $3x10^{-1}$ Torr, it is observed that the longitudinal and lateral dimension of the plume is higher in He environment in comparison to Ar. This is expected, because the higher mass of the ambient atoms leads to better confinement. At this pressure, interpenetration of the plume species and background gas is relatively weak {85}. The plume material pushes more against the ambient gas, which results in the formation of a layer of compressed gas around the plume as sharp boundary.

It should be noted that, the cascade growth should not be favoured at this pressure regime because of the increased energy loss due to elastic collision of the electrons with the neutral particles of the gas. However, at this pressure, greater confinement of the plasma can take place, which can enhance the frequency of elastic and inelastic collisions and thereby increases the probability of excitation.

This effect is illustrated in Fig.3.8, where the confined images in Ar ($P > 10^{-2}$ Torr) are more intense than in He.

It is important to see that the effect of background gas is more pronounced in the lateral direction than in the direction of expansion as evident from the images at 10^{-1} Torr of Ar and 3 Torr of He. A narrow stream of dense emission is observed along the centre-line of the plume, which propagates like free expansion in vacuum. This can be explained in terms of sequence of formation of LBO plume. As discussed earlier, LBO plume consists of a fast and a slow component formed by two different mechanisms. The fast component corresponding to the leading edge of the plume is the result of direct laser ablation at the target. On the other hand, the remaining material is propelled from the substrate in the form of neutral vapour, moving with much lower translational energy as compared to the energetic front. Due to the higher translation energy, energetic fast component of plume penetrates into the ambient gas with little interaction and therefore, has the same velocity as in vacuum. On the other hand, the slow component of the plume represented by the lateral part of the plume undergoes gas hydrodynamic effect resulting in nonlinear expansion in ambient environment.

As mentioned earlier, a sharp and intense contact boundary is formed at the interface between the plasma and ambient gas. It was observed that disturbances on the contact boundary (edge turbulence) appeared with increasing the pressure. This effect is clearly noticed for pressures $>10^{-1}$ Torr of Ar and >1 Torr of He. As already mentioned in part (Sec 3.4.1) of this chapter, at 2.8×10^{-1} Torr Ar pressure, the interface is perturbed due to hydrodynamical instability (e.g. R-T instability) {76-78}. The critical density required to produce the R-T instability is given by, Eq (3.2); where m, the mass of ablated material and R, the plume dimension. Considering the mass of the ablated material as 0.992 μg and the measured plume length ~7.3 mm (at 400 ns), the estimated density of the He gas corresponds to a

pressure of ~ 3 Torr required for R-T instability. This is in agreement with the observed edge turbulence at 3 Torr of He pressure.

Apart from the edge turbulence, the interaction of the expanding plume with the background atoms also affects the central part of the plume. The breaking of plume images is clearly observed for the pressure $\geq 10^{-1}$ Torr of Ar. Though there were no significant changes in the internal structure in He background, some distortion inside the plume however, appeared at 1500 ns time delay and 3 Torr pressure. This might be due to the fact that at higher background pressures (depending on mass of the gas), the ambient gas penetrates into the plume, which could lead to collisions inside the plume. As a result, generation of complex internal structural patterns can take place inside the plume.

As mentioned earlier, one of the most important observations during expansion of plume in Ar ambient is the focusing of the LBO plume in the lateral direction. Similar phenomenon is also observed in He at 3 Torr pressure and for time delay > 1000 ns. Due to limitations of our experimental setup, we could not exceed the ambient pressures greater than 3 Torr in He, in order to confirm the focusing strength and divergence of plume in He. In this case also it is found that the strength of focusing is found to be dependent on the time delay and ambient gas pressure.

From earlier spectroscopic studies of LBO plume {35, 36}, it was established that for these pressures and time delays, most of the emission came from the neutral species. Also, the emission intensity was more pronounced for Li I compared to Li II in ambient environment. In order to verify the focusing effect in the present case i.e., in He ambient, we recorded images with an interference filter corresponding to the neutral lithium line (centre wavelength 670.8 nm) fitted in front of ICCD camera. Similar to the plume images recorded with and without filter in Ar ambient gas, plume focusing found in He ambient also and confirmed that plume focusing is a gas hydrodynamic phenomenon.

Earlier we have discussed the various models available in literature in connection with plume focusing {Sec 3.4}. We have observed the focusing of the plume in both Ar and He, which exhibits dependence on the mass of ambient gas. However, we could not find any shift in the focus position of the plume towards target with increasing the ambient pressure or divergence of plume after focusing.

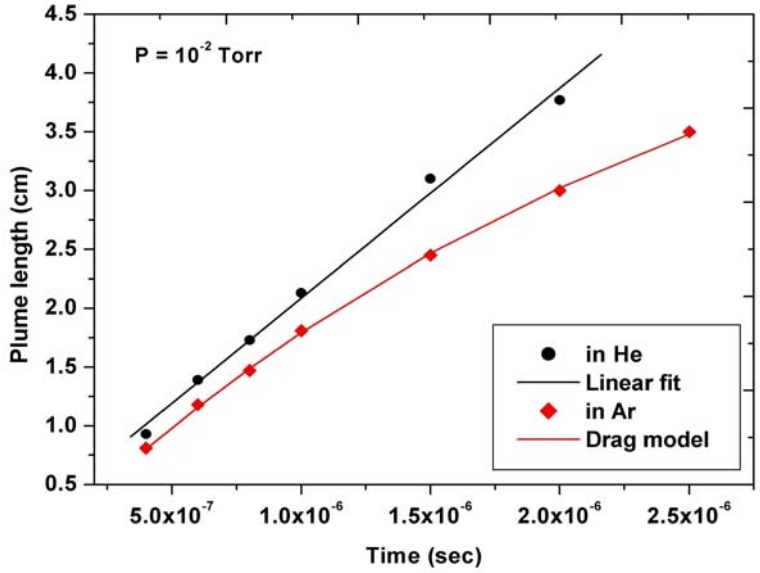

Figure 3.9 *The observed plume length as a function of time delay for three different ambient environments at pressure 10^{-2} Torr of He and Ar pressure. The solid lines represent the best fit of the experimental data with the appropriate models.*

As discussed earlier, the expansion of the plume shows the characteristic dependence on the nature of ambient gas and its pressure regime. To illustrate the plume propagation in different pressure regimes, we have estimated the plume length that corresponds to distance travelled by the plume versus time (Fig.3.9, Fig.3.10) and the observed results are interpreted with appropriate models. A linear dependence of the plume length with time in vacuum suggests free expansion of plasma plume. At 10^{-2} Torr of He pressure, the plume propagation is almost independent of the ambient pressure and follows vacuum-like expansion (Fig. 3.9).

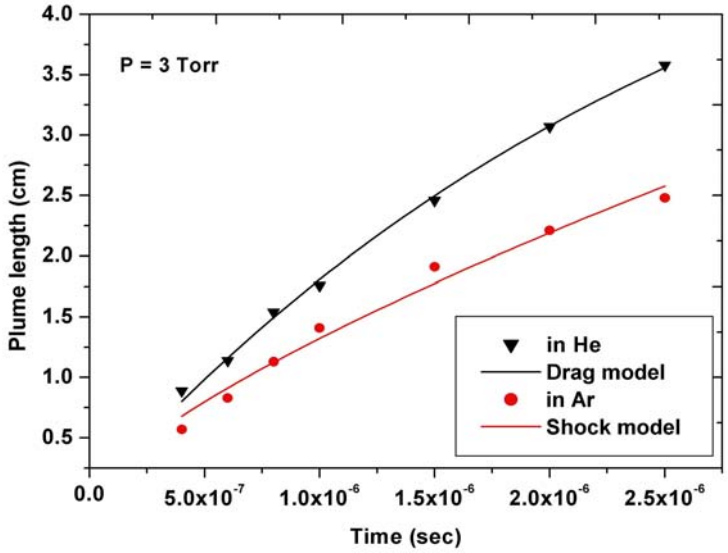

Figure 3.10 *The observed plume length as a function of time delay for different ambient environments at a pressure 3 Torr of He and Ar.*

In the case of 10^{-2} Torr of Ar, plume expands freely up to 1000 ns and thereafter it tends to slow down, as it experiences a viscous drag force exerted by the heavier Ar atoms. The slowing down of ejected species is well fitted{Eqn (3.3)} with the classical drag force model {52, 79}The best fitting parameter gives a slowing coefficient β equal to 3.8 x 10^5/sec and stopping distance equal to 5.6 cm. The plume expansion in 3 Torr of He pressure follows similar behavior as observed in 10^{-2} Torr of Ar (Fig. 3.10). It also follows the drag force model for the fit parameters of β = 3.5 x 10^5/sec and z_f = 6.05 cm. On the other hand, at relatively high pressures (3 Torr) of Ar, a shock wave {80} starts even at 400 ns time delay as the mass of the Ar gas becomes comparable to the mass of the ablated species. In this region, $z \propto t^{0.72}$ dependence of plume propagation is in close agreement with the shock model (Fig.3.10).

We have also compared the measured plume length in different gas pressures using the adiabatic expansion model {88}. According to this model,

plume expansion is stopped as the plasma pressure approaches the ambient gas pressure. The stopping distance and therefore the plume length is then given by Eqn (3.5)

$$L = A[(\gamma - 1)E]^{1/3\gamma} P^{-1/3\gamma} V_i^{(\gamma-1)/3\gamma} \qquad (3.5)$$

where γ is the specific heat ratio, E, the laser energy, P, the ambient pressure and V_i, the initial volume of the plume at the end of the laser pulse and A is the geometrical factor, which depends on the expansion angle θ for a conical plume,

$$A = (1 + 1/\tan\theta)[3\tan\theta/(\pi + 2\pi\tan\theta)] \qquad (3.6)$$

Taking γ = 1.66, E = 200 mJ, $\theta = 30^0$ and $Vi = 4.61\text{x}10^{-4}$ cm^3 (taking initial plume velocity of $7.35\text{x}10^6$ cm/sec and the laser spot and pulse duration 1 mm and 8 ns respectively), the calculated plume length using Eqn.3.5 is shown in Fig. 3.11. The measured plume length at different gas pressures of Ar after 3000 ns of plume initiation are also included in Fig.3.11.

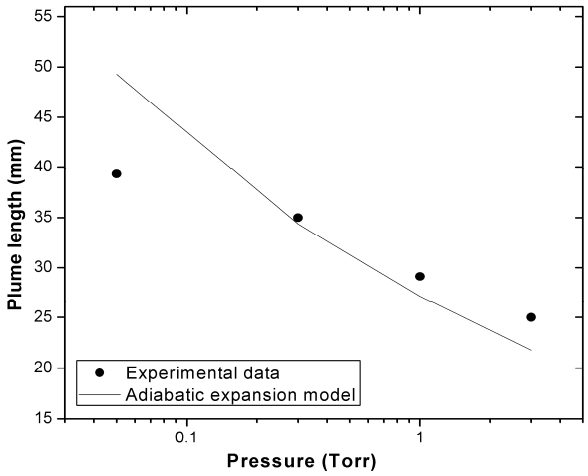

Figure 3.11 *The observed plume length at 3000 ns time delay for different Ar gas pressure. Solid line represents the estimated plume length using the adiabatic expansion model.*

It should be noted that the measured plume length at 3000 ns is not the stopping distance as the plume may further expand with increasing time delay. This conclusion is inferred from the fitting parameters of the drag force model that gives the stopping distance 56 mm for the plume expansion in 10^{-2} Torr of Ar. It can be pointed out that, the observed plume length cannot be compared directly with the calculated plume length. However, the trend of decreasing plume length with ambient gas pressure can be noticed clearly. The LBO plume does not follow the adiabatic expansion model as the plume propagates longer distances as compared to the distance predicted by the model. This may arise due to the formation of energetic plume-front in LBO, which penetrates the ambient gas without much attenuation in temperature and hence similar expansion velocity.

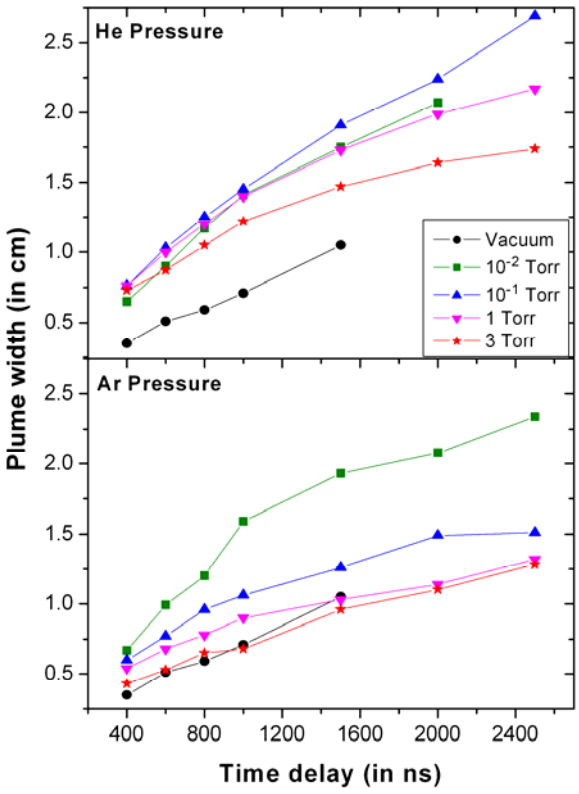

Figure 3.12 *Variation of plume width with the time delay in different pressure regime of (a) He and (b) Ar gas*

To understand the lateral confinement of plume, the variation in plume width with increasing time delay at different gas pressures of He and Ar, are presented in Fig. 3.12. It has been observed that up to the 10^{-1} Torr of He pressure, width of the plume increases with time delay. With further increase in the pressure up to 3 Torr, the plume confinement starts after a time delay of 1000 ns. In the case of He > 10^{-1} Torr, the width of the plume gradually decreases with increasing pressure for any fixed time delay after 1000 ns whereas, in Ar, the maximum width was observed at 10^{-2} Torr and it starts reducing (confining/focusing) with further increase in pressure. The comparison of the plume width in He and Ar reveals that plume width reduces more in Ar than in He. At 2500 ns, the width of the plume at 3 Torr reduces to half of the width observed at 10^{-2} Torr of Ar pressure.

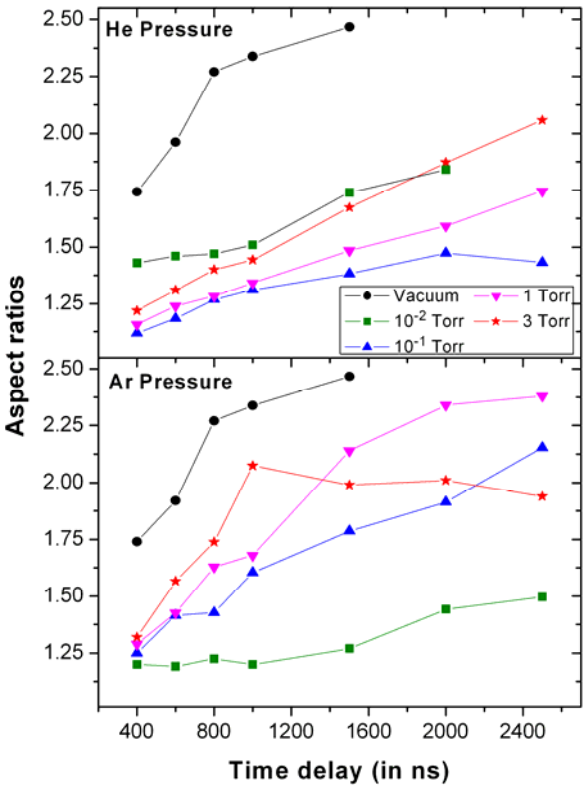

Figure 3.13 *Aspect ratios (width/length) of the plume as a function of time delay in different gas pressure of (a) He and (b) Ar.*

To determine the effect of the ambient environment on the two-dimensional shape of the plume, the aspect ratio (length/width) as a function of time delay is plotted for both the gases (Fig.3.13). For both He and Ar ambient, it has been found that the aspect ratio increases with pressure for fixed time delay, because there is reduction of width with pressure without any appreciable change in length of the plume. However, some differences between the He and Ar ambient are observed especially, at 10^{-2} Torr and 3 Torr pressure. In Ar, plasma plume is nearly hemispherical (width ~ length) up to the 1000 ns for the gas pressure 10^{-2} Torr. The aspect ratios attain close to the saturation for $t \geq 1000$ ns at 3 Torr Ar pressure; it indicates that this pressure restricts the lateral as well as forward motion of the plume species in the same proportion. Those effects are not observed in He environment.

3.6. Conclusions

This chapter details the studies on the expansion dynamics of LBO plasma plume, under the influence of He and Ar ambient pressures using fast imaging technique. It was observed that plume expands adiabatically in vacuum and has an ellipsoidal shape. It showed a three-line structure parallel to the direction of the plume. Enhancement in the plume luminosity and change in size and shape occurred on introduction of ambient gases and these changes were highly dependent on the nature and composition of the background gas used. Velocity of the plume front was found to be higher in He ambient whereas intensity enhancement was greater in Ar environment.

The plume showed maximum size at 10^{-2} and 10^{-1} Torr of Ar and He pressure respectively. With further increase in the background pressure, a high luminescence boundary was formed between ambient gas and the plume. Also the plume gets compressed and focused in the lateral direction. This effect was more pronounced in Ar environment as compared to He. It was found that R-T instability was responsible for the turbulence on the edge region of the plasma plume. At

higher ambient gas pressures (depending on the nature of the gas), structures were developed inside the plasma plume due to hydrodynamic instability. From the length-time plots, it was found that at earlier stages (< 1000 ns) the expansion was almost linear irrespective of the background gas pressure. Later on, velocity plot deviated from linearity due to interaction between the plume and ambient gas. In vacuum, plasma plume followed the linear expansion whereas in presence of ambient gas it followed drag force and shock wave model depending on the nature and pressure of the gas.

The above results could also be useful for improving the hydrodynamic models presently available for simulating the plasma plume expansion dynamics in different gas atmospheres.

3.7. References

1. "*Pulsed Laser Deposition of Thin Films",* D. B. Chrisey and G.K. Hubler., (Wiley, New York, 1994).

2. J. Brandenburg, V. Neu, H. Wendrock, B. Holzapfel, H.-U. Krebs and S. F¨ahler., *"Pulsed laser deposition of metals: consequences of the energy distribution within the laser spot on film growth*", Appl. Phys. A **79**, 1005 (2004).

3. V. Narayanan and R.K. Thareja., *"Emission spectroscopy of laser-ablated Si plasma related to nanoparticle formation"*, Appl. Surf. Sci. **222**, 382 (2004).

4. S. Amoruso, R. Bruzzese, N. Spinelli, R. Velotta, M. Vitiello, X. Wang, G. Ausanio, V. Iannotti and L. Lanotte., "*Generation of silicon nanoparticles via femtosecond laser ablation in vacuum"*, Appl. Phys. Lett. **84**, 4502 (2004).

5. A. G. Gnedovets, A. V. Gusarov and I. Smurov., "*A model for nanoparticles synthesis by pulsed laser evaporation*", J. Phys. D: Appl. Phys. **32,** 2162 (1999).

6. Hassanein A., Sizyuk V., Harilal S. S. and Sizyuk T., *"Analysis, simulation, and experimental studies of YAG and CO_2 LPP for EUVL sources"*, Proc. of SPIE **7636**, 76360A (2010).

7. "EUV Sources for Lithography", V. Bakshi., SPIE, New York, (2006).

8. J. White, G. O'Sullivan, S. Zakharov, P. Choi, V. Zakharov, H. Nishimura, S. Fujioka, and K. Nishihara., *"Tin laser-produced plasma source modeling at 13.5 nm for extreme ultraviolet lithography"*, Appl. Phys. Lett. **92**, 151501 (2008).

9. Abhilasha, P. S. R. Prasad, and R. K. Thareja., "*Laser-produced carbon plasma in an ambient gas* ", Phys. Rev. E **48**, 2929 (1993).

10. Andrey V. Gusarov, Alexey G. Gnedovets and Igor Smurov., "*Gas dynamics of laser ablation: Influence of ambient atmosphere"*, J. Appl. Phys. **88**, 4352 (2000).

11. A. K. Sharma and R. K. Thareja., "*Pulsed laser ablation of aluminum in the presence of nitrogen: Formation of aluminum nitride*", J. Appl. Phys. **88**, 7334 (2000).

12. M. Ohkoshi, T. Yoshitake, and K. Tsushima., "*Dynamics of laser ablated iron in nitrogen atmosphere*", Appl. Phys. Lett. **64**, 3340 (1994).

13. Harilal S. S, Riju C. Issac, C. V. Bindhu, V. P. N. Nampoori and C.P.G. Vallabhan., *"Time resolved analysis of C-2 emission from laser induced graphite plasma in helium atmosphere",* Jpn. J. Appl. Phys. **36**, 134 (1997).

14. *"Fundamentals of Gaseous Ionization and Plasma Electronics",* Essam Nasser., New York : Wiley Eastern (1971).

15. Zhaoyang Chen, Davide Bleiner, and Annemie Bogaerts., "*Effect of ambient pressure on laser ablation and plume expansion dynamics: A numerical simulation*", J. Appl. Phys. **99**, 063304 (2006).

16. S. S. Harilal, C. V. Bindhu, M. S. Tillack, F. Najmabadi, and A. C. Gaeris., *"Internal structure and expansion dynamics of laser ablation plumes into ambient gases"*, J. Appl. Phys. **93**, 2380 (2003).

17. A. K. Shuaibov, L. V. Mesarosh, and M. P. Chuchman., *"Features of the formation of a laser flare from aluminum in the presence of a background gas"*, J. Opt. Technol. **78**, 358 (2011).

18. S. Amoruso, B. Toftmann, and J. Schou., *"Thermalization of a UV laser ablation plume in a background gas: From a directed to a diffusion like flow"*, Phys. Rev. E **69**, 056403 (2004).

19. S Amoruso, J Schou and J. G Lunney., *"Multiple-scattering effects in laser ablation plume propagation in gases"*, Europhysics Lett. **76**, 436 (2006).

20. Yu Quan-Zhi, Z. Jie, Li Yu-Tong, Z. Jun, Yan Fei, Lu Xin, W. Zhe-Bin, Z. Jian, Yu Chang-Xuan, Jiang Xiao-Hua, Li Wen-Hong, Liu Shen-Ye and Zheng Zhi-Jian., "*Thomson scattering process in laser-produced plasmas*", Chinese Phys. Lett. **22**, 1717 (2005).

21. S.Amoruso, B.Toftmann, J.Schou, R.V elotta and X.W ang."*Diagnostics of laser ablated plasma plumes "*, Thin Solid Films **453**, 562 (2004).

22. A Misra, A. Mitra, and R. K. Thareja.,"*Diagnostics of laser ablated plasmas using fast photography*", Appl. Phys. Lett. **74**, 929 (1999).

23. R.K. Thareja, Abhilasha and R.K. Dwivedi., *"Optical emission spectroscopy of laser-produced carbon plasma at moderate and low irradiance in an ambient atmosphere*", Laser and Part. Beams **13**, 481 (1995).

24. O B Anan'in, Yu A Bykovskiĭ, Yu V Eremin, E L Stupitskiĭ, I K Novikov and S P Frolov., "*Investigation of laser plasma expansion in an ambient gas by high-speed photography"*, Sov. J. Quantum Electron. **21**, 787 (1991).

25. Ya B. Zel'dovich and Yu P. Raizer., "*Physics of shock waves and high temperature hydrodynamics phenomena"* (Academic, New York, 1966).

26. Y Tao, M S Tillack, S S Harilal, K L Sequoia, B O'Shay and F Najmabadi., "*Effect of shockwave-induced density jump on laser plasma interactions in low-pressure ambient air*", J. Phys. D: Appl. Phys. **39**, 4027 (2006).

27. Ajai Kumar, R. K. Singh, Jinto Thomas, and S. Sunil., *"Parametric study of expanding plasma plume formed by laser-blow-off of thin film using triple Langmuir probe"*, J. Appl. Phys. **106**, 043306 (2009).

28. O. Barthélemy, J. Margot, M. Chaker, M. Sabsabi, F. Vidal, T. W. Johnston, S. Laville and B. Le Drogoff., "*Influence of the laser parameters on the space and time characteristics of an aluminum laser-induced plasma*", *Spectrochim. Acta B*, **60** (7-8), 905-914 (2005).

29. B. Le Drogoff, J. Margot, F. Vidal, S. Laville, M. Chaker, M. Sabsabi, T. W. Johnston and O. Barthélemy., "*Influence of the laser pulse duration on laser-produced plasma properties*", Plasma Sources Sci. Technol. **13,** 223 (2004).

30. H. C. Ong and R. P. H. Chang., *"Effect of laser intensity on the properties of carbon plasmas and deposited films"*, Phys. Rev. B **55**, 13213 (1997).

31. Abhilasha, R. K. Dwivedi, and R. K. Thareja., *"Wavelength dependence of the photoablation of carbon at low irradiance"*, J. Appl. Phys. **75**, 8237 (1994).

32. Harilal S. S., "*Influence of spot size on propagation dynamics of laser-produced Sn plasma",* J. Appl. Phys **103**, 123306 (2007).

33. Ajai Kumar, Sony George, R. K. Singh and V. P. N. Nampoori., *"Influence of laser beam intensity profile on propagation dynamics of laser-blow- off plasma plume"*, Laser and Part. Beams, **28**, 387 (2010).

34. Sony George, Ajai Kumar, R. K. Singh and V. P. N. Nampoori.,*"Effect of ambient gas on the expansion dynamics of plasma plume formed by laser blow off of thin film"*, Appl. Phys. A., **98**, 901 (2009).

35. R. K. Singh, Ajai Kumar, B. G. Patel, and K. P. Subramanian.,"*Role of ambient gas and laser fluence in governing the dynamics of the plasma plumes produced by laser blow off of LiF-C thin film",* J. Appl. Phys. **101**, 103301 (2007).

36. R. K. Singh, Ajai Kumar, V. Prahlad and H. C. Joshi.,*"Generation of fast neutrals in a laser-blow-off of LiF-C film: A formation mechanism"*, Appl. Phys. Lett. **92**, 171502 (2008).

37. A. I. Ledyankin, C. De Michelis, R. Guirlet, W. Hecq, W. R. Hess and P. Monier-Garbet.,*"On the possibility of measuring peripheral electron density and temperature profiles in Tore Supra using a laser blow-off lithium and fluorine atomic beam"*, Phys. Lett. A **230,** 209-Z 17 (1997).

38. Michaud, D. Ross, G. G. Haddad, E. Mai, H. H. Pospieszczyk, A. St Germain, J. P., *"Measurements of ne(r) and Te(r) in TdeV boundary layer by injection of laser ablated Li and C*", Rev. Sci. Instrum. **63**, 5698 (1992).

39. S. Sasaki, Y. Uesugi1, S. Takamura, H. Sanuki, and K. Kadota., *"Temporal behavior of the electron density profile during limiter biasing in the HYBTOK-II tokamak"*, Phys. Plasmas **1**, 1089 (1994).

40. Ajai Kumar, R. K. Singh, V. Prahlad, and H. C. Joshi.,"*Comparative study of laser produced Li plasma plumes from thin film and solid target"*, J. Appl. Phys. **104**, 093302 (2008).

41. M. Ohkoshi, T. Yoshitake, and K. Tsushima., "*Dynamics of laser ablated iron in nitrogen atmosphere*", Appl. Phys. Lett. **64**, 3340 (1994).

42. Z. Chen, D. Bleiner, and A. Bogaerts., "*Effect of ambient pressure on laser ablation and plume expansion dynamics: A numerical simulation*", J. Appl. Phys. **99**, 063304 (2006).

43. Z. Chen and A. Bogaerts., "*Laser ablation of Cu and plume expansion into 1 atm ambient gas*", J. Appl. Phys. **97**, 063305 (2005).

44. K. F. Al-Shboul, S. S. Harilal, A. Hassanein, and M. Polek., "*Dynamics of C_2 formation in laser-produced carbon plasma in helium environment* ", J. Appl. Phys. **109**, 053302 (2011).

45. Noor Batcha, Robert R. Lucchese, and Yehuda Zeiri., "*Monte Carlo simulations of gas phase collisions in rapid desorption of molecules from surfaces*", J. Chem. Phys. **86**, 5816 (1987).

46. Dieter Sibold, Herbert M. Urbassek., *"Effect of gas phase collisions in pulsed laser desorption: A three dimensional Monte Carlo simulation study*", J. Appl. Phys. **73**, 8544 (1993).

47. J. N. Leboeuf, K. R. Chen, J. M. Donato, D. B. Geohegan, C. L. Liu, A. A. Puretzky, and R. F. Wood.,*"Modeling of plume dynamics in laser ablation processes for thin film deposition of materials"*, Phys. Plasmas **3**, 2203 (1996).

48. A.V. Bulgakov and N.M. Bulgakova., *"Dynamics of laser-induced plume expansion into an ambient gas during film deposition"*. J. Phys. D: Appl. Phys., **28**, 8, pp 1710-1718 (1995).

49. P. W. Rambo and J. Denavit., *"Time-implicit fluid simulation of collisional plasmas"*, J. Comput. Phys. **98**, 317 (1992).

50. Zel'dovich, Ya. R. and Raizer, Yu. P., *"Physics of Shock Waves and High-Temperature Hydrodynamic Phenomena"*, Dover, Cambridge, Massachusetts (2001).

51. "*Physics of Shock Waves in Gases and Plasmas",* M. A . Liberman and A. L. Velikovich, (Springer, Berlin, 1986).

52. D.A. Freiwald, R.A. Axford.,*"Approximate spherical blast theory including source mass"*, J. Appl. Phys. **46**, 1171 (1975).

53. S. I. Anisimov, D. Bäuerle, B. S. Luk'yanchuk.,*"Gas dynamics and film profiles in pulsed-laser deposition of materials"*, Phys. Rev. B **48** 12076 (1993).

54. Arnold, N., Gruber, J. and Heitz, J., *"Spherical expansion of the vapor plume into ambient gas: an analytical model"*, Appl. Phys. A **69**: S87 (1999).

55. J. Gonzalo, F. Vega, and C. N. Afonso., *"Plasma expansion dynamics in reactive and inert atmospheres during laser ablation of Bi(2)Sr(2)Ca(2)O(7-y)",* J. Appl. Phys. **77**, 6588 (1995).

56. A. V. Bulgakov and N. M. Bulgakova.,*"Gas-dynamic effects of the interaction between a pulsed laser-ablation plume and the ambient gas: analogy with an underexpanded jet"*, J. Phys. D: Appl. Phys. **31**, 693 (1998).

57. R. F. Wood, K. R. Chen, J. N. Leboeuf, A. A. Puretzky and D. B. Geohegan., *"Dynamics of plume propagation and splitting during pulsed-laser ablation",* Phys. Rev. Lett. **79**, 1571 (1997).

58. Tatiana E. Itina, Jörg Hermann, Philippe Delaporte, and Marc Sentis., *"Laser-generated plasma plume expansion: Combined continuous-microscopic modelling"*, Phys. Rev. E **66**, 066406 (2002).

59. Riju C. Issac, K. Vasudevan Pillai, S. S. Harilal, Geetha K. Varier, C. V. Bindhu, Pramod Gopinath, P. Radhakrishnan, V. P. N. Nampoori and C. P. G. Vallabhan., *"Dynamics of laser produced silver plasma under film deposition conditions studied using optical emission spectroscopy"*, Appl. Surf. Sci. **125**, 2, 227 (1998).

60. Salvatore Amoruso, Riccardo Bruzzese, Nicola Spinelli, Raffaele Velotta, Marco Vitiello, and Xuan Wang.,*"Dynamics of laser-ablated MgB_2 plasma expanding in argon probed by optical emission spectroscopy"*, Phys. Rev. B **67**, 224503 (2003).

61. David B. Geohegan.,*"Fast intensified CCD photography of $YBa_2Cu_3O_{7-x}$ laser ablation in vacuum and ambient oxygen"*, Appl. Phys. Lett. **60**, 2732 (1992).

62. Misra. A and Thareja. R. K., "*Investigation of laser ablated plumes using fast photography*", IEEE Transactions on Plasma Sci. **27**, 1553 (1999).

63. A. Misra, A. Mitra, and R. K. Thareja., "*Diagnostics of laser ablated plasmas using fast photography*", Appl. Phys. Lett. **74**, 929 (1999).

64. S. Abdelli-Messaci, T. Kerdja, S. Lafane and S. Malek.,"*Fast imaging of laser-induced plasma emission from a ZnO Target"*, Spectrochimica Acta Part B **64** , 968 (2009).

65. R. K. Singh and J. Narayan., *"Pulsed-laser evaporation technique for deposition of thin films: Physics and theoretical model"*, Phys. Rev. B **41**, 8843 (1990).

66. Amoruso, S., *"Modeling of UV pulsed-laser ablation of metallic targets",* Appl. Phys. A **69**, 323 (1999).

67. A. Bailinia & P. M. Ossi.,*"Modelling the propagation of an ablation plume in a gas",* Radiation Effects and Defects in Solids, 163, 4-6, (2008) Special Issue: 3rd Workshop 'Plasma Production By Laser Ablation-2007' (PPLA) (2007).

68. ZhiHua Li, DuanMing Zhang, and Li Guan., *"Discussion on plasma shock waves generated by high-power pulsed laser"*, MRS Proceedings, **793**: S8.21, (2003).

69. P. Yeates and E. T. Kennedy., *"Spectroscopic diagnostics of plume rebound and shockwave dynamics of confined aluminum laser plasma plumes"*, Phys. Plasmas **18**, 063106 (2011).

70. Q.L. Ma, V. Motto-Ros, W.Q. Lei, M. Boueri, X.S. Bai, L.J. Zheng, H.P. Zeng and J. Yu., *"Temporal and spatial dynamics of laser-induced aluminum plasma in argon background at atmospheric pressure: Interplay with the ambient gas",* Spectrochimica Acta Part B:, **65**, 11, pp-896-907 (2010).

71. Jeong Dae Suh, Gun Yong Sung and Kwang Yong Kang., *"Effects of oxygen pressure and target-substrate distance on the density of particulates on pulsed laser deposited YBa2Cu3O$_{7-x}$ thin film surfaces"*, J. Materials Sci. Lett. **14**, 832 (1995).

72. P. E. Dyer and J. Sidhu., *"Spectroscopic and fast photographic studies of excimer laser polymer ablation"*, J. Appl. Phys. **64**, 4657 (1988).

73. S. S. Harilal, C. V. Bindhu, M. S. Tillack, F. Najmabadi, and A. C. Gaeris., *"Plume splitting and sharpening in laser-produced aluminium plasma*", J. Phys. D **35**, 2935 (2002).

74. Ajai Kumar, Vishnu Chaudhari, Kiran Patel, Sony George, S. Sunil, R. K. Singh and Ranjeet Singh., "*An experimental setup to study the expansion dynamics of laser blow-off plasma plume in variable transverse magnetic field"*, Rev. Sci. Instrum. **80**, 033503 (2009).

75. W. D. Westwood., *"Calculation of deposition rates in diode sputtering systems"*, J. Vac. Sci. Technol. **15**, 1 (1978).

76. L. Rayleigh, Proc. London Math. Soc. **14**, 170 (1883).

77. R. Betti, V. N. Goncharov, R.L. McCrory and C. P. Verdon., "*Growth rates of the ablative Rayleigh–Taylor instability in inertial confinement fusion*", Phys. Plasmas **5**, 1446 (1998).

78. R. P. Drake and P. A. Keiter., *"Rayleigh–Taylor growth at decelerating interfaces",* Phys. Plasmas **9**, 382 (2002).

79. "*Pulsed Laser Deposition of Thin Films"*, D. B. Geohegan, edited by D. B. Chrisey and G. K. Hubler (Wiley, New York, 1994).

80. Kumuduni, Wanniarachchi K. A, Nakayama, Yasushi, Nakata, Yoshiki, Okada, Tatsuo, Maeda, Mitsuo.,*"Transport of YO molecules produced by ArF laser ablation of $YBa_2Cu_3O_7$ - delta in ambient oxygen gas"*, J. Appl. Phys. **74**, 7510 (1993).

81. D. J. Lichtenwalner, O. Auciello, R. Dat and A.I. Kingon.,*"Investigation of the ablated flux characteristics during pulsed laser ablation deposition of multicomponent oxides"*, J. Appl. Phys. **74**, 7497 (1993).

82. T. Kerdja, S. Abdelli, D. Ghobrini and S. Malek., "*Dynamics of laser-produced carbon plasma in an inert atmosphere"*, J. Appl. Phys. **80**, 5365 (1996).

83. C. Timmer, S. K. Srivastava, T.E. Hall and A. Fucaloro., *"Enhanced line emission from laser-produced plasmas",* J. Appl. Phys.**70**, 1888 (1991).

84. G. M. Weyl, in *"Laser-Induced Plasmas and Applications"*, edited by L. J. Radziemski and D. A. Cremers (Dekker, New York, 1989), Chap. 1

85. Y. Iida.,*"Effects of atmosphere on laser vaporization and excitation processes of solid samples"*, Spectrochim. Acta B **45**, 1353 (1990).

86. S. S. Harilal, C. V. Bindhu, V. P. N. Nampoori and C. P. G. Vallabhan., *"Influence of ambient gas on the temperature and density of laser produced carbon plasma"*, Appl. Phys. Lett. **72**, 167 (1998).

87. J.A. Aguilera and C. Aragon., *"A comparison of the temperatures and electron densities of laser-produced plasmas obtained in air, argon, and helium at atmospheric pressure"*, Appl. Phys. A **69**, S475–S478 (1999).

88. P. E. Dyer, A. Issa and P. H. Key.,*"Dynamics of excimer laser ablation of superconductors in an oxygen environment"*, Appl. Phys. Lett. **57**, 186 (1990).

Chapter 4

Effect of Laser Intensity Profile on the Plasma Formation Mechanism

Abstract

This chapter discusses the influence of energy density profile of ablating laser on the dynamics of laser-blow-off plume by using fast imaging technique. Visualization of the expanding plume in vacuum reveals that geometrical shape and divergence of the plume is highly dependent on the laser intensity profile. Present result demonstrated that the Gaussian profile laser produces a well-collimated, low divergence plasma plume as compared to plume formed by laser having top hat intensity profile. Another interesting feature observed is the formation of laser plasma induced shock wave, when the plasma expands in an ambient medium. Results clearly demonstrate that, highly directional plume produces the strong shock wave in comparison to shock produced by the diverging plume. It has also been found that shock parameters are strongly dependent on the pressure and nature of the ambient gas.

4.1. Introduction

Dependence of the ambient medium and its pressure on the laser blow off (LBO) plume has already been discussed in the previous chapter {Chapter 3}. In LBO scheme, the size, shape and divergence of the expanding plume are highly dependent on the thickness of the film, laser spot size and laser fluence. Numerous experimental and theoretical studies have been made to address the effect of film thickness and laser fluence on the LBO generated beam {1-6}. However, little attention has been paid towards investigating the role of intensity profile of laser beam on the geometrical aspect of the LBO plume {7} and its dynamics, which are highly relevant in thin film deposition, neutral beam injection in plasma environment and other LBO induced beam applications.

Several attempts have been made to optimize the expanding laser produced plasma plume (LPP) by varying experimental factors like, ambient gas, focal spot size, laser pulse width, irradiance and wavelength of ablating laser {8-17} General observation is that the lateral velocity of the plume species increases with an increase in the laser fluence. Besides this, the plume expansion becomes cylindrical in shape with increase in the laser spot size.

In view of the above, experiments were conducted to understand the expansion dynamics of the LBO plume formed by two different laser systems having different intensity profiles *viz* Gaussian and top-hat. In this work, emphasis was given to the comparison of the shape, size, directionality and angular divergence of the LBO plume observed with two different laser profiles by fast time resolved imaging spectroscopy. Study has also been extended to investigate the laser profile dependency of plume formed in an ambient environment and this will be presented in the second part of this chapter.

4.2. Experimental details

A detailed description of experimental setup has been described in chapter 2 {18}. Only the additional parts are briefly summarized here. The experiment was

carried out in a cylindrical stainless steel chamber, evacuated to a base pressure less than $2x10^{-5}$ Torr. The target was composed of uniform layers of 0.05 μm LiF and 0.5 μm thick carbon film, deposited on a 1.2 mm thick quartz substrate.

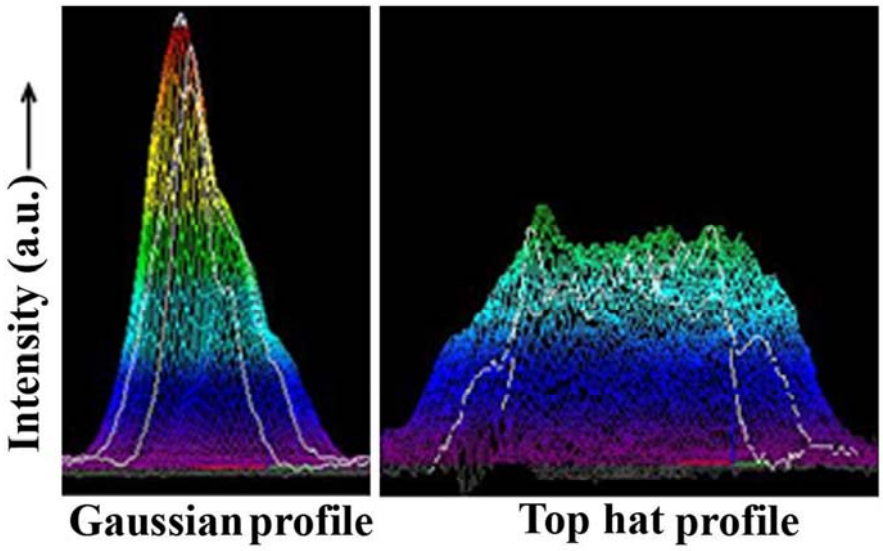

Figure 4.1 *Recorded intensity profiles of laser; Gaussian beam profile, "GP" and top hat profile, "THP".*

Nd: YAG (λ = 1064 nm) lasers having two different intensity profiles, top-hat laser beam profile (referred as 'THP') of 8 ns pulse width and Gaussian beam profile (referred as 'GP ') of 5 ns, were used in this study. Intensity profiles for both lasers are shown in Fig. 4.1. The spot size of the laser beam was ~ 1 mm diameter at the target. By adjusting the operating parameters of the laser, fluence ~ 20 J/cm^2 was set at the target surface for both lasers. An ICCD camera (*4 Picos Stanford Computer Optics, Inc*.) having variable gain and gating on time, was used to record the time resolved images of the plume luminescence in the spectral range of 350-750 nm. In the present experiment, gate opening time is set at 4 ns. Temporal evolution of the LBO plume has been obtained by varying the time delay from 100 to 4000 ns, between the laser pulse and the opening time of ICCD gate. Five images

were recorded under similar experimental conditions in order to confirm the reproducibility.

In order to measure the distributions of ablated ions across the expansion axis, an electrical ion probe mounted in front of the plume propagation direction {18}. The ion probe was constructed with a tungsten wire of 0.4 mm diameter. The length of the probe, which was exposed to the plasma and separation between the probe and target plate were set as 3 mm and 45 mm, respectively. In order to get the better spatial resolution in the transverse direction, orientation of the probe was aligned along the axis of plume expansion. The probe assembly was mounted on a linear motion feed-through, which enables the positioning of probe in the plume expansion axis. A negative bias voltage of 22 V was applied to the probe to measure the ion current in the saturation limit. A 2 mF capacitor was used to decouple the measuring circuit from the applied bias voltage. The ion signal across the 50 Ω resistance was recorded on a fast digital oscilloscope.

4.3. Plume formation in vacuum

4.3.1. Fast imaging

Fast imaging of the electronically excited plume species, driven by collisional processes between electrons, ions, and neutrals generated by laser-film interaction provides the two dimensional snap shot of the expanding LBO plume. Expansion dynamics of the species as well as geometrical aspect of the expanding plume such as local structure, directionality and divergence, can be studied by observing these emissions as a function of time. Typical ICCD images of expanding plume formed by THP and GP lasers in vacuum and at various time delays are shown in Fig. 4.2. The visual examination of the plume images reveals following interesting effects.

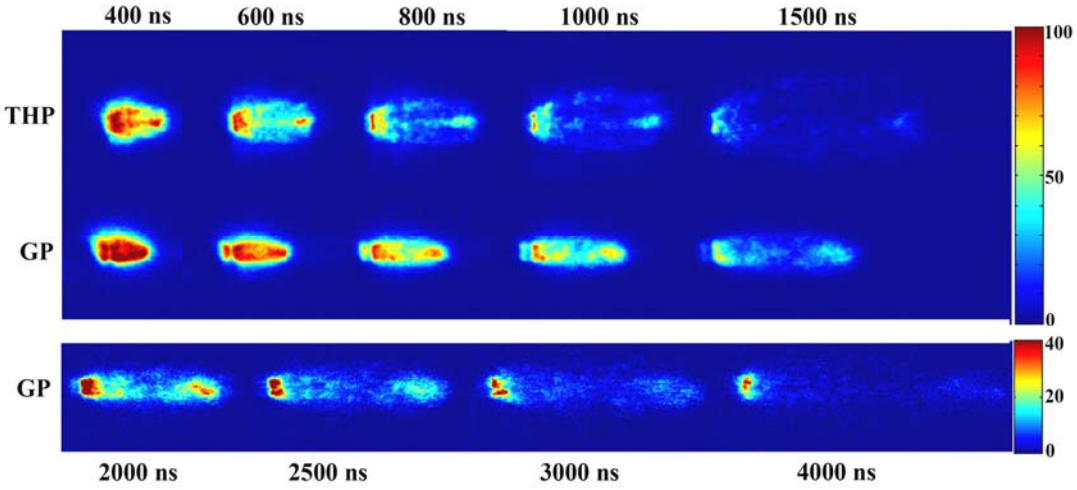

Figure 4.2 *The sequence of images of expanding LBO plume in vacuum formed by THP and GP laser at different time delays. The integration time of ICCD was fixed as 4 ns. Colorbar shows the normalized intensity in arbitrary units.*

For both laser beam profiles, plume expands linearly and their intensities gradually diminish with time. The plume expansion in vacuum under the influence of pressure gradient inside ablated plume is treated as adiabatic expansion {19}, where the thermal energy of plume species is rapidly converted into the kinetic energy. This leads to decrease in electron temperature and density with time and hence decrease in electron impact process {6}. Therefore, considerable reduction in the emission intensity of the plume with increase in the time delay can be anticipated. Moreover, linear dependence of the plume front position with time delay confirms free expansion of the plume (Fig.4.3). Average translational velocities of 1.8×10^6 and 1.1×10^6 cm/sec for the plume by THP and GP lasers respectively are obtained from the slopes of the curve. However, it is observed that the lifetime of the emissive plume, directionality /divergence and shape are highly dependent on the intensity profile of the laser beam.

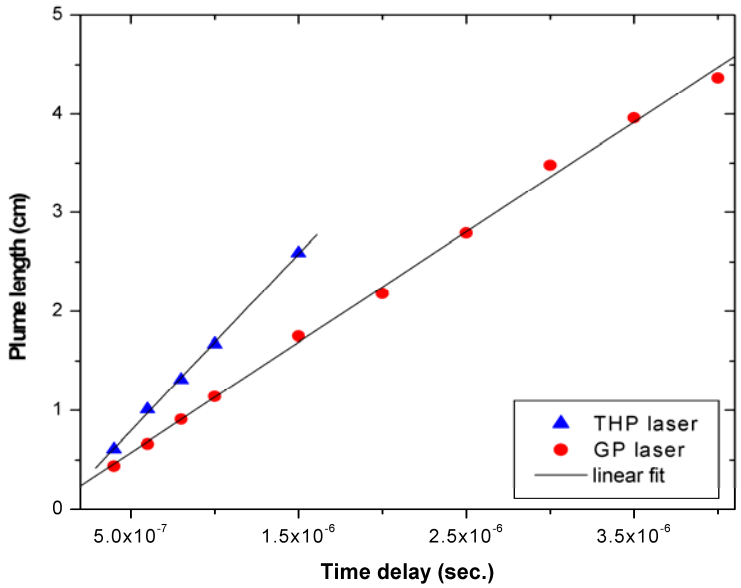

Figure 4.3 *Observed plume length versus time plot for the THP and GP laser generated plumes. The solid lines represent the linear fit for the experimental data.*

In the case of THP, the plume is ellipsoidal in shape i.e. the velocity component along the expansion axis is larger than the lateral direction. The recorded images for THP show a non-uniform intensity pattern parallel to the direction of the plume expansion and are more intense at the leading edge of the plume and at points closer to the target. During the expansion, emission intensity decreases rapidly and finally becomes highly diffused after t > 1500 ns and is almost beyond the detection limit of the ICCD.

On the other hand, plume formed by GP laser expands linearly with smaller lateral velocity in comparison to that observed with THP laser. In this case, plume has nearly cylindrical shape. Moreover, the lifetime of the emissive plume is found to be significantly larger and is clearly visible up to a time delay t > 4000 ns. Unlike THP produced plume, it has a uniform intensity distribution; of course, it has bright patches at leading and trailing edges of the plasma. Another noteworthy observation is that the overall integrated intensities in the vertical section with a width of

Δz = 0.5 mm of plumes produced by THP and GP laser are nearly the same. The calculated value is within 5% uncertainty at any fixed location of the plume. However, due to confined geometry, images with GP laser look brighter as compared to THP plume.

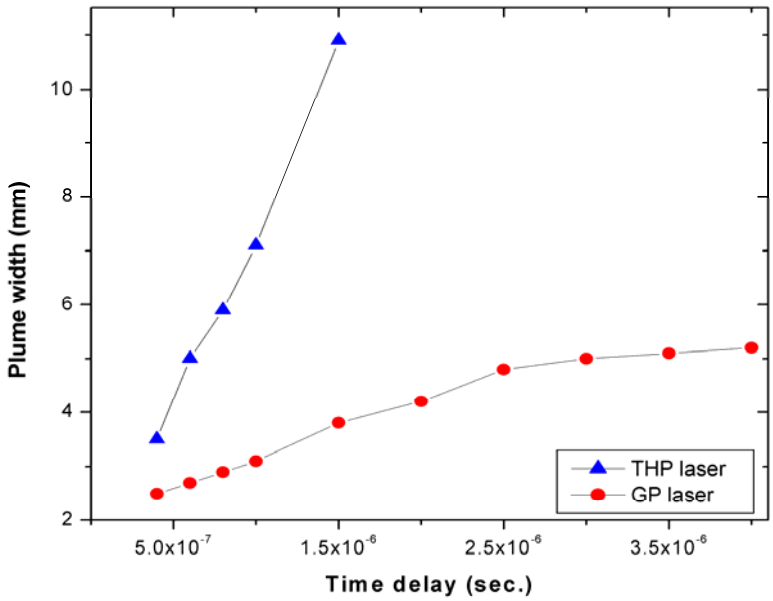

Figure 4.4 *Variation of plume width as a function of time delay for the both THP and GP laser.*

The difference in lateral expansion for these cases is clearly visible in plume width versus time plot as shown in Fig. 4.4. In the case of THP laser, width of the plume gradually increases with time. On the other hand, plume width with GP laser slowly increases up to t = 2500 ns and attains nearly constant value with further increase in the time delay. Figure 4.4 shows that the transverse velocity of THP plume is higher than the transverse velocity of GP plume in the overlapping region; and after t > 2500 ns, GP plume follows one-dimensional motion with negligible transverse velocity component.

4.3.2. Divergence measurement

Visible inspection of Fig.4.2 reveals that there is a significant difference in the divergence of the expanding plume formed by THP and GP lasers. The divergence of plume can be estimated by measuring the diameter of the plume at two separate points 'd_i' and 'd_f' separated by a distance 'x' and using the relation,

$$Divergence = A\tan^{-1}\left(\frac{d_f - d_i}{2x}\right) \qquad (4.1)$$

Divergence measurement has been carried out over one set of plume images formed at t = 800 ns. The portion of the plume has been considered up to the maximum acquired diameter, which is nearly equal to half of the total length of the plume. Diameter of the plume at different locations of the plume and separation between them are used to estimate the divergence of plume for both laser systems. The estimated values of divergence of plumes formed by THP and GP lasers at t = 800 ns are 1.5 rad and 40 mrad respectively. This indicates that transverse expansion in the case of THP produced plume is larger in comparison with GP-plume by a factor of ~ 40. The measured divergence, 40 mrad with GP laser further reduces at later stages (t > 2500 ns) where the plume width is almost invariant with time. This is an important finding in the sense that GP produces low divergence and long lived highly collimated plume. The persistence of low divergence for longer time is highly suitable for producing collimated atomic/ionic beams.

Further, while comparing the directionality of THP and GP laser induced plumes; it is worthwhile to see the angular dependence of ejected species in the respective plumes extracted from the recorded images {20}. The recorded image is divided into radial slices of specific width and the emission intensity is integrated along each axis. A typical intensity distribution obtained by normalizing to the maximum intensity of LBO plumes formed by THP and GP laser respectively at a time delay, t = 800 ns is shown in Fig. 4.5.

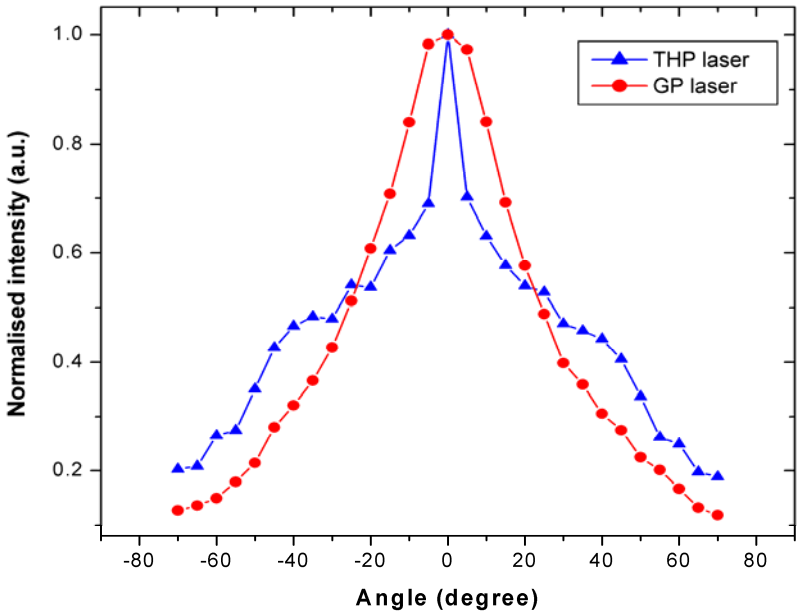

Figure 4.5 *Angular dependence of emission intensity of the LBO plumes produced by THP and GP laser at 800 ns time delay.*

It should be noted that, the difference in angular distributions for THP and GP is not as prominent as observed in the visible inspection of the plume images, shown in Fig.4.2. This discrepancy is due to the limitation of the adopted method, where the major portion of the angular slice is lying in the intense portion of the plume close to the target, especially at higher angles, which gives wrong information at these angles. In spite of this, some features are still comparable for these two cases and we have observed some differences as well. For both the cases, one can see that distribution of species is highly peaked in the forward direction and shows isotropic behavior. Almost similar distributions are observed for different time delays. The intensity distribution profile of THP plume appears to have two types of distributions (i) a narrow one lying near the central position and (ii) a broader one appearing as a shoulder. On the other hand, species in the GP-plume lie in a narrow angular region and vary smoothly with the angle of incidence.

4.3.3. Ion probe studies

Since the ICCD images provide the information only about the excited plume species, it is worthwhile to verify the above results with other diagnostic techniques. In this regard, the ion distributions across the expansion axis have been measured using an electrical ion probe. Experimental details for this studies has already been discussed in chapter 2.

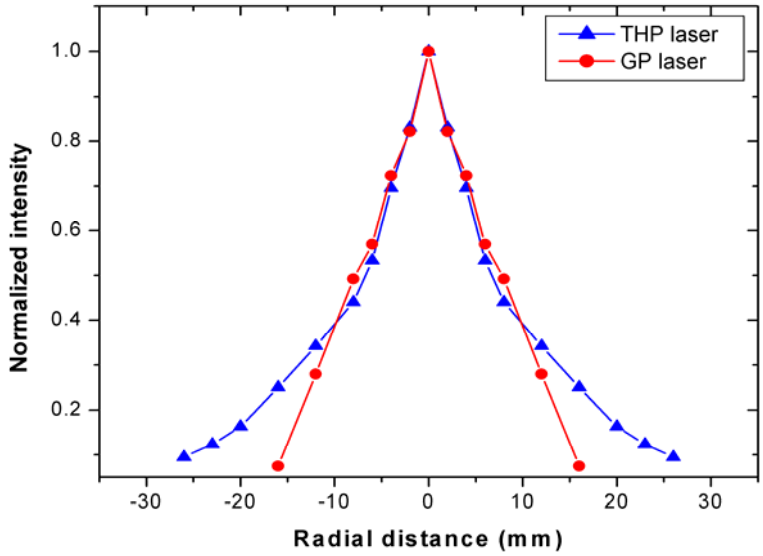

Figure 4.6 *Ion distributions of the LBO plumes as function of radial distance for the both THP and GP laser. The distance between the ion probe and target plate was set as 45 mm.*

The total intensity of ions at any probe position is obtained by the area under the temporal profile of ion current. This has been normalized with the maximum intensity and the intensity variation of ejected ions as a function of radial distance for both THP and GP lasers are shown in Fig. 4.6. It clearly shows that the ion distribution is peaked in the forward direction for both the laser systems and also the ions formed by GP laser have narrow distribution as compared to that of THP laser. Thus, the ion probe results further support the fact that the plume formed by GP laser is of low divergence.

4.3.4. Plume Formation Mechanism

It has already been mentioned earlier that the THP plume has larger divergence in comparison to plume formed by GP laser. For similar power density range, Singh & Narayan {19} and others {21} have modelled the plume formation and its expansion for the conventional solid ablation. According to their proposed models, the pressure driven acceleration is larger along the direction where the plume has smaller size. Since at the initial stage, plume size along the expansion direction is small. Therefore, the velocity component along the expansion axis is much larger than the lateral one and hence the plume acquires an ellipsoidal shape. It is observed that the plume shape during expansion is elliptical in the case of THP, which is in close agreement with the proposed model. However, the plume shape is close to cylindrical for GP plume. The plume size in the transverse direction varies negligibly with time, especially at higher time delays, which could not be fully predicted by the above model. This difference in the divergence of both plumes during their expansion should be related to the difference in plume formation

The GP-plume moves with smaller velocity as compared to the THP-plume, which can be understood in terms of a qualitative mechanism for the sequence of the processes in the formation of the LBO plume {1} e. g. melting of the film after the laser strikes the front surface, propagation of the melt front towards the back surface and propelling of the material due to increased vapour pressure. In the case of thin film target where skin depth attaining time is less than laser pulse duration, all these events are completed before the termination of laser pulse. Therefore, the propelled material further interacts with the laser and forms the plasma plume. The time required for the melt front to reach the back surface is called melt-through. This parameter plays an important role in the film removal process, which should depend on the power density of the laser, thickness and thermal properties of the target film.

In the case of THP laser, uniform heating of target film within the irradiated region is expected. For the considered power density, the super-heated front surface having high vapor pressure causes explosive rupture of the vacuum-film interface. Therefore, the propelled material is propagated in the forward direction with significant transverse velocity component. On the other hand, in the case of GP produced plume, a non-uniform heating/melting of the film favors bubble formation in between the substrate and film interface {22}. With increase in vapor pressure, ultimately an opening may be formed to release the material rather than the occurrence of explosive rupture. Since peak intensity of the GP laser is higher than the intensity of the THP, a smaller region of the film near the Gaussian peak will reach melt-through rapidly and propulsion may start through a small area. This will reduce the build-up of vapor pressure. Therefore, the material removal will take place through a small orifice similar to gas expansion through a smaller size nozzle but with less stagnation pressure, which may result in a relatively low velocity collimated plume with GP.

4.4. Conclusions

The above discussed results clearly showed the dependence of characteristic expansion of the LBO plume on the laser beam intensity profile. The geometrical shape, velocity and directionality of the plumes formed by the GP and THP laser were significantly different. One of the important observations reported in the present work was the very low divergence plume produced by GP in comparison to the plume generated by THP. The present observations are explained on the basis of the formation mechanism of plasma using two different intensity profiles. However, more theoretical work is required to understand it quantitatively. The present observations will be of significant importance in shaping laser generated plasma plumes and understanding and controlling the geometrical aspect of the LBO generated atomic/ionic beam.

4.5. Plume expansion in an ambient medium: Effect of laser intensity profile

In the previous section, we have seen that laser intensity profile significantly controls the LBO plume geometry. The fast imaging spectroscopy of the LBO plume in vacuum has revealed that the ablating laser having the Gaussian energy density profile produced the LBO plume of cylindrical geometry and expands with little lateral divergence as compared to plume formed by top-hat intensity profile laser {Sec. 4.3}. In this context, we were motivated by the fact that the geometrical shape and divergence of plume play the crucial role in plume-ambient atom interaction, especially in shock front formation {23}. We therefore attempted to look more closely the above phenomena by considering the LBO plume expansion in different ambient conditions. For this, the study was extended to investigate the expansion dynamics of LBO plume for three different ambient gases: helium(He), oxygen(O_2) and argon(Ar).

Compared to the adiabatic expansion into vacuum, the interaction of the plasma plume with an ambient gas is a complex gas dynamic process, which we have already discussed in chapter 3 {6, 24-27}. During the initial period after plasma formation, plume has a very high driven pressure and the effect of ambient gas is not significant. In this stage plume expands just as in vacuum. However, expansion dynamics is fully controlled by the interaction between the ablated species and the ambient atoms at the time delay of hundreds of nanoseconds depending on the pressure and atomic weight of the ambient gas. After the termination of laser pulse plume, particles move with high velocity into the surrounding gas with continuous interaction of ambient atoms. When the mass of the ablated plume is equivalent to the mass of the ambient gas, plume material compresses the ambient gas and as a result, strong shock wave is formed. The strength, shape and velocity of the shock front are highly dependent on the velocity and angular distribution of the plume and nature of the ambient gas.

In view of the above, experiments were conducted using the fast imaging to understand the dynamics of LBO plume and shock formation in He, O_2 and Ar environment. In this study, emphasis was given to the shape, strength and velocity of the shock wave and their dependence on the pressure and nature of the ambient gases. Helium and argon as ambient environment has been chosen for comparison due to the large difference in their atomic masses and ionisation potentials whereas oxygen provides the information regarding the chemically reactive aspect.

4.5.1. Imaging results

LBO plasma plume has been recorded using an ICCD fast imaging system and the results are presented in the coming sections.

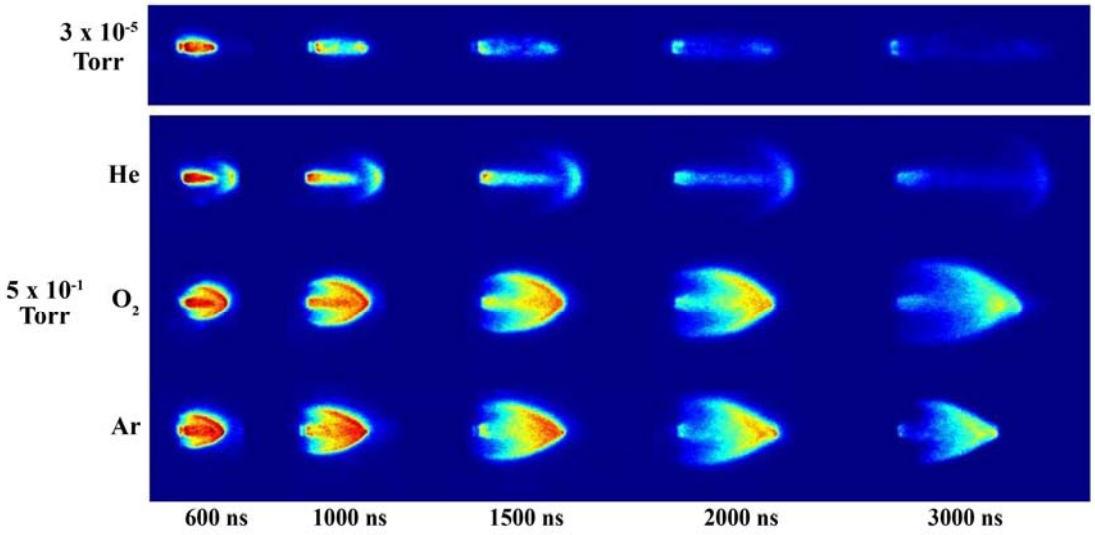

Figure 4.7 *Images of LBO plume at a background pressure of 3 x 10^{-5} Torr of vacuum and 5 x 10^{-1} Torr of three ambient gases He, O_2 and Ar at five different time delays after the onset of plasma formation.*

In order to understand the effect of pressure and atomic/molecular weight of ambient gas on the geometrical structure and hydrodynamical movement of the expanding LBO plume, the temporal evolution of emitting plume are recorded at different pressure levels of He, O_2 and Ar under the similar experimental conditions.

Figure 4.7 shows the sequence of images recorded at different time delays, varying from 600 ns to 3000 ns at vacuum and ambient pressure of 3 x 10^{-1} Torr of He, O_2 and Ar gases. All these images are recorded at a laser irradiance of ~ 3 GWcm^{-2} and normalized to their maximum intensity. Each image represents the spectrally integrated emission intensity in the range 350–750 nm emitted from different species within the plume.

As can be seen from Fig.4.7, in vacuum plume propagates linearly and their intensities decrease gradually with time. Intensity distribution is almost uniform throughout the plume volume, though it has bright patches at leading and trailing edge of the plasma. In vacuum, plume expands under the influence of pressure gradient and is treated as adiabatic expansion {28}, where electron temperature and density decrease with time and hence electron impact process also decreases. Therefore, considerable reduction in the emission intensity of the plume with increase in the time delay is observed. Similar studies have already been performed using top-hat profile laser {Chapter 3}. In the present case Guassian profile laser was used and compared to the earlier studies. One of the peculiar observations is that, the plume expands with negligible lateral velocity and has nearly cylindrical shape in comparison with conventionally observed elliptical shape {Chapter 3}. Due to the highly directional nature, the lifetime of the emissive plume is found to be significantly larger and is clearly visible up to t > 4000 ns. Very low divergence and long lived highly collimated plume is attributed by film ablation mechanism with laser having Gaussian intensity profile {Sec. 4.3}.

Plume was completely modified upon introducing the ambient gas. These images show distinct features of the plasma plume in 10^{-1} Torr of He, O_2 and Ar pressures in terms of emission intensity, duration and geometrical shape of expanding plasma plume. Visible examinations of the images clearly demonstrate the effect of nature of the ambient gas, e.g. atomic mass, ionisation energy and thermal conductivity on the expanding plasma plume. In the case of He, major

portion of the geometry is nearly identical to that observed in vacuum and travel almost with the same distance as in the case of vacuum expansion. An additional luminous cone-shaped structure starts to appear in front of the plume in the presence of ambient gas. This added component is attributed to shock front and propagates with a higher velocity as compared to the plume velocity and therefore well separated from plasma plume in He environment.

In the case of heavier ambient gas, e.g. O_2 and Ar, the images are significantly different as compared to the observed images in He environment. Apart from the more intense and sharper contact boundary i.e, the shock front, a drastic enhancement in emission intensity especially in the centre portion of the plume are observed in presence of Ar and O_2. In this case, ($P < 10^{-1}$ Torr) conical structure remains intact with plume front and not well separated as in the case of He environment.

In order to get more insight into the plume dynamics under various environments, plume images as a function of gas pressure of He, O_2 and Ar are shown in Fig. 4.8. The background gas pressure varies from high vacuum to 3 Torr pressure and time delay is set as 1000 ns. Careful examination of Fig. 4.8 reveals the following general features. Under the same ambient pressure, the shock front moves with higher velocity in lighter gases (He) compared to the velocity in heavier gases like O_2 and Ar.

At a fixed time delay, shock front is more luminous in higher atomic/molecular gas and becomes more intense and sharper with increasing the background gas pressure. A second intensity discontinuity just behind the shock front is observed in Ar and O_2 at pressure > $1x10^{-1}$ Torr. This effect is not visible at lower pressure of heavier gases and all the considered pressure range of He.

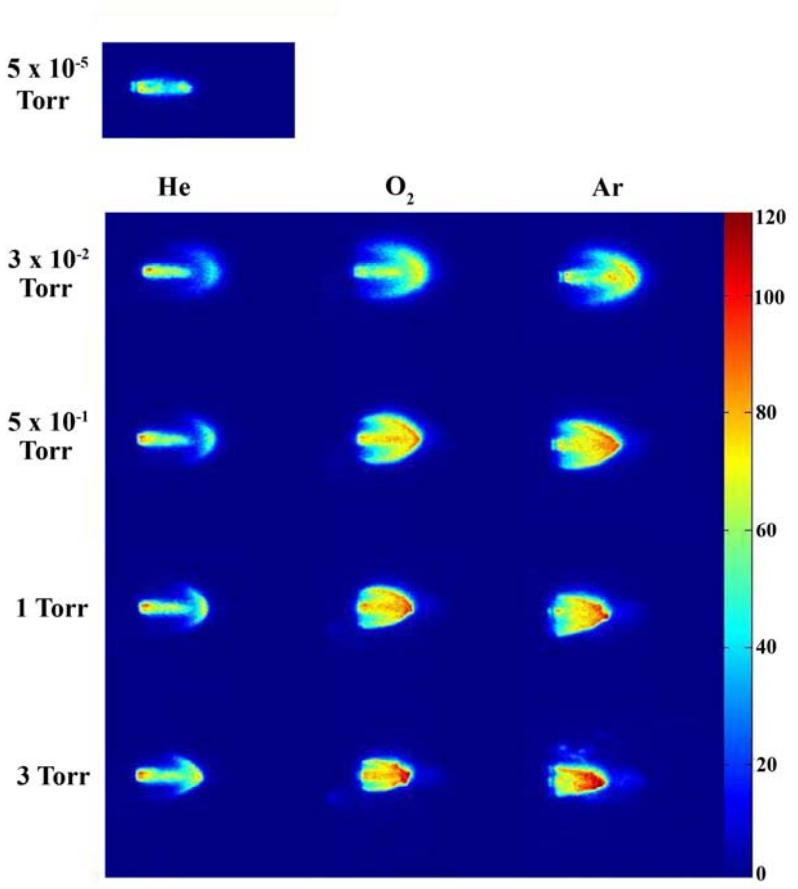

Figure 4.8 *Images of LBO plume at different background pressures of three ambient gases He, O_2 and Ar at a time delay of 1000 ns after the onset of plasma formation. Colorbar shows the normalized intensity in arbitrary unit.*

Further, the enhancement in emission intensity, especially inside the plume is not much significant with increasing the He pressure. However, drastic enhancement is observed in shock front and inside the plume in the case of both Ar and O_2. For a fixed time delay (1000 ns) and at pressure 10^{-1} Torr, it has been found that there is an overall enhancement in intensity of 1.52 times in Ar and 1.45 times in O_2 as compared to that in He. As usual, plume experiences more resistive force i.e, drag force, in heavier gas environment in comparison to that of He gas, and

therefore axial as well as lateral confinement is dominant with increasing the pressure of Ar and O_2. This can be clearly seen in the measured plume length for the different pressures of He, Ar and O_2 at fixed time delay as shown in Fig.4.9.

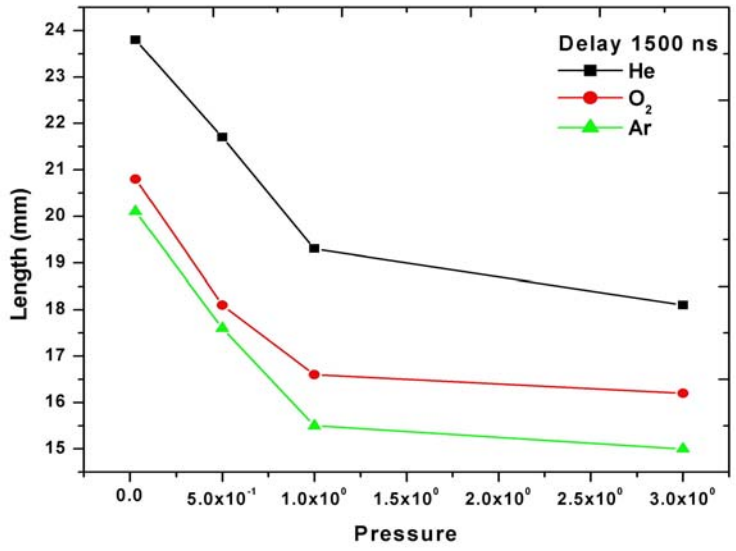

Figure 4.9 *Observed plume length at 1500 ns for the different pressures of He, Ar and O_2.*

The difference in enhancement in emission intensity inside the plume in different gasses can be explained in terms of electron impact excitation which is the dominant process to excite the plume species {Chapter 3}. Since the ionization energy of He is greater than O_2 and Ar, more increase in electron density during the plume-ambient gas interaction is expected in O_2 and Ar environment. Another mechanism which contributes to the increase in electron density in different ambient gases is the cascade growth of the electron number density and absorption coefficient of the plasma in ambient environment {Chapter 3}.

4.5.2. Shock structure

The shape of the plume and its divergence control plume-gas interaction and hence influences the shock front formation and expansion. The highly

directional plume with insignificant lateral movement and cylindrical geometry as in the present case, efficiently compresses the ambient gas and therefore provides better chance to form strong shock front. This can be clearly seen in the Fig. 4.7 where, the appearance of shock wave structure and their visibility in ICCD images are more clear as compared to reported results in the past {6, 24}.

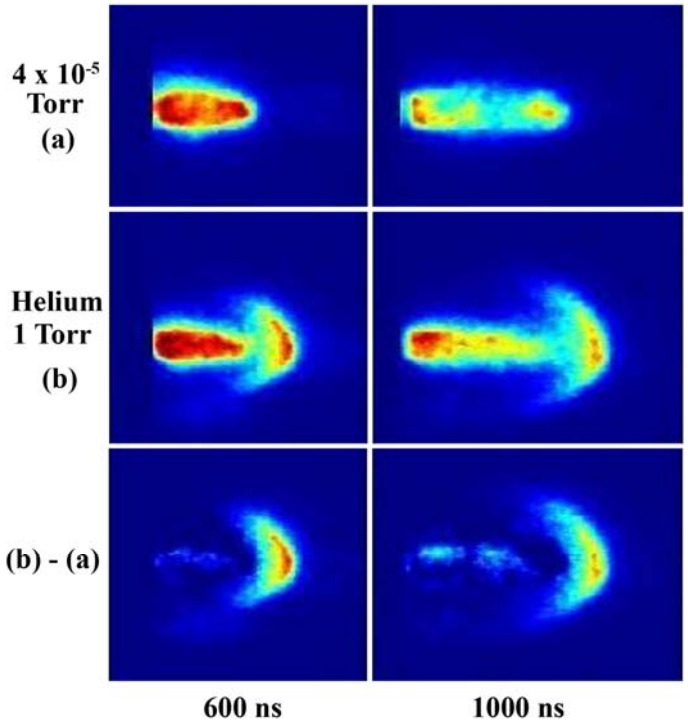

Figure 4.10 ***(a)*** *plume formed in vacuum 4 X* 10^{-5} *Torr* ***(b)*** *plume formed in Helium pressure of 1 Torr* ***(c)*** *subtraction of image 'a' from image 'b'.*

In order to confirm the presence of shock front, we have subtracted the plume image formed in vacuum from the images observed at 600 ns and 1000 ns in He medium as shown in Fig. 4.10. Interestingly the major portion of the plume is completely eliminated after the image subtraction process and only the cone shaped front portion remains visible. This method confirmed that, the shape and intensity of plume observed in vacuum remains unchanged in He environment even at a

relatively high pressure of 1 Torr and the intense shock front is formed only due to the compression of background gas by the plume front.

The explosive hot plume expands adiabatically, with high velocity creating a high pressure material front and pushing the surrounding gas. Its expansion velocity rapidly decreases and it transfers its energy and momentum to the ambient gas, thus sending out a shock wave which gradually separates from the plume. Taylor-Sedov {29} model the spherical blast wave expansion by considering the blast wave originating from a point explosion where the shock swept the ambient gas mass such that $M_a >> M_p$, where M_a and M_p are the masses of ambient gas and mass of the ablating species respectively. This model is valid for the strong shock condition where the ambient gas pressure is negligible in comparison with the to pressure behind the shock front. The shock wave model has limiting characteristic distance 'R_1', for a particular gas and pressure, below which this model is not valid {30}. R_1 is set by the requirement that the mass of the gas encompassed by the shock wave (in volume $= 2/3\pi R^3$) is much greater than the initial ablated mass m. This requires

$$R_1 >> R = \left(\frac{3m}{2\pi\rho_b}\right)^{1/3} \tag{4.2}$$

Due to the cylindrical geometry in present case, one cannot directly estimate the distance where the shock initiated, but it is clear that in the case of heavier background gas and high-pressure region, shock is initiated at early stage of plasma compared to that of lighter gas and relatively low pressure region. The above inference is clearly visible in the present observation as shown in Fig. 4.8.

4.5.3. Shock wave analysis

In order to compare the shock wave condition in different gases the density (ρ_s), temperature (T_s) and velocity (V_s) in the shocked region in He, Ar and O_2 is

estimated by using the mass, momentum and energy conversation, and is given by {31, 32}

$$V_s \approx (\frac{\gamma+1}{2})V_a \tag{4.3}$$

$$T_s \approx \frac{2\gamma}{\gamma+1}\left[\frac{(\gamma-1)}{(\gamma+1)}M^2+1\right]T_b \tag{4.4}$$

$$\rho_s \approx \rho_b(\frac{(\gamma+1)}{(\gamma-1)}) \tag{4.5}$$

where V_a is the velocity of expanding plume, M is the Mach number (M = V_a /sound velocity), γ is the specific heat ratios of background gas and T_b and ρ_b is the temperature and density of the undisturbed background gas. Using the time-of-flight of plume, velocities of expanding plume at 10^{-1} Torr of He, O_2 and Ar are estimated as $1.63x10^4$, $1.36x10^4$ and $1.26x10^4$ m/sec respectively. Using the relation (4.3, 4.4), the estimated velocity in the shock region in He, O_2 and Ar are $2.16x10^4$, $1.62x10^4$ and $1.67x10^4$ m/sec respectively. The above estimate indicates that at fixed background pressure, shock front moves with highest velocity in He compared to the velocity in O_2 and Ar and therefore clear separation between the plume front and shock front is observed in He environment (Fig. 4.7). Further, the estimated temperature at the shock region in He, O_2 and Ar pressure of 10^{-1} Torr are 2.07, 11.55 and 12.23 eV respectively. The high temperature in O_2 and Ar is correlated with the observed luminosity of the shock front.

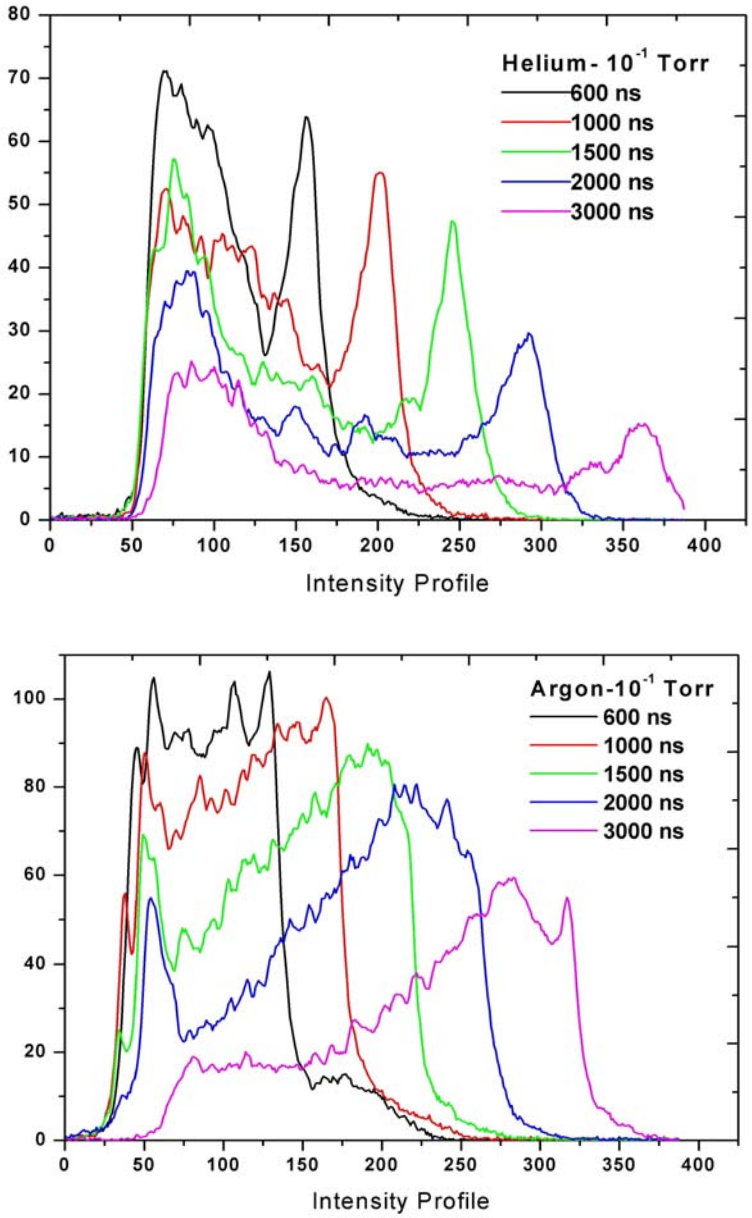

Figure 4.11 *Intensity profiles for various time delays for the plume formed in (a) Helium and (b) Argon gas pressure of 5 x10^{-1} Torr.*

In order to get a better presentation of the shock propagation, intensity variation of the ICCD images along the expansion axis are binned for the different delay at 10^{-1} Torr of He and Ar as shown in Fig.4.11.

Figure 4.11 clearly demonstrate most of the evolution features, e.g., intensity variation with time, shock formation and its expansion, plume confinement and their differences in He and Ar environment. Two well separated components corresponding to the expanding plume and shock front are clearly observed in He environment. The separation between the plume and shock front increases with increase in time delay and the intensity of the shock front reduced with time. On the other hand, in the case of Ar, the plume portion and shock front are not resolved as observed in the case of He. However, at lower time delays, one can easily identify the ionized front (discussed later) and the shock front merging in intense plume front with increasing time delay due to the increase in the resistive force with time. The rate of decrease of shock intensity with time is higher in He as compared to decrease in Ar environment. This is because of the large temperature difference in He and Ar environment which is ~ 2 eV and 12 eV in He and Ar respectively. Because of the higher thermal conductivity of He, shock front is rapidly cooling in He environment {24}.

The above intensity profile can also be used to estimate the shock strength in different ambient conditions. The shock strength which is the reciprocal of the shock thickness, is obtained by using the density gradient in pre-shock to post shock region {33},

$$\frac{1}{S} = \delta = \frac{I_{\max} - I_0}{Z_a - Z_b} \tag{4.6}$$

where, I_{max} is the peak intensity, Z_a and Z_b are the distance from the target where the intensity is 75% and 25% of the peak intensity. I_0 is the pre-shock intensity, ≈ 0. Figure 4.12 shows the typical intensity profile at 600 ns time delay in

He adopted for calculating the shock strength. From the intensity profile of the plume images, the second peak away from the target is considered as shock region and inverse of the width of 25 % and 75 % of the falling edge of the lobe represent the shock strength. The shock strength at different pressure levels of He and Ar plotted as a function of time are shown in Fig 4.13.

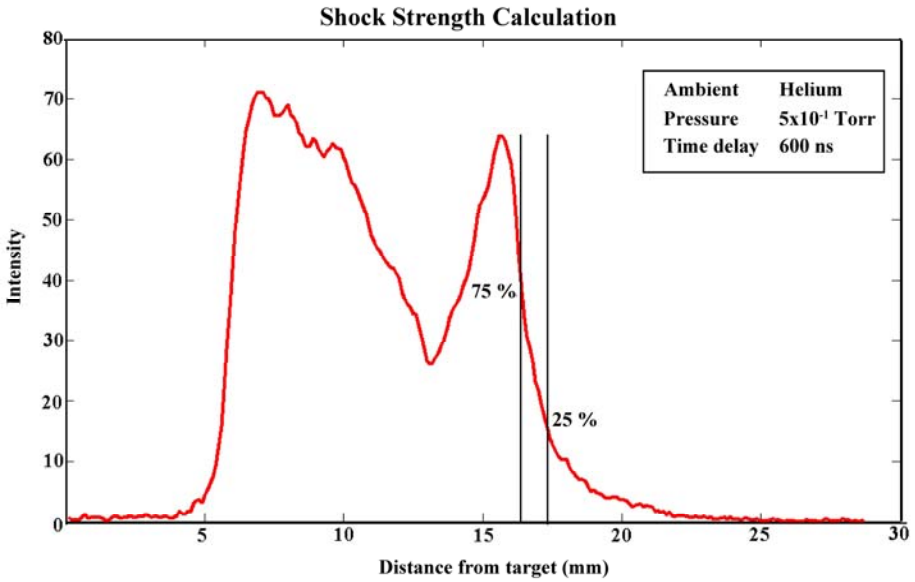

Figure 4.12 *Method adopted to calculate shock strength from intensity profile plot.*

This gives information regarding the development of different stages of shock front propagation in time domain. The calculated shock parameter values clearly shows the dependency of shock wave formation and its dynamics over the ambient gas medium and are highly influenced by the mass of ambient gas. From the first sight it is clearly visible that shock strength increases with rise in pressure of surrounding gas medium. Upon introducing the gas, shock wave forms in the medium and continuously interact with the gas and decreases with time. Maximum shock strength is observed at 3 Torr pressure in both He and Ar environment. Increase in pressure cause more resistance from the external medium which causes increase in blast pressure, and hence maximizes the shock strength. During the

initial period of plume formation t < 1500 ns, the higher plume pressure causes larger shock strength and then gradually decreases with further increase in time delay. Obviously, the shock strength is maximum in Ar because of heavier atoms.

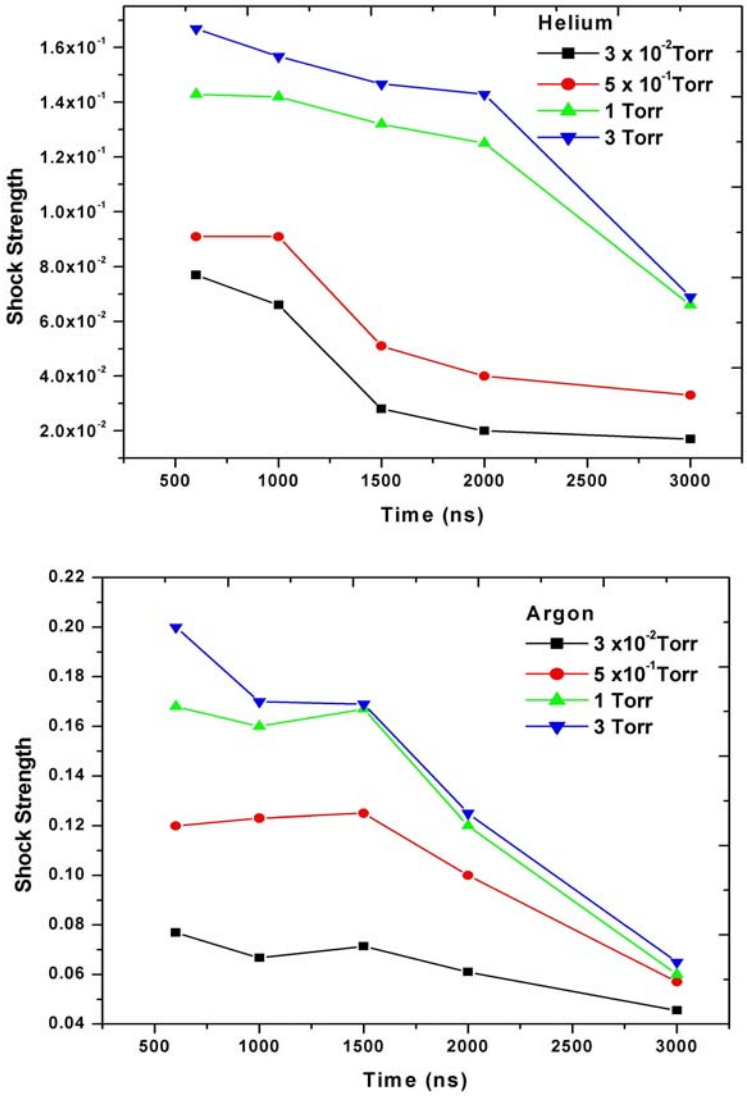

Figure 4.13 *Shock -strength calculated from the ICCD images recorded for plume formed in (a) Helium and (b) Argon ambient gases.*

As already mentioned, a sharp and more intense boundary, just behind the shock front is observed in Ar and O_2 at pressure > $1x10^{-1}$ Torr. This can be

explained in terms of elastic scattering of plume front species with the ambient atoms/molecules. The highly directional plume species are scattered in collision with the ambient atoms and deviate from the original direction. Scattering angle depends on the mass and radii of the plume and background species. The scattering angle of the carbon atoms which is the major constituent in the plume has been estimated and it is observed that there is a change in direction by ~15^0, ~75^0 and ~78^0 in single collisions with He, O_2 and Ar atoms respectively {34}. Since the temperature in the shock region is very high ~ 12 eV in O_2 and Ar, there is a finite chance of ionization of scattered plume species. Therefore, due to the higher scattering angle and higher shock temperature, the second intense boundary behind the shock front is attributed to ionized plume front. Due to low scattering angle and shock temperature ~2 eV, the ionized front is not visible in He environment. Here we ignore the inelastic scattering and chemically reactive scattering, especially in the case of O_2 gas as reported in past {35}. In the case of inelastic scattering or oxidation of plume species i.e., chemically reacted with dissociated oxygen, width of the plume in O_2 is narrower than plume width in Ar because of low scattering angle of heavier molecules. The reduction of plume width and length with increasing pressure is mainly due to the increase of resistive force of ambient gas and hence this effect is maximum in heaviest gas like O_2 and Ar.

4.6. Conclusions

In summary, the characteristic expansion of LBO plasma plume and the formation of shock wave in different gas pressure, ranging from high vacuum to 3 Torr of He, O_2 and Ar have been studied experimentally with fast gated ICCD camera. The enhancement in emission intensity, structure formation, drag force and confinement effect is maximum in Ar environment in comparison to He and O_2 environment. The associated physical processes responsible for the production of these differences were briefly discussed. The present observations suggest that highly collimated, low divergence plume produces substantially strong shock wave

in comparison to the previously reported shock produced by the diverging plume. It has been found that shock velocity is highest in He and the shock front is completely detached from the plasma plume. However, the shock temperature and strength is maximum in high pressure and heaviest ambient gas. We could not observe any significant difference in the plume shape in Ar and O_2 environment and therefore ignore the possibility of chemically reactive processes in the present case. Further, an ionizing front just behind the shock front is observed in Ar and O_2 at pressure $P > 1x10^{-1}$ Torr and this effect is not visible for the entire pressure range in the case of He. We feel that this study will give additional information to explore the above subject.

4.7. References

1. F. J. Adrian, J. Bohandy, B. F. Kim, A. N. Jette, and P. Thompson., *"A study of the mechanism of metal deposition by the laser-induced forward transfer process"*, J. Vac. Sci. Technol. J. Vac. Sci. Technol. **B5**, 1490 (1987).

2. Robert J. Baseman and Nan M. Froberg., "*Time-resolved transmission of thin gold films during laser blow-off",* Appl. Phys. Lett. **55**, 1841 (1989).

3. Z. Kántor, Z. Tóth and T. Szörényi., *"Laser induced forward transfer: The effect of support-film interface and film-to-substrate distance on transfer"*, Appl. Phys. A **54**, 170 (1992).

4. D. Toet, P. M. Smith, T. W. Sigmon, and M. O. Thompson., *"Experimental and numerical investigations of a hydrogen-assisted laser-induced materials transfer procedure"*, J. Appl. Phys. **87**, 3537 (2000).

5. R. K. Singh, Ajai Kumar, B. G. Patel, and K. P. Subramanian.,*"Role of ambient gas and laser fluence in governing the dynamics of the plasma plumes produced by laser blow off of LiF–C thin film",* J. Appl. Phys. **101**, 103301 (2007).

6. Sony George, Ajai Kumar, R. K. Singh, and V. P. N. Nampoori.,*"Fast imaging of laser-blow-off plume: Lateral confinement in ambient environment"*, Appl. Phys. Lett. **94**, 141501 (2009).

7. V. Schultze and M. Wagner.,*"Blow-off of aluminium films".* Appl. Phys. A **53**, 241 (1991).

8. M. H. Key, W. T. Toner, T. J. Goldsack, J. D. Kilkenny, S. A. Veats, P. F. Cunningham, and C. L. S. Lewis., *"A study of ablation by laser irradiation of plane targets at wavelengths 1.05, 0.53, and 0.35 μm"*. Phys. Fluids **26**, 2011(1983).

9. G. J. Pert.,*"Models of laser-plasma ablation. Part 3. Steady-state theory: deflagration flow"*, J. Plasma Phys **39**, 241 (1988).

10. S.Witanachchi and P. Mukherjee., "*Spot-size-dependent bifurcation of laser-ablated plumes"*, J. Appl. Phys. **78**, 4099 (1995).

11. Nadezhda M. Bulgakova, Alexander V. Bulgakov, and Oleg F. Bobrenok., *"Double layer effects in laser-ablation plasma plumes"*. Phy. Rev. E **62**, 5624 (2000).

12. Salvatore Amoruso, Riccardo Bruzzese, Nicola Spinelli, Raffaele Velotta, Marco Vitiello, and Xuan Wang., *"Dynamics of laser-ablated MgB_2 plasma expanding in argon probed by optical emission spectroscopy"*, Phys. Rev. B **67**, 224503 (2003).

13. S.S Harilal., *"Influence of spot size on propagation dynamics of laser-produced tin plasma"*, J. Appl. Phys. **102**, 123306 (2007).

14. Isak I. Beilis., *"Laser plasma generation and plasma interaction with ablative target"*. Laser Part. Beams **25**, 53 (2007).

15. L. Laska, K. Jungwirth, J. Kra´ SA, E. Krousky´, M. Pfeifer, K. Rohlena, A. Velyhan, J. Ullschmied, S. Gammino, L. Torrisi, J. Badziak, P. Parys, M. Rosinski, L. Ryc´ and J. Wolowski., *"Angular distributions of ions emitted from laser plasma produced at various irradiation angles and laser intensities"*, Laser Part. Beams **26**, 555 (2008).

16. M.S. Rafique, M. Khaleeq-Ur-Rahman, I. Riaz, R. Jalil, and N. Farid., *"External magnetic field effect on plume images and X-ray emission from a nanosecond laser produced plasma"*. Laser Part. Beams, **26**, 217 (2008).

17. J. Hoffman, T. Moscicki, Z. Szymanski., *"The effect of laser wavelength on heating of ablated carbon plume"*., Appl. Phys. A **104**, 3 (2011).

18. Ajai Kumar, Vishnu Chaudhari, Kiran Patel, Sony George, S. Sunil, R.K. Singh and Ranjeet Singh.,"*An experimental setup to study the expansion dynamics of laser blow-off plasma plume in variable transverse magnetic field"*, Rev. Sci. Instrum. **80**, 033503 (2009).

19. R. K. Singh and J. Narayan.; *"Pulsed-laser evaporation technique for deposition of thin films:Physics and theoretical model"*, Phys. Rev. B **41**, 8843 (1990).

20. Salvatore Amoruso, Alessia Sambri, and Xuan Wang., *"Propagation dynamics of a $LaMnO_3$ laser ablation plume in an oxygen atmosphere"*, J. Appl. Phys. **100**, 013302 (2006).

21. S. I Anisimov and B. S Luk'yanchuk., *"Selected problems of laser ablation theory"*, Physics-Uspekhi **45**, 293. (2002).

22. D. J. Broer and L. Vriens., *"Laser-induced optical recording in thin films"*, Appl. Phys. A **32**, 107 (1983).

23. A Misra and R. K. Thareja., *"Laser-ablated plasma for deposition of aluminum oxide films",*Appl. Surf. Sci., **143**, 56 (1999).

24. Sony George, Ajai Kumar, R. K. Singh and V. P. N. Nampoori., *"Effect of ambient gas on the expansion dynamics of plasma plume formed by laser blow off of thin film"*, Appl. Phys. A., **98**, 901 (2009).

25. S. S. Harilal, C. V. Bindhu, M. S. Tillack, F. Najmabadi, and A. C. Gaeris., "*Internal structure and expansion dynamics of laser ablation plumes into ambient gases"*, J. Appl. Phys. **93**, 2380 (2003).

26. R. K. Singh, Ajai Kumar, B. G. Patel, and K. P. Subramanian.,"*Role of ambient gas and laser fluence in governing the dynamics of the plasma plumes produced by laser blow off of LiF–C thin film"*, J. Appl. Phys. **101**, 103301 (2007).

27. S. Amoruso, J. Schou and J. G Lunney.,*"Multiple-scattering effects in laser ablation plume propagation in gases"*, Euro Phys. Lett. **76**, 436 (2006).

28. P. E. Dyer, A. Issa, and P. H. Key., *"Dynamics of excimer laser ablation of superconductors in an oxygen environment"*, Appl. Phys. Lett. **57**, 186 (1990).

29. *"Similarity and Dimensional Methods in Mechanics",* L. I. Sedov., (Academic Press, New York, 1959).

30. P. E. Dyer and J. Sidhu., *"Spectroscopic and fast photographic studies of excimer laser polymer ablation"*, J. Appl. Phys. **64**, 4657 (1988).

31. *"Physics of Shock Waves in Gases and Plasmas"*, M.A. Liberman and A. L. Velikovich., Springer-Verlag, Berlin (1986).

32. J. J. Chang and B. E. Warner.,*"Laser-plasma interaction during visiblelaser ablation of methods"*, Appl. Phys. Lett., **69**, 4 (1996).

33. Charles Phelps, Carl J Druffner, Glen P Perram and Rand R Biggers.,"Shock front dynamics in the pulsed laser deposition of $YBa_2Cu_3O_{7-x}$", J. Phys: D Appl Phys 40, 4447 (2007).

34. W. D. Westwood., *"Calculation of deposition rates in diode sputtering systems"*, J. Vac. Sci. Technol. **15**, 1 (1978).

35. A. Sambri, S. Amoruso, X. Wang, F. Miletto Granozio, and R. Bruzzese., *"Plume propagation dynamics of complex oxides in oxygen"*, J. Appl. Phys. **104**, 053304 (2008).

Chapter 5

Image Analysis of Lithium Plasma Plume in Variable Transverse Magnetic Field

Abstract

Effect of transverse magnetic field on the geometry and features of the lithium plasma plume generated from solid and thin film target has been studied using fast imaging and emission spectroscopy. Enhancement in the overall emission intensity as well as appearance of distinct structures in the plasma plume in the presence of magnetic field has been observed. By introducing a variable magnetic field, the influence of various atomic processes in expanding plasma plume across the transverse magnetic field has been studied.

5.1. Introduction

The interaction that occurs between an externally applied magnetic field and plasma is an important topic with potential applications ranging from astrophysics to pulsed power and fusion. In recent years, the effect of magnetic field on the expansion of laser-produced plasma plume has been the subject of intensive research because of its relevance in various applications like thin film deposition, debris mitigation, development of extreme ultra-violet (XUV) lithographic sources, analytic detection limit enhancement in laser-induced breakdown spectroscopy (LIBS) etc{1-8}. Earlier studies revealed that expansion of plasma in the presence of magnetic field may initiate several interesting physical phenomena in the overall plume dynamics such as conversion of the plasma thermal energy into kinetic energy, plume confinement, ion acceleration, emission enhancement, plasma instabilities etc. Among this, there is a particular interest to investigate the influence of magnetic field for the plasma confinement {9-11}. In pulsed laser deposition (PLD), plasma confinement in a converging magnetic field leads to more excited plasma and a reduction in the deposition temperature {17, 18}. It has also been observed that magnetic field can control the external plasma parameters in a variety of ways {9, 11, 13, 21}

In this chapter, we discuss the influence of external magnetic field on the propagation dynamics of laser plasma formed from Li solid as well as LiF-C thin film target. Uniform magnetic field applied in the transverse direction to the expanding plasma and the field strength was varied from zero to 4000 Gauss. Imaging of the expanding plasma was carried out using ICCD. Li spectral line emission analysis also performed in order to confirm the results obtained from the imaging data. Analysis of the experimental data revealed several interesting observations at different time periods. The overall plume shape and intensity variations are major characteristics, which have been studied.

5.2. Review of earlier works

Considerable work has already been carried out both theoretically and experimentally to understand the influence of external magnetic field on laser produced plasma. Bhadra et al {19} theoretically studied the expansion of plasma in the presence of magnetic field and has postulated that, cloud of plasma will be stopped by the magnetic field B at a distance $R \sim B^{-2/3}$. The periodic pulsations of the plasma boundary against the magnetic field when $\beta > 1$ observed by Tuckfield et.al.{20}were in approximate agreement with the theory proposed by Bhadra with inclusion of a condition that the energy losses due to radiation and particle losses along and possibly across the field lines been taken into account.

Peyser et al {21} demonstrated that, plasma expansions strongly collimated in the direction transverse to both the initial flow and the magnetic field, but jet-like in the direction parallel to the initial flow. Structural changes in the plasma geometry and instabilities generated as result of the magnetic field were studied using fast framing cameras. Further, they attributed that E x B is responsible for the jet like structures, whereas instabilities caused the edge structures. Plume emission enhancement when the plasma expands in a magnetic field was another interesting observation reported in many cases {10-13}. Enhancement in emission was found to be dependent on the intensity of external magnetic field and correlated with an increase in confinement of laser produced plasma as well as generation of instabilities in the plasma. Mostovych et. al {26} investigated the expansion of laser-produced barium plasma in 0.5- 1 T transverse magnetic fields, and reported the focusing of plasma jet in the plane perpendicular to the field, while in the plane of the field the plasma expands along the field lines and this appears as flute-like striations. The narrowing of the plasma jet was understood in terms of the configuration of the plasma polarization fields, while the flute structure was identified as electron-ion hybrid velocity shear instability. Dimote and Wiley {27} measured the magnetic profile and plasma structure for nearly spherical exploding plasmas in a magnetic field. The diamagnetic cavity and plasma radii scale with the

magnetic containment radius over a wide range of ion magnetization. Plasma instabilities were also observed which evolve from short to long wavelengths and affect the evolution of the magnetic field

Bryunetkin et al {28} reported the first experimental demonstration of the difference in the emission of spectral lines by ions of different degrees of ionization in a laser-plasma expanding in vacuum in the presence of a transverse external magnetic field strength of 0.3 T. Enhancement in line emissions were observed and they concluded this result as the action of plasma focusing due to the magnetic field. A qualitative explanation of the observed emission pattern has also been provided with numerical modeling.

Confinement of the laser-produced plasma by a curved magnetic field was investigated by Tsui et. al. {29, 30}. In this study, an axial magnetic field with a maximum strength of 2.2 kG was used to confine and guide a laser produced carbon plasma. The measurement has been conducted using an array of Faraday cups positioned at the exit of the guide field and found that approximately 20% of the original plasma was confined by the magnetic field.

Plume splitting was another interesting observation noticed in the presence of magnetic field. Combined diagnostics using emission spectroscopy and fast imaging by Neogi and Thereja {31} reported the splitting of plume into two assymetric lobes in the presence of an inhomogeneous magnetic field. Each of these lobes has three components viz. the fast, intermediate, and slow. The plume spitting has been explained on the basis of J x B force acting on the plume. Moreover, oscillations were also observed in the temporal profile of the plume, in the presence of magnetic field. These oscillations were observed at a location where species are at the outermost front, and this is attributed to edge instability in magnetic field. Harilal et al. {32, 33} suggested the role of backflow of particles towards the target for the appearance of lobes. Qindeel et al. {34} studied the plume behaviour with imaging CCD for varying magnetic field for Al, Cu and brass targets. They

suggested that plume structure might result from the Lorentz force exerted by the field. Jet-like structures in the plume in the presence of magnetic field has been attributed to instabilities by Rafique et al. {35}. Despite these reports, a comprehensive temporal imaging study with varying field is necessary to understand the field effect. Studies carried out in this direction are described in this chapter.

5.3. Experimental details

The investigations were carried out by means of the experimental setup described in chapter 2. Only the main features and additional parts are briefly summarized here. The experiment was carried out in a cylindrical stainless steel chamber, evacuated to a base pressure < $2x10^{-5}$ Torr. For LPP studies, ½ inch diameter solid Li rod with purity 99.999% and for LBO studies LiFC thin film target was used. Fundamental emission (1064 nm) from an Nd:YAG laser was used to ablate the target. The spot size of the laser beam was set to about 1 mm diameter at the target to achieve average power density of ~ 10^9 W/cm^2. A pulsed power system consisting of capacitor bank and a wire wound solenoid was used to produce a magnetic field in the range, 0 – 3000 G with a flat-top duration of of 40 μs which was much larger than the plume duration {36}.

Both OES and imaging diagnostics were performed simultaneously on the two sides of the chamber. Each of these techniques has its on merits and demerits for plasma diagnostics. Due to certain limitations, some results cannot be correlated with each other. For instance, enhancement of emission that comes out from distinct lines was easier to understand by analysing OES data. On the other hand, plume geometry alterations induced due to magnetic field were more visible in ICCD images than in OES data. To investigate the effects of the magnetic field on the plasma plume, the emission spectrum for two characteristic emissions from lithium neutral and from lithium ion has been recorded by varying the field.

An ICCD camera (*4 Picos, Stanford Computer Optics, Inc.*) having variable gain and gating on time, has been used to record the time resolved images of the plume luminescence in the spectral range of 350 - 750 nm. In the present experiment, gate opening i.e., image integration time was set at 4 ns. Temporal evolution of the LPP plume has been obtained by varying the time delay from 100 to 4000 ns between the laser pulse and the opening time of ICCD gate. Five images were recorded under similar experimental conditions. These images were found to be nearly identical in shape and the reproducibility of the emission intensity was better than 5 %. To find the emission profile along the direction of plume expansion, plume images were binned along the vertical column of images.

5.4. LPP of Li in magnetic field

The plasma expansion from solid Li target across the transverse magnetic field was recorded by ICCD camera at different magnetic field strengths, varying from 0 to 2800 G and is shown in the Fig 5.1.

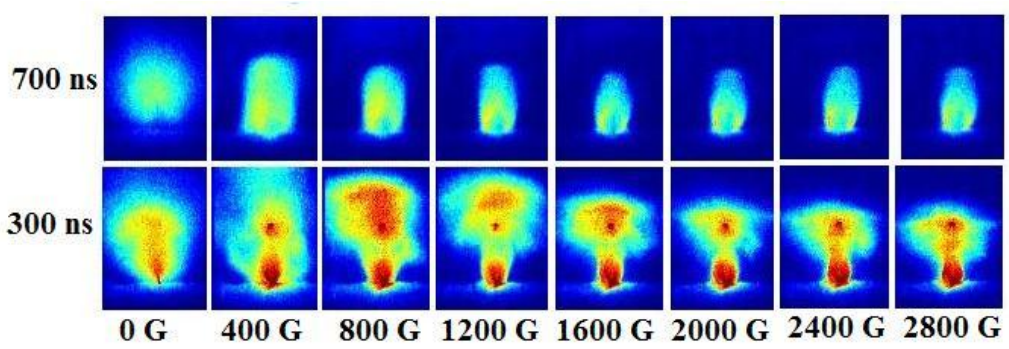

Figure 5.1 *Images of plume recorded at two different time delays 300 ns and 700 ns as a function of the field strength.*

These images were recorded in vacuum with a time delay of 300 ns and 700 ns with respect to the laser pulse. Images at these particular delays are showing interesting features on the plume intensity distribution. Each of these images represents spectrally integrated emission intensity in the region 350 – 750 nm emitted from different plume species for a fixed value of magnetic field.

From Fig.5.1, it is clearly visible that, the plume was modified drastically by the influence of uniform magnetic field. The changes induced under the influence of field include the enhancement in intensity and modification in the plume geometry. These two aspects are explained separately in the coming sections of this chapter. Emission spectroscopy was also conducted in every case to have better understanding of the dynamics under magnetic field.

5.4.1. Plume emission under magnetic field

In the absence of the magnetic field, ablation of lithium into vacuum produces an intense luminous plume that expands normal to the target surface. The expansion is primarily governed by the initial density/ pressure gradient inside the plume and is well explained theoretically in terms of adiabatic and self-similar expansion model {18}. Comparison of the images recorded at different field strengths shows that, the shape and the intensity of the plasma plume are completely modified on introducing the transverse magnetic field.

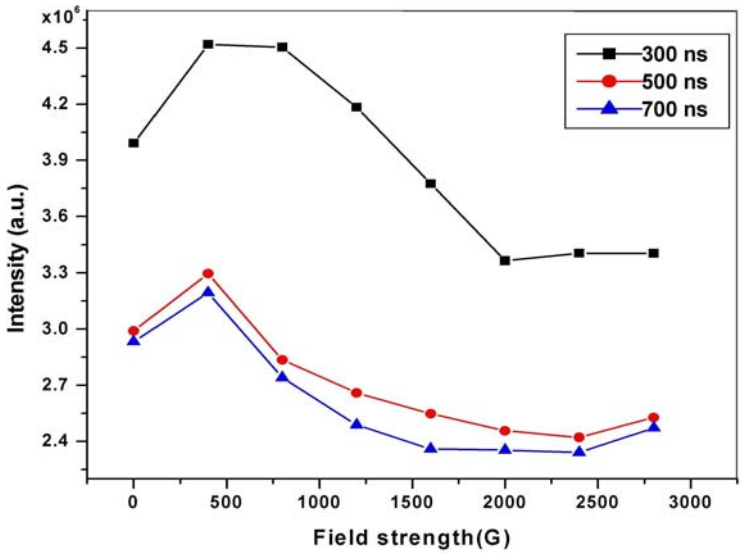

Figure 5.2 *Variation of the total integrated intensities of plume images recorded at three specific time delays after the laser hit.*

Figure 5.1 shows plume geometry and emission as a function of field strength at three different time intervals. For field strength 0 to 800 G, plume size has increased and with further increase in field i.e., > 800 G plume becomes confined. Many authors have already reported the enhancement of emission in the presence of magnetic field. To get degree of enhancement quantitatively, we have integrated the intensity of the plume images recorded using ICCD and are shown in Fig.5.2

The above figure (Fig 5.2) gives an understanding of the plume intensity variations as a function of field strength at three specific time delays. Initially for field strength of 400 to 800 G, the plume undergoes significant enhancement in intensity and with further increase in field strength, the enhancement goes down. This information can be correlated to the ICCD image data shown in Fig.5.1. On increasing the field strength beyond some range (> 800 G), the plume size becomes smaller as a result of plume confinement and intensity increases over a small area. Since the dynamic range of ICCD camera limits the maximum intensity that can be recorded, and this makes the integrated plume intensity data exhibiting a different trend with increase in field.

In order to confirm the plume enhancement, we have recorded the Li neutral emission lines. Figure. 5.3 show the temporal evolution of Li (I) 670.8 nm ($2s\ ^2S_{1/2} \leftarrow 2p\ ^2P_{3/2,1/2}$) line at different magnetic fields. It can be seen that enhancement in the emission takes place when the field is increased. Moreover, the profile is broadened with some small structures. However, unlike 670.8 nm, for 610.3 nm ($2p\ ^2P_{1/2,3/2} \leftarrow 3d\ ^2D_{3/2,5/2}$) line shows a decrease in emission although the profile shows some broadening (Fig. 5.3).

To explain enhancement in line emission, various mechanisms like increase in ionization, confinement, increase/ decrease in effective plasma density, increased radiative recombination and increase in both confinement and radiative recombination have been proposed. As most of the earlier experiments were

performed at constant magnetic field, no definite mechanism for enhancement could be identified.

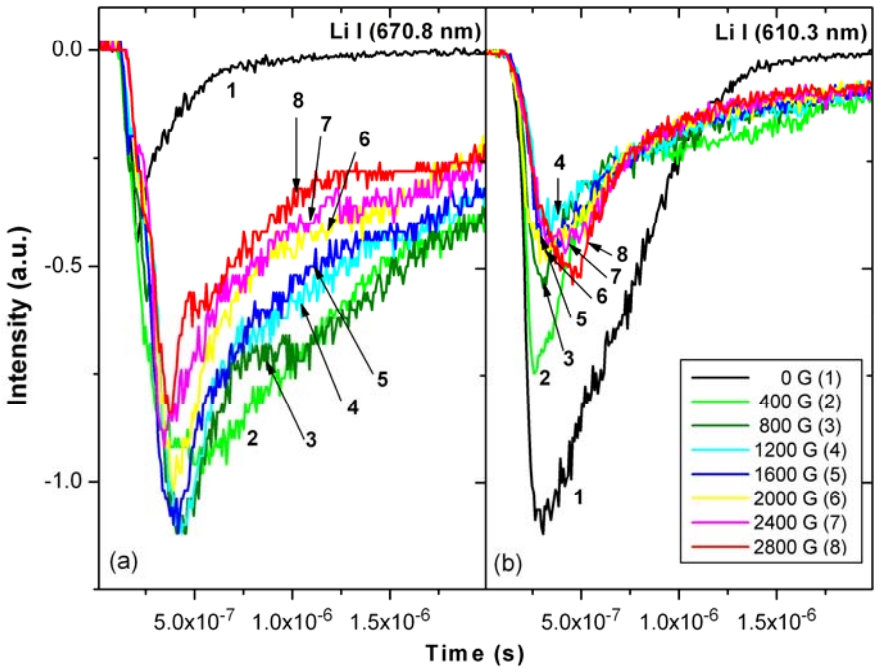

Figure 5.3 *Intensity variations with magnetic field of (a)670.8 nm line and (b)610.3 nm line*

A recent study explained the role of atomic process during the plume dynamics under the influence of magnetic field {44, 45}. For this, the photoemissivity coefficients (PEC), has been calculated from Atomic Data Analysis Structure (ADAS) database {46}. This research addressed the difference in enhancement on the basis of change in PEC's. For 670.8 nm, coefficients for electron impact excitation(PEC_{ex}) is significantly higher than coefficients for recombination(PEC_{re}) indicating that electron impact dominates over recombination and hence will result in the enhancement in intensity with the increase in field because of increase in electron temperature although a small increase in electron

density is also expected because of confinement. However, the overall effect of Joule heating appears to be dominating. On the other hand, for 610.3 nm lines, there is less difference in PEC_{re} and PEC_{ex}. As the LPP plume is expected to have ionic species, it appears that net contribution from recombination dominates in this case. This explains the decrease in intensity with increase in field as PEC_{re} decreases with increase in temperature.

In addition to the enhancement of the plume emission, various instabilities like structures and splitting are also induced in the plume under the influence of magnetic field and these results are presented below.

5.4.2. Plume geometry under magnetic field

Plume modifications are most pronounced in the range of field from 400 G to 1600 G. The degree of modification of the plume was not so visible after a field of B > 1600 G.

In order to get a better presentation of axial variation of emission intensity in the presence of magnetic field, the cross-section of the plume emission intensity along the expansion axis is binned and included in Fig.5.4. Binned intensity profile plot of the plume images gave precise information about the plume splitting and spatial location at which the intensity peak appears. Initially in the presence of magnetic field above 400 G, the plume splits into two lobes (P1 and P2) in the direction of expansion. Figure 5.4 also shows the formation of another structure P3 with increase in the magnetic field (> 400 G) and this well-defined third lobe (P3) is clearly visible at a field of 1200 G field. However, P3 diminishes with further increase in the field and almost disappears when the field is B > 1600 G and finally attains a two lobe structure. Here we rule out the possibility of P2 and P3 being merged. Had the merger caused it, a large enhancement in the emission intensity should have taken place for higher field values, which, of course, is not observed in the present case. Another noticeable observation is that the increase in magnetic

field largely affects the leading portion of the plasma plume as compared to the initial portion closer to the target.

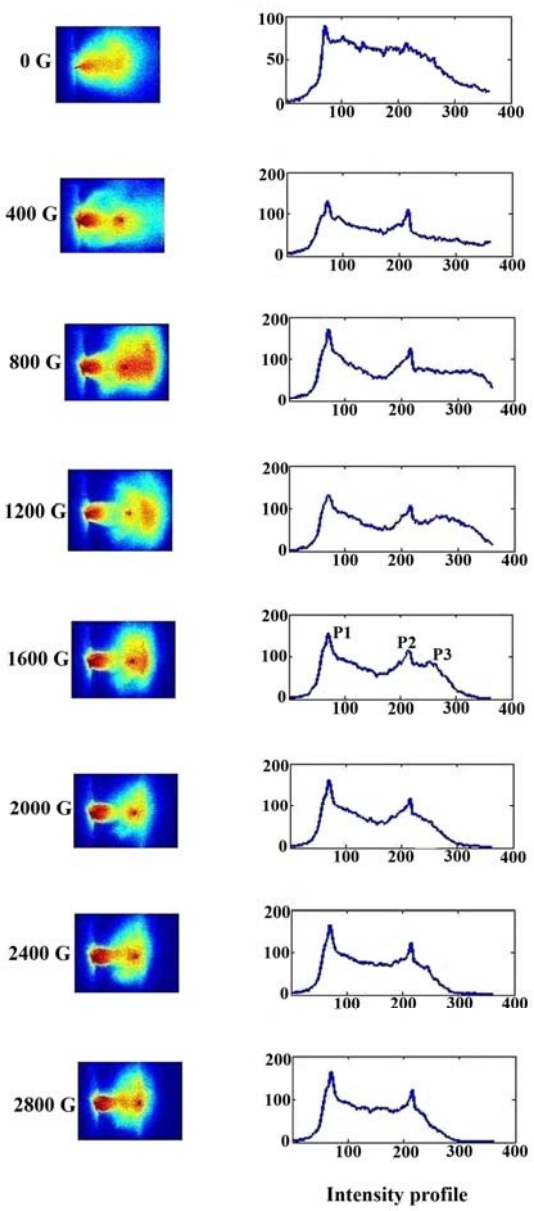

Figure 5.4 *Sequence of images at 300 ns along with the corresponding intensity profiles for different magnetic fields*

Plume splitting in the presence of magnetic field has been observed previously by several authors {32, 33, 37} and they explained this phenomenon on the basis of fluid MHD model. According to this model, plasma plume can be treated as a conductive medium, which expands in external magnetic field and an internal diamagnetic current arises to exclude the field from the interior. This diamagnetic current interacts with the magnetic field through $\boldsymbol{J} \times \boldsymbol{B}$ force that accelerates or decelerates different regions of the plasma plume, depending on the direction of the diamagnetic current within the plume causing the plume splitting along the expansion direction.

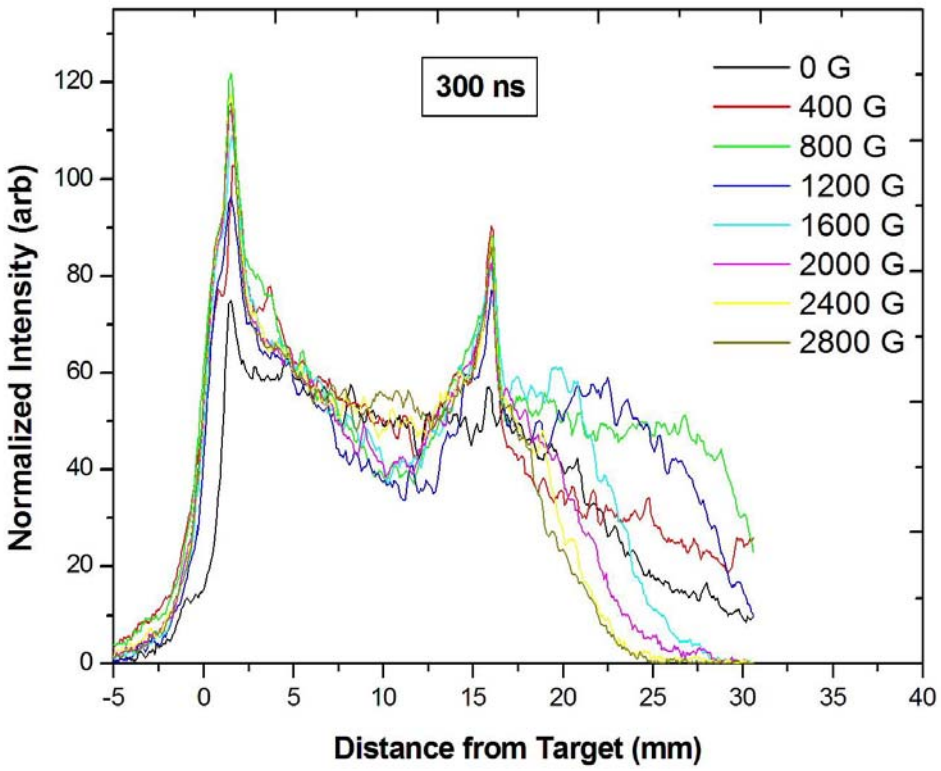

Figure 5.5 *Overlapped intensity profiles for various magnetic fields for 300 ns delay.*

It can be noted that the above conclusions drawn in most of the previous reports were based on experimental results with fixed magnetic field. Hence,

experiments with variable magnetic field are essential to explore the role of $\boldsymbol{J} \times \boldsymbol{B}$ force in expanding plasma plume across the transverse magnetic field. We, therefore, attempted to look more closely at the plume splitting in the magnetic field by investigating the splitting pattern for variable field strength. In this regard binned emission intensity profiles along the expansion axis corresponding to different magnetic fields are overlapped as shown in Fig.5.5.

Interestingly, the peak positions of P1 and P2 are independent of the field strength and appear at the same axial position for the entire field range. However, front portion of the plume slowly converges with increasing the magnetic field. This is an important observation because variation in the separation between two components is expected with increase in the field, if $\boldsymbol{J} \times \boldsymbol{B}$ force is responsible for the splitting. This indicates that instead of $\boldsymbol{J} \times \boldsymbol{B}$ force**,** some other processes should be responsible to produce the above phenomenon.

Another suggestion for the presence of lobes observed in the imaging study was given by Harilal et al. {33} where the studies were carried out at a fixed magnetic field. They estimated the bubble time and found that splitting takes place at longer times than the bubble time and subsequently attributed it to the backflow of particles. We have also calculated bubble radius and hence calculated bubble time from it. A typical bubble radius

$$R_b = \left(\frac{3\mu_0 E_l}{2\pi B^2} \right)^{1/3} \tag{5.1}$$

where E_l is laser energy and B is magnetic field strength. For the experimental parameters E_l = 200 mJ and at 400 G field the calculated value of bubble radius is ~ 4.2 cm and corresponding bubble time (2Rb/v) which comes to about ~ 760 ns for an expansion velocity of ~1.1×10^7 cms^{-1}. Since the lobes appear even at the lowest field (400 G) and at 300 ns time delay, it is difficult to correlate

the presence of lobes to the collapse of the bubble and subsequent backflow of particles, as the bubble lifetime is comparatively longer.

Another aspect that can result in instabilities in the plume is the self-generated magnetic field. The self-generated field can be estimated by {38-40}

$$B\ (kT/ezv)\ e \leq /\ (2) \qquad (5.2)$$

where k is Boltzmann constant, T_e is the plasma temperature, e is electronic charge, z is the distance at which field is to be calculated and v is the expansion velocity of the plume. For z = 6 mm distance, the maximum value of B is ~ 80 G, which is much less as compared to the external applied field values. Hence any instability due to the interaction of self generated magnetic field and applied magnetic field can be simply ruled out.

We feel that the magnetic field significantly influences the plasma parameters and hence the associated atomic processes in different regions to different extents in the plume as the composition changes along the expansion direction, causing the structure formation in magnetic field. The presence of magnetic field increases the electron temperature due to Joule heating {11} and electron density due to magnetic confinement {10, 11, 29}. Moreover, the plume expansion in the transverse magnetic field may result in the cyclotron motion of electrons and ions. This will significantly increase the probability of electron-atom/ion collisions, which in turn lead to enhancement in the emission intensity of the expanding plume. Therefore, the overall enhancement in emission intensity can be considered as the net contributions from electron impact excitation as well as recombination processes.

It is known from earlier studies that LPP plume front is mainly composed of energetic ionic species and therefore ionic emission is supposed to form the plume front in the observed images. On the other hand, the slow moving species dominated by neutrals represent the trailing portion of the plume. The above argument is strongly supported by optical emission spectroscopic data {45} where

strong Li II emission line appeared at shorter time delays as compared to that of Li I emission. Further, it is evident that the typical electron temperature and electron density of Li plasma are around 2 eV and 10^{17} cm^{-3} under similar experimental conditions {45}.

Conclusions are made on the basis of the above discussion that enhancement in the emission intensity; especially at the plume front and the appearance of elongated leading portion of the plume (P3) in the presence of the magnetic field is mainly due to the increase in excited ionic species by recombination processes. It is likely that with the introduction of the field, confinement may take place, which will result in increased electron density and hence increase the electron-ion recombination.

Careful examination of Fig.5.1 reveals that the magnetic field largely influences the front portion of the plume as compared to that of the trailing part. Plume front gradually converges into small volume with increase in the field. This could be understood as follows. The leading portion of the plume is mainly composed of energetic ions. It appears that ejected ions experience the resistive force in the presence of magnetic field and are gradually confined in small volume with increasing the magnetic field. For the present experimental conditions, the estimated bubble radii for the magnetic fields of 400 G and 2800 G are 4.2 and 1.15 cm respectively. The average deceleration (g = v2/2R) in the presence of 2800 G magnetic field is 5.3 $x10^{13}$ cm/s^2. Here the initial velocity of the plume (v = 1.1 $x10^7$cm/sec) is obtained by the plume image at 300 ns in the absence of magnetic field. The deceleration is also calculated by considering the plume images in the absence and presence of magnetic field using time of flight method. The agreement between the experimentally observed deceleration (~ 4.0 $x10^{13}$ cm/s^2) and calculated one suggests the confinement of ion rich plume front in the presence of magnetic field.

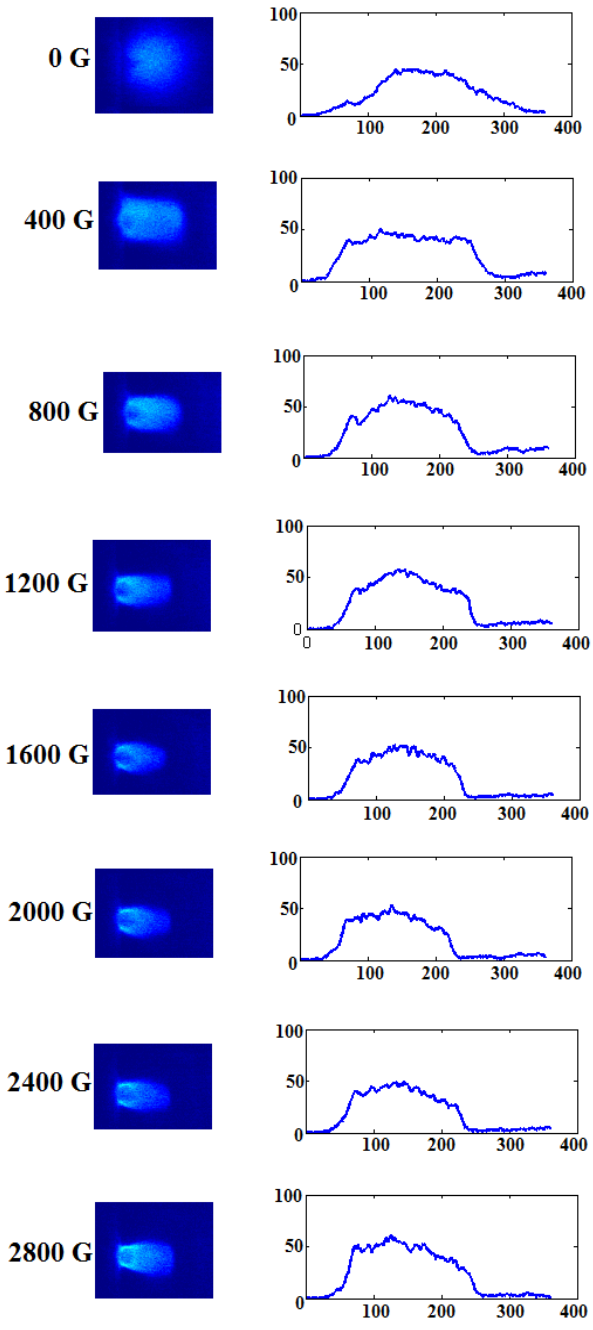

Figure 5.6 *Sequence of images at 700 ns along with the corresponding intensity profiles for different magnetic fields*

Similar analyses were performed for the images taken at 700 ns delay and is shown in Fig.5.6. The shape of the plume is entirely different from those observed at 300 ns. It can be noted that the emission intensity of the emitting species thermalizes rapidly with increasing time delay. It appears that emission from the ionic species i.e., front portion of the plume represented by P2 & P3 is decreased significantly or disappears and only neutral-rich trailing portion of the plume appears at this time delay. The confinement of neutral species can be understood in the following manner.

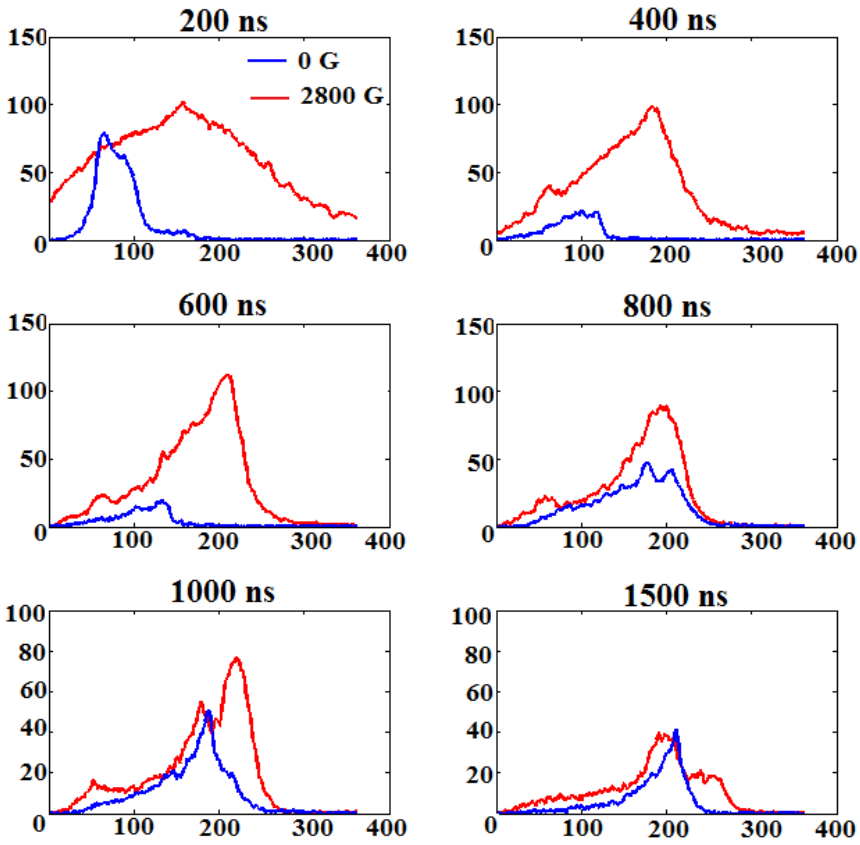

Figure 5.7 *Intensity profiles of images showing intensity enhancement. All these images were recorded at an argon pressure of 10^{-2} Torr at various time delays after the plasma formation*

At 700 ns, plume emission comes from both slow moving neutrals as well as neutral produced by the recombination of ionic species. As we have already discussed the ionic species experience the resistive force in the presence of magnetic field, which is reflected in the reduction of emission length from neutrals. Further, the images at 700 ns clearly show that the emission intensity at the edge of the plume (near the pole) is high in the presence of the magnetic field. This is because electron current density at the outer most boundary of the plume is expected to be high in the presence of the magnetic field.

Experiments were also conducted to understand the effect of magnetic field when the plasma is generated in an ambient gas environment. For this, we introduced argon gas into the chamber. As we had discussed in the earlier chapters, the presence of ambient gas enhances the intensity and lifetime of the plume. Figure 5.7 shows the images of plasma created from solid lithium target kept in ambient gas in the absence and presence of a uniform field of 2000 G.

5.5. LBO of LiFC in magnetic field

In the previous section of this chapter, we have been discussing the influence of external magnetic field on the dynamics of laser-produced plasma from Li solid targets. From the analysis, we found many interesting changes in the presence of field and alteration in the geometrical shape with varying magnitude of field

This section of the chapter discusses the study conducted to investigate the effect magnetic field on the propagation dynamics of plasma generated from LiFC thin film target. Super-thermal neutral atomic beams lithium and carbon, produced by laser-blow-off (LBO) technique are extensively used to measure the edge parameters of high temperature Tokamak plasma. The presence of Tokamak's magnetic field is expected to considerably affect the neutral and atomic ion beams. This motivated us to conduct experimental study to investigate the effect of magnetic field on the lithium plasma produced from LiFC target by LBO scheme.

The experimental setup used is same as the one described in the earlier part (Sec 5.3) of this chapter. The target used is a thin film LiFC coated over a quartz substrate. Optical emission spectroscopy and/or imaging techniques were used as diagnostics for studying the dynamics of these plasma plumes.

During the initial phase of the studies, we have recorded the plume images at various time delays as well as at different field strengths.

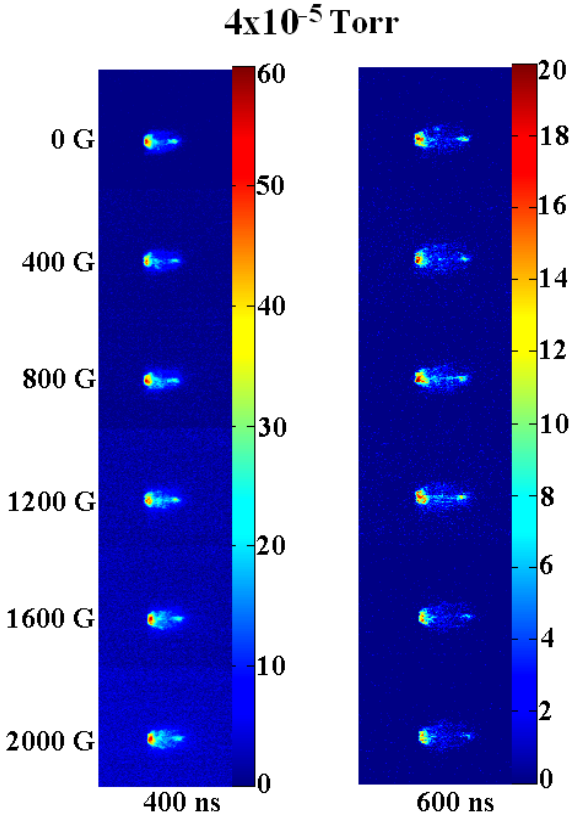

Figure 5.8 *ICCD images of the plume recorded in vacuum for different magnetic fields. Above images are recorded at 400 ns and 600 ns. Colorbar shows the normalized intensity in arbitrary unit.*

In order to study the influence of varying magnetic field, the magnitude of field was varied from 0 G to 2000 G and the images were recorded using ICCD (Fig.5.8). In general, enhancement of the plume intensity is observed at different

magnetic field strengths. Plume shape changes are not as prominent as that observed in the case of LPP plasma from Li solid target. Similar to the observations in solid Li target, changes induced for the LBO plume is maximum for the field strength in the range 400 G to 1600 G.

It has already been discussed that plume undergoes significant changes when it expands in an ambient medium. In the present investigation, we have studied the combined effect of magnetic field and ambient gas over the expanding LBO plasma. Figure 5.9 shows the images recorded at different pressure levels of argon gas and the field was varied from 0 to 2000 G.

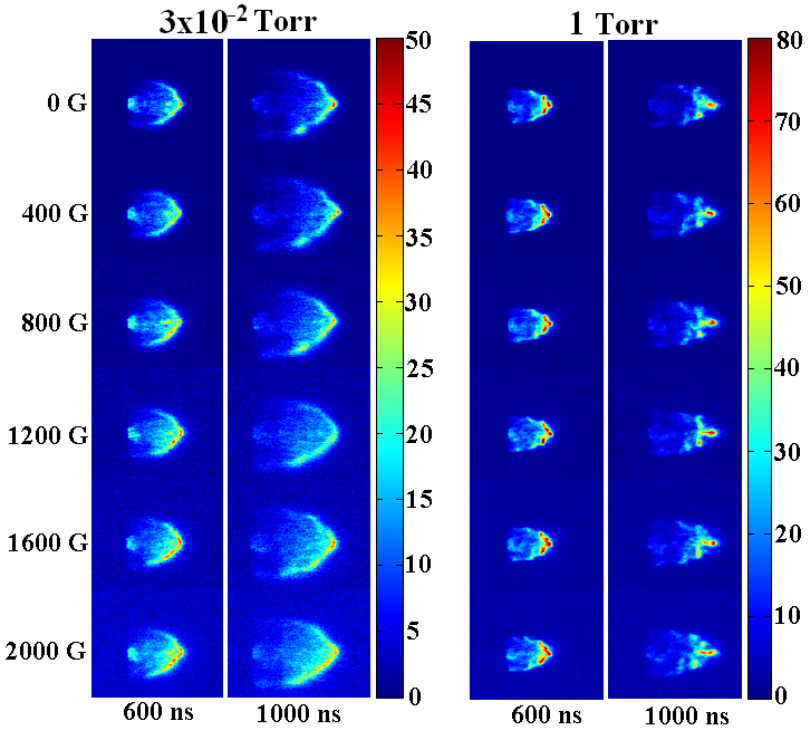

Figure 5.9 *ICCD images of the plume recorded at an argon pressure of 10^{-2} Torr and 1 Torr for different magnetic fields. Above images are recorded at 600 ns and 1000 ns. Colorbar shows the normalized intensity in arbitrary unit.*

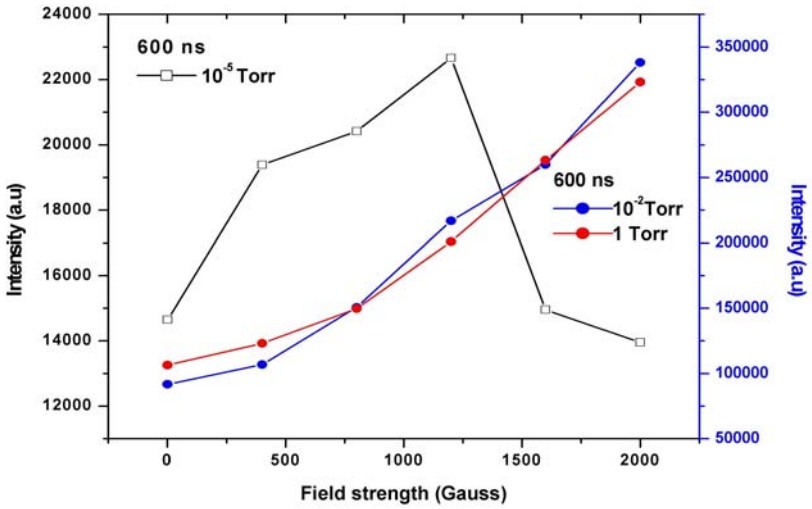

Figure 5.10 *Variation of the total integrated intensities of LBO plume for different magnetic fields in vacuum, 10^{-2} Torr and 1 Torr after a delay of 600 ns of laser ablation*

Since it is difficult to get a quantitative measure of the overall plume enhancement from the images, the plume images are integrated and are shown in Fig.5.10. It is clear from the Fig. 5.10 that plume intensity enhanced with increase in magnetic field. This effect was almost similar in both pressure levels 10^{-2} Torr and 1 Torr. Considering the plume structure changes at different magnetic field strengths, the changes induced is almost negligible as compared to the plume modifications observed in the case of plasma plume from Li solid target.

Imaging studies produce resultant signals derived from the overall emission of the plasma. Due to these limitations, ICCD imaging alone would not make it possible to understand the exact details on the changes that plasma expands in a magnetic field. From the earlier studies, it is clear that the magnetic field affects in a different way on various emission lines. So the results obtained using the fast imaging technique has confirmed and/expanded by relating the same with corresponding emission spectroscopy data which are recorded for the same ablation.

For spectroscopic studies, we have chosen two spectral lines of neutral lithium Li (670.8 nm) and Li (610.3 nm). Figure 5.11 shows the variation in the neutral emissions 670.8 nm and 610.3 nm for different magnetic fields in the range 0 –2000 G observed at a distance z = 6 mm from the target.

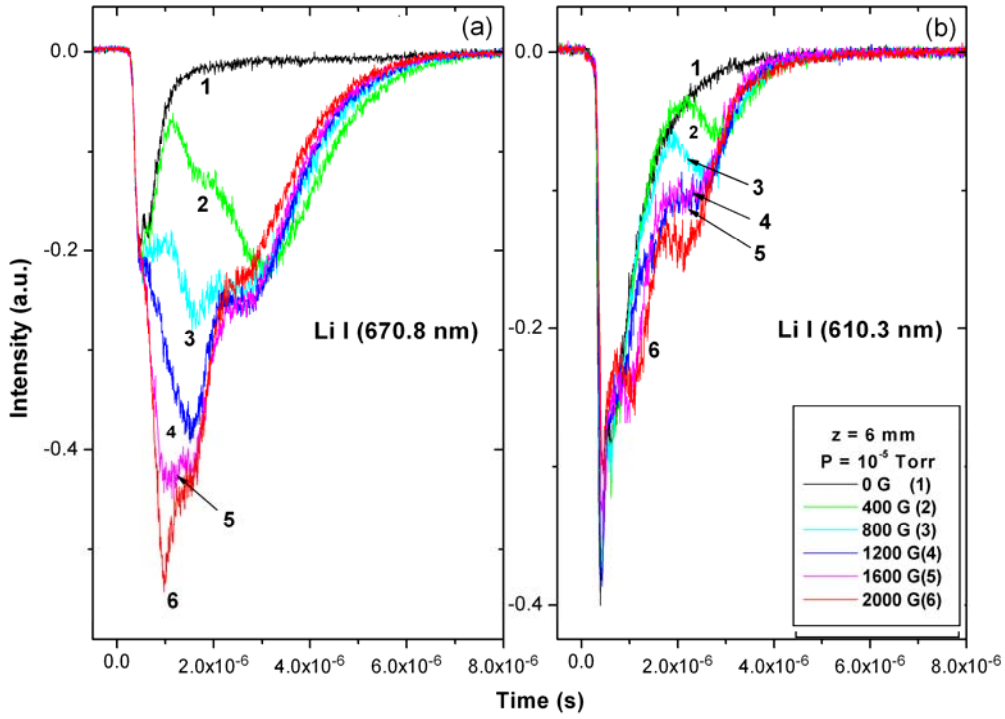

Figure 5.11. *Temporal profiles of 670.8 nm line (a) and 610.3 nm (b) for various magnetic fields at z =6 mm.*

There is a significant difference in the shapes of temporal profiles of neutrals obtained with and without magnetic field. In vacuum, with increase in the magnetic field, the profile shows structure formations as well as intensity enhancement. The enhancement in intensity for 670.8 nm line is significantly higher as compared to the neutral line 610.3 nm. Enhancement of 7.3 times for 670.8 nm in overall intensity was observed in the presence of magnetic field.

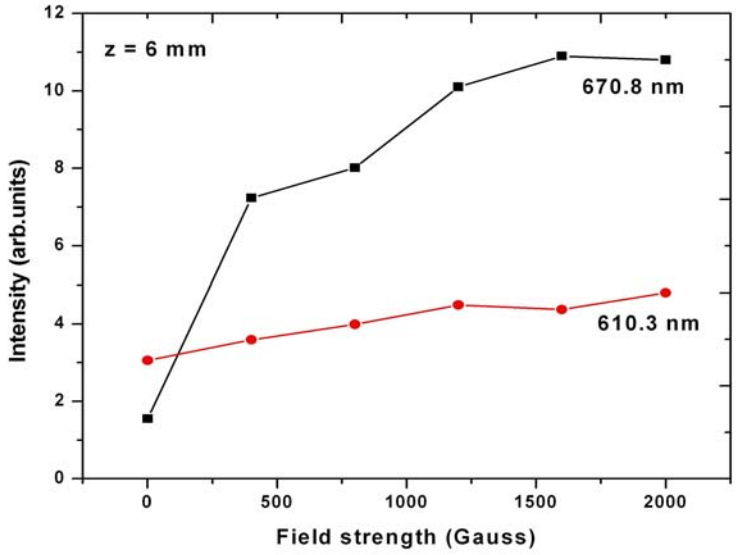

Figure 5.12 *Variation of the total integrated intensities of 670.8 nm and 610.3 nm spectral lines with magnetic field at z = 6 mm.*

The effect of magnetic field when the plasma formed in an ambient environment is entirely different as compared to that in vacuum. When the ambient pressure increased to $3x10^{-2}$ Torr of argon, the temporal profile of 670.8 nm line exhibits an interesting change with increase in the field. Its leading part shrinks sharply and the overall profile becomes narrower although there is an increase in the overall intensity as compared to the field free case. However, 610.3 nm emission line shows a different trend. The overall emission enhancement in the intensity particularly at the trailing part as the field is increased, which is prominently different to what is observed in the case of 670.8 nm line. Furthermore, unlike in the case of vacuum, the structures in the temporal profile are not evident at this pressure (Fig.5.13). With further increase in pressure to 1 Torr, there is not much pronounced effect of the magnetic field on both 670.8 nm and 610.3 nm temporal profiles unlike in the case of $3x10^{-2}$ Torr.

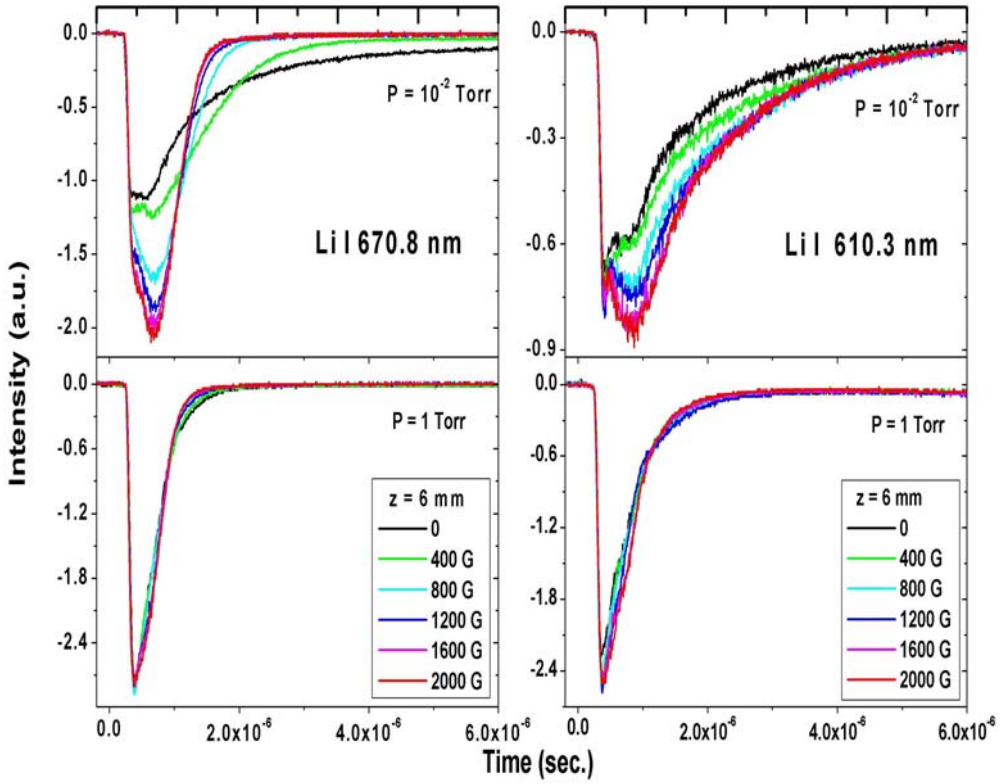

Figure 5.13 *Temporal profiles of 670.8 nm (left panel) and 610.3 nm (right panel) in 10^{-2} Torr and 1 Torr for different magnetic fields. The profiles were recorded at z=6 mm.*

A similar observation, i.e., the difference in temporal profiles for the two neutral lines (670.8 nm and 610.3 nm) under the influence of magnetic field has been discussed in the earlier part of this chapter. The change has been qualitatively understood in terms of computed photon emissivity coefficients (PEC) using atomic data and analysis structure (ADAS) {46} for both the lines.

The observed behavior in the intensity of these two transitions in the presence of the magnetic field and at different ambient pressures can be explained by considering the following processes (i) Joule heating due to the presence of the magnetic field and hence an increase in electron temperature {11}, (ii) increase in

electron confinement in the presence of the magnetic field {42, 43}, (iii) heating due to the ambient gas itself {49} and (iv) increase in electron density as a result of interaction between plume plasma and ambient gas.

Earlier studies reported {44, 45} the enhancement in the intensity of these lines in the presence of magnetic field in vacuum. This was attributed to an increase in electron impact excitation, which increases with increase in electron temperature as well as electron density. The difference in the intensity enhancement for these two lines has been attributed to the difference in electron impact excitation for these transitions due to increase in Joule heating (increased electron temperature) {11}. Moreover, the temporal evolution of the plume in vacuum and in the presence of the field is correlated to the magnetic diffusion time i.e., time essential for Joule heating, which is ~4 to 1 μs for our experimental parameters. This means that with increase in the field, the plume will be affected at shorter time delays.

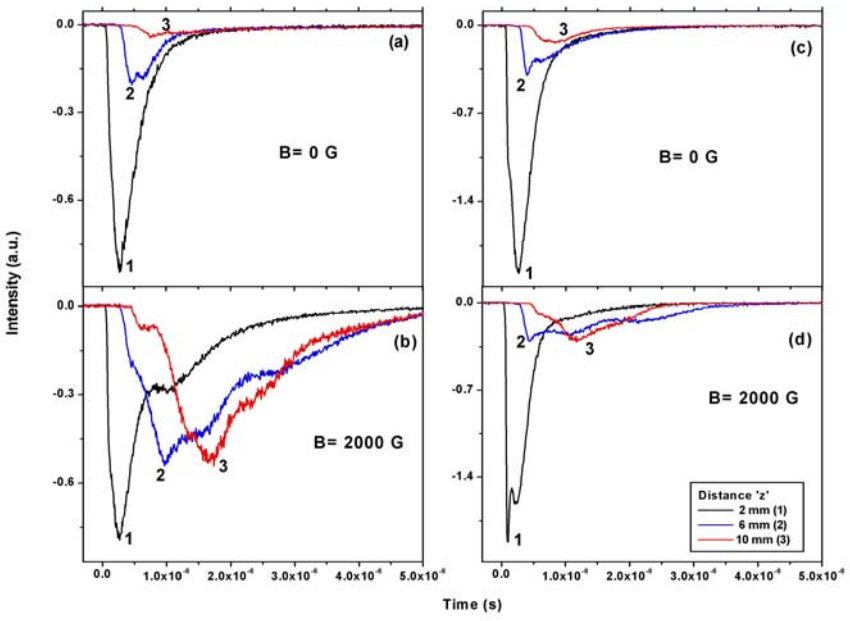

Figure 5.14 *Temporal profiles of Li I 670.8 nm (a) without field, (b) 2000 G; Li I 610.3 nm (c) without field and (d) 2000 G for various distances.*

In the presence of the ambient gas, it should be noted that collisions start between the plume species and ambient atoms, when the plume dimensions are of the order of the mean free path of the ejected species {49, 50}. We have already discussed the influence of ambient gas on an LBO plume in chapter 3. Using the Westwood model {47}, the estimated mean free path for lithium atoms is ~4.8 mm at $3x10^{-2}$ Torr. This value of mean free path reconfirm the fact that the plume expands into collisional regime at this pressure for z = 6 mm. In this regime, interpenetration of the plasma plume into the ambient gas occurs, which causes an increase in the collisions between the plume species and the ambient gas atoms. Hence, there will be an increase in the electron density in this pressure regime. It is also observed that at this pressure, plume front temperature is increased (~7 eV) {52}. However, as the time evolves, plasma electrons quickly lose their kinetic energy through elastic and inelastic collisions with the ambient gas atoms. As a result, plasma with high density and low temperature especially at the trailing portion of the plume is presumably formed.

At sufficiently higher pressures (1 Torr), the plume material pushes away the background gas. The compressed gas restricts the diffusion of the plume material and an interface is formed. On the development of the interface boundary between the plume and the surrounding gas, the expansion transforms from collisional regime to hydrodynamical regime {Chapter 3}. The compressed gas restricts the expansion of the plume, thereby confining the plume in a smaller volume {48, 49}. Combined effect of the magnetic field and the ambient gas on the temporal evolution of neutral emission lines can be understood as follows. Apart from the heating of the plume front and increase in electron density in the presence of the ambient gas, the presence of magnetic field also increases the electron temperature due to Joule heating and electron density due to magnetic confinement {11}. In vacuum, the appearance of broad component with field can be attributed to the presence of slow neutrals emanating from the direct vaporization of lithium.

This explains the appearance of a broad shoulder as well as greater intensity enhancement for the 670.8 nm line with increasing magnetic field

At z = 6 mm, plume-atom collision causes an increase in the electron temperature as well as density and hence increase in the electron impact excitation dominates for 670.8 nm which is strongly dependent on the temperature and density. Further at 1 Torr pressure, plume already gets confined and hence it is expected that magnetic field may not bring about any more prominent changes in the line emission.

It was found that there is a drastic reduction in the intensity of P4 as a function of magnetic field. This can be attributed to the role of electron drift induced by the penetrating magnetic field lines. As the temperature in this region is very low, the magnetic field lines can easily penetrate and cause the electrons to drift away from the region of observation causing reduction in the number deinsity of electrons. As the observed intensity is directly proportional to the electron density, a significant reduction in intensity as a function of magnetic field is not unexpected.

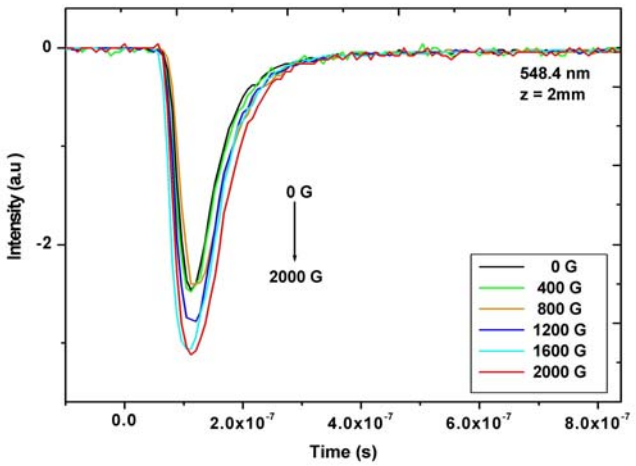

Figure 5.15 *Temporal profiles of 548.4 nm line for various magnetic fields at z = 2 mm.*

Scenario is different for the ionic spectral line. Interestingly, the temporal behavior of Li II 548.4 nm ionic line did not show any significant changes in the presence of the ambient gas and magnetic field as shown in Fig. 5.15. The dominant mechanism for the excitation of 548.4 nm ionic line has been found to be the recombination mechanism {51}. In vacuum and for low fields, the electron density is not affected much and hence the intensity is not expected to get changed significantly. However, for higher fields due to increase in confinement a small increase in density is expected, which, of course, will result in increased intensity. For $3x10^{-2}$ Torr pressure, as the confinement may take place even for lower fields, we can expect an increase in intensity due to increased electron density. For higher fields, electron temperature also increases resulting in decreased recombination and hence decreased intensity.

In this section, we have discussed the effect of magnetic field on the plasma plume formed from LiFC target. The emission was monitored by fast imaging using ICCD and two distinct neutral emission lines from lithium have been observed . In the presence of magnetic field, the temporal profiles of these lines showed distinct features with an enhancement in their intensity.

5.6. Conclusions

In this chapter, we have discussed the results of the experiments conducted to understand the effect of magnetic field on the dynamics of plasma created from Li solid as well as LiFC thin film target. Plume images at various experimental conditions were recorded using ICCD. Optical emission spectroscopy also employed in all cases to get better insight into the plume evolution in the presence of magnetic field. Enhancement of the overall emission of the plume as well as structural modifications was observed as a function of field strength.

First section of the chapter demonstrates the plume formed from a solid lithium target under the influence of magnetic field. Fast imaging of the laser produced plasma plumes showed the appearance of structures in presence of

transverse magnetic field. The observed findings indicated that instead of J × B force, atomic processes get affected by magnetic field in different regions to different extents causing the structure formation. Evidence of instability or collapse of the bubble has not been found to be the cause of the structures.

Influence of field on plasma formed from LiF-C thin film target was the subject of matter in the second part of this chapter. Plume imaging and spectroscopy was performed for plume formed in vacuum and in argon ambient gas. Analysis of imaging data showed the enhancement of the plume in the presence of magnetic field while OES data illustrate the presence of various structures. The temporal profiles for the two neutral lines (670.8 nm, 610.3 nm) showed distinct features at the trailing part at $3x10^{-2}$ Torr argon pressure. At further higher pressures (1 Torr) the effect of field was not that prominent. Lithium ionic lines (548.4 nm) were not influenced much by the magnetic field. The difference was explained by considering electron impact excitation and recombination processes and ambient gas diffusion in collisional and hydrodynamical regimes.

5.7. References

1. W. Gekelman, M. Van Zeeland, S. Vincena, and P. Pribyl.,*"Laboratory experiments on Alfvén waves caused by rapidly expanding plasmas and their relationship to space phenomena"*, J. Geophys. Res., Space Phys. **108**, 1281 (2003).

2. Hiroharu Kawasaki, Kazuya Doi, Satoshi Hiraishi, Yoshiaki Suda., "*Effects of cross-magnetic field on thin film preparation by pulsed Nd:YAG laser deposition"*, Thin Solid Films **374**, 278 (2000).

3. P. R. Willmott and J. R. Huber.,*"Pulsed laser vaporization and deposition",* Rev. Mod. Phys. **72**, 315 (2000).

4. S. S. Harilal, B. O'Shay and M. S. Tillack.,*"Debris mitigation in a laser-produced tin plume using a magnetic field*", J. Appl. Phys. **98,** 036102 (2005).

5. Shinsuke F, Hiroaki N, Katsunobu N, Noriaki M, Yasukazu, Kunioki M, Yoshinori S and Atsushi S., *"Laser production of extreme ultraviolet light source for the next generation lithography application"*, Plasma and Fusion Research **4**, 048 (2009).

6. Y. Watanabe, K. Ota, H. Franken, and V. Banine, in Proceedings of the EUV Source Workshop, San Diego, 2005 (International SEMATEC, Austin, 2005), p.1, www.sematech.org/meetings.

7. Katsunobu Nishihara et.al.,*"Plasma physics and radiation hydrodynamics in developing an extreme ultraviolet light source for lithography"*, Phys. Plasmas **15**, 056708 (2008).

8. Y. Godwal, M. T. Taschuk, S. L. Lui, Y. Y. Tsui, and R. Fedosejevs., *"Development of laser-induced breakdown spectroscopy for microanalysis applications"*, Laser Part. Beams **26**, 95 (2008).

9. X. K. Shen, Y. F. Lu, T. Gebre, H. Ling and Y. X. Han.,*"Optical emission in magnetically confined laser-induced breakdown spectroscopy"*, J. Appl. Phys. **100**, 053303 (2006).

10. Alan F. Haught, Donald H. Polk and Walter J. Fader., *"Magnetic field confinement of laser irradiated solid particle plasmas"*, Phys. Fluids **13**, 2842 (1970).

11. Harilal, S.S., Tillack, M.S., O'shay, B., Bindhu, C.V.F. and Najmabadi, F., *"Confinement and dynamics of laser-produced plasma expanding across a transverse magnetic field",* Phys. Rev. E **69**, 026413 (2004).

12. L. Torrisi, D. Margarone, S. Gammino and L. Ando., *"Ion energy increase in lasergenerated plasma expanding through axial magnetic field trap"*, Laser Part. Beams **25**, 453 (2007).

13. Y. Li, C. Hu, H. Zhang, Z. Jiang and Z. Li., *"Optical emission enhancement of laser-produced copper plasma under a steady magnetic field"*, Appl. Optics, **48** B 105-B 110 (2009).

14. A. Huber, U. Samm, B. Schweer and Ph. Mertens., *"Results from a double Li-beam technique for measurement of both radial and poloidal components of electron density fluctuations using two thermal beams"*, Plasma Phys. Control. Fusion **47**,409 (2005).

15. *"Principles of Fusion Energy",* A. A. Harms, K. F. Schoepf, G. H. Miley, and D. R. Kingdon., World Scientific, Singapore, (2000).

16. R. Bhattacharyay et.al.*"Study of magnetic configuration effects on plasma boundary and measurement of edge electron density in the spherical tokamak compact plasma wall interaction experimental device using Li sheet beam",* Phys. Plasmas **15**, 022504 (2008).

17. "*Pulsed Laser Deposition of Thin Films"*, D. B. Chrisey and G. K. Hubler., (Wiley, New York, 1994).

18. R. K. Singh and J. Narayan.,*"Pulsed-laser evaporation technique for deposition of thin films: Physics and theoretical mode"*, Phys. Rev. B **41**, 8843 (1990).

19. D. K. Bhadra., *"Expansion of a resistive plasmoid in a magnetic field",* Phys. Fluids **11**, 234 (1968).

20. R. G. Tuckfield and F. Schwirzke.,"*Dynamics of laser created plasma expanding in a magnetic field"*, Plasma Phys. **11**, 11 (1969).

21. T. A. Peyser, C. K. Manka, B. H. Ripin and G. Ganguli., "*Electron–ion hybrid instability in laser-produced plasma expansions across magnetic fields"*, Phys. Fluids B **4,** 2448 (1992).

22. B. H. Ripin, E. A. McLean, C. K. Manka, C. Pawley, J. A. Stamper, T. A. Peyser, A. N. Mostovych, J. Grun, A. B. Hassam and J. Huba., "*Large-Larmor-radius interchange instability*", Phys. Rev. Lett. **59**, 2299 (1987).

23. Virendra N. Rai, Hansheng Zhang, Fang Y. Yueh, Jagdish P. Singh and Akshaya Kumar.,"*Effect of steady magnetic field on laser-induced breakdown spectroscopy*", Appl. Opt. **42**, 18 (2003).

24. R.A. Cairns and B. Rau., *"Effects of magnetic fields on wave propagation in dense laser-produced plasmas*", Laser and Part. Beams, **18**, 355 (2000).

25. H.C. Joshi, Ajai Kumar, R.K. Singh and V. Prahlad.,*"Effect of a transverse magnetic field on the plume emission in laser-produced plasma: An atomic analysis"*, Spectrochimica Acta Part B **65**, 415 (2010).

26. A. N. Mostovych, B. H. Ripin, and J. A. Stamper., *"Laser produced plasma jets: Collimation and instability in strong transverse magnetic fields"*, Phys. Rev. Lett. **62**, 2837 (1989).

27. G. Dimonte and L. G. Wiley., *"Dynamics of exploding plasmas in a magnetic field"*, Phys. Rev. Lett. **67**, 1755 (1991).

28. B.A. Bryunetkin, U.Sh. Begimkulov, V. M. Dyakin, G.A. Koldashov, S. N. Priyatkin, A. Yu. Repin, E. L. StupitskiT, and A. Ya. Faenov., *"Laser plasma expansion in a magnetic field"*, Sov. J. Quantum Electron. **22**, 223 (1992).

29. Y. Y. Tsui, D. Vick and R. Fedosejevs., *"Guiding and confinement of a laser produced plasma by a curved magnetic field"*, Appl. Phys. Lett. **70**, 1953 (1997).

30. Y. Y. Tsui, H. Minami, D. Vick, and R. Fedosejevs., *"Debris reduction for copper and diamond-like carbon thin films produced by magnetically guided pulsed laser deposition"*, J. Vac. Sci. Technol. A **20**, 744 (2002).

31. Raj K. Thareja and A. K. Sharma., *"Reactive pulsed laser ablation: Plasma studies"*, Laser Part. Beams **24**, 311 (2006).

32. Harilal, S.S., O'shay, B., Tao, M. and Tillack *M., "Ion debris mitigation from tin plasma using ambient gas, magnetic field and combined effects",* Appl. Phys. B **86**, 547 (2007).

33. Harilal S.S., O'Shay B, Tillack M.S, Bindhu C.V and Najmabadi F., "*Fast photography of a laser generated plasma expanding across a transverse magnetic field",* IEEE Trans. Plasma Sci. **33**, 474 (2005).

34. Rabia Qindeel, Noriah Bte Bidin and Yaacob Mat daud., *"Dynamics expansion of laser produced plasma with different materials in magnetic field"*, J. Phys.: Conf. Ser. **142**, 012069 (2008).

35. M.S. Rafique, M. Khaleeq-UR-Rahman, I. Riaz, R. Jalil and N. Farid., *"External magnetic field effect on plume images and X-ray emission from a nanosecond laser produced plasma"*, Laser and Part. Beams **26**, 217 (2008).

36. Ajai Kumar, Vishnu Chaudhari, Kiran Patel, Sony George, S. Sunil, R.K. Singh and Ranjeet Singh., "*An experimental setup to study the expansion dynamics of laser blow-off plasma plume in variable transverse magnetic field"*, Rev. Sci. Instrum. **80**, 033503 (2009).

37. A. Neogi and R. K. Thareja., *"Physics of plasmas laser-produced carbon plasma expanding in vacuum, low pressure ambient gas and non-uniform magnetic field"*, Phys. Plasmas **6**, 365 (1999).

38. F. Schwirzke and R. Tuckfield.,"*Observations of enhanced resistivity in the wave front of a laser-produced plasma interacting with a magnetic field"*, Phys. Rev. Lett. **22**, 1284 (1969).

39. *"Laser Interaction and Related Plasma Phenomena",*Schwirzke F., Schwarz H. and Hora H., eds., New York: Plenum (1974).

40. Raj K. Thareja and A. K. Sharma.,*"Reactive pulsed laser ablation: Plasma studies"*, Laser Part. Beams **24**, 311 (2006).

41. A. K. Sharma and R. K. Thareja.,*"Anisotropic emission in laser-produced aluminum plasma in ambient nitrogen"*, Appl. Surf. Sci. **253**, 3113 (2007).

42. Virendra N. Rai, Jagdish P. Singh, Fang Y. Yueh and Robert . Cook.,*"Study of optical emission from laser-produced plasma expanding across an external magnetic field"*, Laser and Part. Beams, **21**, 65 (2003).

43. Virendra N. Rai, Awadhesh K. Rai, Fang-Yu Yueh and Jagdish P. Singh., *"Optical emission from laser-induced breakdown plasma of solid and liquid samples in the presence of a magnetic field*", Appl. Opt. **42**, 12 (2003).

44. Ajai Kumar, R. K. Singh, V. Prahlad, H.C. Joshi., *"Effect of magnetic field on laser blow-off Li plasma plume: Role of atomic processes"*, Laser Part. Beams **28**, 121 (2010).

45. H.C. Joshi, V. Prahlad, R. K. Singh, Ajai Kumar.,"*Emission analysis of expanding laser produced lithium plasma plume in presence of ambient gas"*, Phys. Lett. A **373**, 3350 (2009).

46. Atomic Data Analysis Structure (ADAS).online at http://adas.ac.uk

47. W. D. Westwood., *"Calculation of deposition rates in diode sputtering systems"*, J. Vac. Sci. Technol. **15**, 1 (1978).

48. Sony George, Ajai Kumar, R. K. Singh and V. P. N. Nampoori., *"Fast imaging of laser blow off plume: lateral confinement in ambient environment",* Appl. Phys. Lett. **94**, 141501 (2009).

49. S. Amoruso, B. Toftmann, J. Schou, R. Velotta and X. Wang., *"Diagnostics of laser ablated plasma plumes"*, Thin Solid Films 453–454, 562 (2004).

50. Ajai Kumar, H.C. Joshi, V. Prahlad, R.K. Singh.,*"Effect of magnetic field on laser-blow-off lithium plasma plume: structured temporal emission profile"*, Phys. Lett. A **374**, 2555 (2010).

51. S.D. Loch, C.J. Fontes, J. Colgan, M.S. Pindzola, C.P. Ballance, D.C. Griffin, M.G.O'Mullane and H.P. Summers., "*Collisional-radiative study of lithium plasmas*", Phys. Rev. E **69**, 066405 (2004).

52. Ajai Kumar, R. K. Singh, Jinto Thomas, S. Sunil.,*"Parametric study of expanding plasma plume formed by laser-blow-off of thin film using triple Langmuir probe",* J. Appl. Phys. **10,** 043306 (2009).

Chapter 6

Laser Induced Plasma from Solid and Thin Films: Comparative Study

Abstract

The evolution features of lithium plasma generated by two different schemes viz. the laser-blow-off (LBO) of multicomponent LiF-C thin film and conventional laser ablation referred to here as laser produced plasma (LPP) from solid lithium have been studied using fast imaging and optical emission spectroscopic techniques. Modifications of the plume structure in different experimental conditions are monitored as a function of ambient gas pressure and distance from the target. Apart from their similarities, some interesting differences are noticed in temporal profiles of the plumes generated by LPP and LBO both in vacuum as well as in the presence of the ambient gas.

6.1 Introduction

In previous chapters, we have discussed the expansion dynamics of lithium ions and neutrals produced by laser-blow-off (LBO) of LiFC thin film in different experimental conditions. We found certain striking differences in comparison with the conventional solid ablation i.e., laser produced plasma (LPP). Therefore, we were motivated to perform investigation specifically to study the lithium plasma generated from solid lithium target. Also, it is of interest to study the differences in the dynamics of plasma plumes generated by the LBO and LPP.

In conventional laser ablation of solid targets i.e., in LPP, laser of few nanosecond pulse width with energy above the ablation threshold is incident on a solid target, the formation of plasma plume involves the following stages. The leading edge of the laser pulse ejects an envelope of material from the front surface. At an early stage, the ejected material mostly consists of atoms and a small fraction of ions and electrons. As the temperature increases, boiling and explosive boiling/phase explosion occur which then changes the composition and dynamics of ejected species {1, 2}. Even for density well below the critical density for absorption of laser light, some portion of incident radiation is absorbed by plume resulting in strong heating of the plume. During the initial phase of expansion, particle density is high, and the particles move with strong collisions between them. A layer called Knudsen layer, in contact with the target in which reflections and collisions occur which will tend to thermally equilibrate the plasma {3-5}.

In contrast, the mechanism for the formation of LBO is impulsive heating of the film. This heating process continues until the vapor pressure at the film support interface becomes large enough to expel the film material {6-9}. The expansion dynamics in LBO strongly depends on the thickness of the thin film. If the thickness is less than the skin depth -defined as the penetration depth of the laser in solid target, then it would result in explosive expansion of plume with less

number of collisions. It has been found that neutral species are the main constituents of the LBO plumes {10, 11}.

We have already discussed the important applications of LPP and LBO plasmas {Sec.1.5}. One of the most important applications of LPP is the thin film deposition with pulsed laser (PLD) {12-14}. LBO technique is one of the most commonly used tools for production of neutral atomic beams in Tokamak plasma diagnostics {15-18}. Lithium is particularly important because of the low mass and high penetration speeds and its simple structure of emission spectra. Therefore, the Li beam is extensively used to determine the parameters of edge plasma in Tokamak. Several experimental investigations related to laser induced lithium plasma formed by thin film as well as solid targets have been reported in the past {18-25}.

We present here a direct comparison between the conventional solid ablation (LPP) and laser blow off (LBO) of thin films using fast imaging and OES. The image analysis of the plume has been largely employed as a diagnostic technique of laser ablation plume {26-32}and is capable of revealing different changes occurring during the propagation of the ablated species. Since the plasma formation mechanism in these two schemes, i.e., LBO and LPP are entirely different, a direct comparison in the plume geometry is not much relevant. Keeping this in view, more emphasis has been given to emission spectroscopy. The evolution features of the spectral lines of Li I and Li II generated by LPP and LBO are compared on a one-to-one basis in high vacuum and in different ambient gas pressures.

6.2 Experimental details

A detailed description of experimental setup has been explained in chapter 2. Plasma was created inside a vacuum chamber, which was evacuated to a base pressure of 10^{-6} Torr. In order to study the effect of ambient gas, argon gas was

introduced into the chamber and the pressure was controlled by a fine controlled needle valve. For LPP studies, solid Li rod with purity of 99.999% purity and for LBO studies, LiFC thin film target was used. Nanosecond pulses from Nd:YAG (λ = 1064 Å) laser having 8 ns pulse width with maximum pulse energy 1.6 J was used to ablate target. Same fluence was used for the LBO and LPP experiments. Time resolved images were recorded using an intensified CCD (ICCD) camera having variable gain, gate time and spectral response in 350-750 nm region. In the present experiment, the gate time was set to 4 ns. To measure the spatio-temporal evolution of emitting plume species, the plasma plume was viewed normal to the direction of expansion and imaged at the entrance slit of a monochromator ($\Delta\lambda$= 12.5 Å). The temporal profile of emission signal was detected by a photomultiplier tube (PMT) {33}.

6.3 Expansion dynamics in vacuum

A detailed picture of plume formation and dynamics has been given in Sec.1.2 of this thesis. As the laser hit on the target, the laser energy is absorbed by the electrons in the target (solid/ thin film) and leads to strong heating of the irradiated volume. This causes the ablation of the irradiated area and the evaporated material continuous to absorb the incoming laser radiation. After the termination of the laser pulse, the initial gas layer expands in all directions. In the case of LBO, plume propagation is in the laser direction and is opposite in the case LPP. In both cases, plume expansion is driven by the energy, which is accumulated as thermal energy and energy which is stored as excitation and ionization in the initial layer. This energy is converted to kinetic energy of the atoms in the plume, and eventually all atoms will move with an asymptotic, constant velocity distribution. In this part of the thesis, a comparative study has been discussed between plume generated by LBO and LPP schemes in a low-pressure region (10^{-6} Torr).

6.3.1 Fast imaging of LPP and LBO plasma in vacuum

After the formation, plume dynamics is highly depends on the medium through which it expands. This part of the thesis present the results obtained using the imaging studies of plume expansion formed by solid and thin film targets in vacuum.

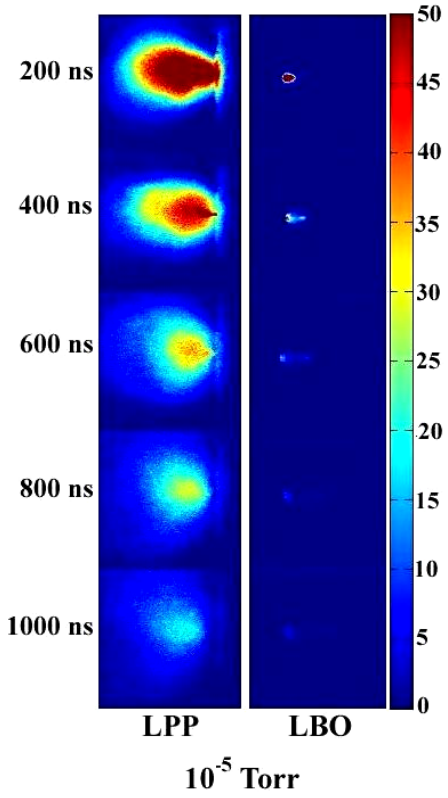

Figure 6.1 *Plume images of Li plasma recorded using ICCD at a pressure of 10^{-5} Torr, at different time delays after the onset of plasma formation. Colorbar shows the normalized intensity in arbitrary units.*

Since the formation mechanism of these two schemes (LBO and LPP) is completely different, a direct comparison of the plume geometry cannot be appropriate. However, it gives rough idea about the differences in geometry of the plume generated from LPP and LBO schemes in vacuum. For this, plume images

are recorded at various time delays (0-1000 ns) after the plume initiation. Figure 6.1 shows the recorded plume images generated from LiF-C thin film and Li solid targets. All these images are representative of the geometrical shape of plume in a time domain, which was normalised to their maximum intensity for better representation and comparison. Analysis of the images revealed many interesting features regarding the plasma generated under two different schemes.

We have already seen in chapter 3 that, LBO plume expands adiabatically and has an ellipsoidal shape {19, 20}. During the expansion, electron density reduces rapidly and hence the probability of electron impact excitation is reduced. This leads to reduction in the emission intensity of the plume and for a time delay $t > 1000$ ns, emission intensity is beyond the detection limit of the ICCD due to lower dynamic range of the camera. On the other hand, plasma generated in LPP scheme exhibits an entirely different shape in vacuum. During initial period, the plume expansion shows an elongated shape and as time progresses, intensity at the leading edge of the plume decreased drastically. This dissimilarity in plume geometry may be attributed by the difference in formation mechanism of plasma in the two cases LBO and LPP. We have already discussed earlier that plume formation in LBO is by impulsive hearing of the film and complete irradiated area is converted to plasma in each ablation {Chapter 4}. In contrast to LBO where the plume is detached from the target surface after a time delay, LPP plume found to be attached to the solid target (Fig.6.1). At later time intervals ($t > 400$ ns), LPP plume acquires a spherical shape with maximum intensity at the center portion. Size of the LBO plume is found to be much smaller compared to that of LPP plume.

In vacuum, intensity of LBO plume is much lower compared to the emission intensity of LPP and hence the lifetime also. This is because of the limitation of ablated material in the case of LBO scheme. From the recorded images and also from earlier analysis (Sec.3.4), it has been observed that there exist a linear behaviour between the plume front position and time delay in the case of LBO

plume. On the other hand, in LPP expansion, part of plume is found to be static with respect to the target. The scattered structure of the LPP plume boundary, limit the possibility of measuring the exact plume front position. An approximate estimated of the LPP plume length in comparison with the length of LBO plume at the same time delay, shows that LPP plume front propagates larger distance. For a fixed delay 600 ns, plume length is found to be 10 mm in LBO whereas it is 22.5 mm in the case of LPP.

6.3.2 Emission spectroscopy of LBO and LPP in vacuum

In the previous section, we have been discussing a comparative analysis between plume geometry of plasma generated by LBO and LPP scheme. Though it gives information about the plume geometry, there exist few limitations for ICCD imaging for explaining the exact plume dynamics as it acquire the resultant emission of all the wavelengths present in the plume. To get a better understanding, we compared the time and space resolved emission spectroscopy of the evolution features of the two ionic lines 478.8 nm ($3p\,^1P_1 \leftarrow 4d\ \ ^1D_2$) and 548.4 nm ($2s\ ^3S_1 \leftarrow 2p\ ^3P_{2,1,0}$) and two neutral lines 610.3 nm ($2p\ ^2P_{1/2,3/2} \leftarrow 3d\ ^2D_{3/2,5/2}$) and 670.8 nm ($2s\ ^2S_{1/2} \leftarrow 2p\ ^2P_{3/2,1/2}$) respectively. Due to similarities in the expansion features of the ionic spectral lines (478.8 versus 548.4 nm) and neutral lines (610.3 versus 670.8 nm) and for the sake of simplicity, all the discussions are based on the observations for only one ionic line Li II (548.4 nm) and one neutral line Li I (670.8 nm).

On comparing the recorded spectral lines (Fig. 6.2), it can be seen that during the initial phase of LBO plume expansion (z=2 mm), the temporal profile of ionic and neutral species exhibits double peak structure, designated as ‘fast’ (first peak) and ‘slow’ (delayed peak) components (Fig. 6.2). Away from the target ($z \geq 6$ mm), slow component disappears and only the fast component with reduced intensity was present in the ionic profile. On the other hand the neutrals in LBO maintained their

double peak structure throughout the distance of observation i.e. upto z =12 mm (Fig. 6.2).

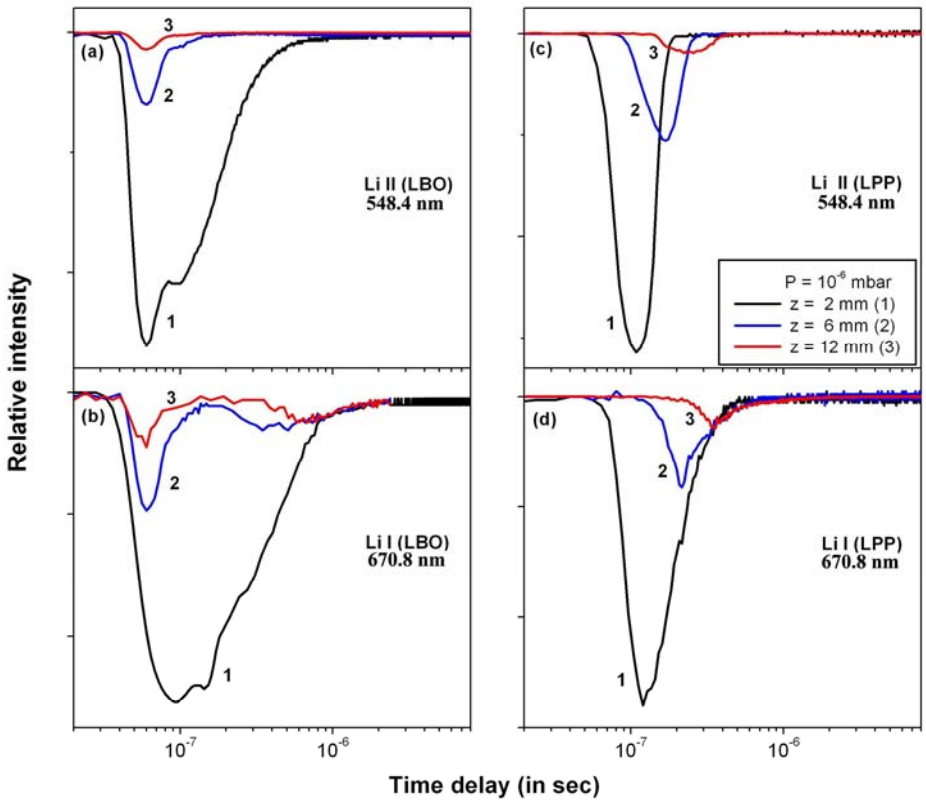

Figure 6.2 *Spatially resolved OES spectra of the LBO and LPP plume at high vacuum measured at distances (z) 2 mm, 6 mm and 12 mm.*

Entirely different results are observed in the case of LPP. No splitting of the profiles is observed for any of the emission lines (both ionic and neutral species), and a single peak structured profiles are maintained throughout the distance z = 2–12 mm. During the initial phase of evolution (z = 2 mm), ion and neutral species move with approximately same velocity (1.9×10^6 cm/sec). With increasing distance, i.e., z > 2 mm, ions were moving with much higher velocity as compared to neutral species. At larger distance (at z = 12 mm) the ion velocity was almost double that of neutrals. Another remarkable difference between the LBO and LPP

scheme is that the arrival time distributions of ejected species observed by LBO is much broader than those of profiles observed in LPP.

In order to investigate further we attempted to compare the plasma temperatures of LBO and LPP. The spectral line intensity ratio of Li II 478.8 nm and Li II 548.4 nm lines are used to estimate the electron temperature of LBO as well as LPP plumes. It is found that the peak electron temperature of LBO (11 eV) corresponding to fast component is greater than that of LPP (2 eV).

The above observations can be interpreted as follows. In LBO, the observed splitting of LBO profile in vacuum is basically due to the formation of species by two different mechanisms that can produce two different velocity distributions {5, 6}. When the laser heats the thin film, the front surface of the film (towards the substrate) is superheated and produces the energetic ion species. These energetic ions form the leading edge of the plume {Sec.6.3.1}. On the other hand, majority of the materials propel from the substrate in the form of neutral vapor, moving with much low translational energy as compared to its faster counterpart. The slow components of both neutrals and ionic profiles are formed by collision processes mainly, electron impact processes of the neutral species {38}. As the time evolves, the plume expands in vacuum causing a rapid reduction in electron density. As a result, probability of ionization/excitation reduces and for sufficiently large distances from the target ($z > 6$ mm), slow component disappears from the ionic profile.

Situation is quite different in LPP. Here the laser pulse heats the bulk of material and the ablated material consists of electrons, ions and neutrals. These particles escape from the target and undergo multiple collisions between themselves. During the early stage of plasma, both ions and neutral move with same velocity. In general, for transient plasma plumes, the larger mobility of electrons induces a self-generated and localized electric field {34, 35}. This electric field

accelerates the ions in addition to the pressure gradient. Therefore, at the latter stage, ionic species move with higher velocity as compared to neutrals.

6.4 Effect of ambient gas on the plume expansion dynamics

The presence of ambient gas significantly affects temporal and spatial distribution of ejected species. In order to compare the influence of ambient gas on the dynamics plasma formed by LBO and LPP scheme, we have analysed various aspects of the plume generated from both solid and thin film target as a function of ambient pressure and is presented in the coming sections.

6.4.1 Fast imaging of LPP and LBO plasma in an ambient medium

Figure 6.3 shows the plume images recorded at various delay times with LBO and LPP scheme as a function of ambient gas pressures. These images are representative of the plume expansion for argon pressure levels 10^{-2} and 1 Torr. We have seen in earlier discussions that plume follows linear expansion in vacuum. Upon increasing the pressure, plume is found to experience resistive force from the ambient gas.

As we have seen in chapter 3, plume geometry is completely modified upon introducing the ambient gas {Sec.3.2}. Though there are some similarities, the way in which ambient medium influenced the plume expansion is entirely different in the case of plume formed by LBO and LPP. Some observations are common for plume formed by LBO and LPP in ambient gas. At 10^{-2} Torr of argon pressure, plasma plume becomes wider and intense in comparison to that observed in vacuum (Fig.6.1). A bright luminescence on the plume boundary (wake like) is formed at the leading edge of the plume (Fig.6.3).

Overall intensity of the plume is increased and lifetime of the plume persists upto $t > 2500$ ns after the plume initiation. Plume penetrates into the ambient gas and this caused an increase in collision between the plume species and ambient gas

{36}. With further increase in pressure, P > 1 Torr, plume became more confined. Intensity of the plume also increased with increase in pressure. Increase in ambient pressure results in the confinement of the plume and in turn increase in collisions. This leads to more and more emission from the expanding plume (increase in the lifetime of the excited species in the plasma) and hence plume is sustained for a longer time at high pressures.

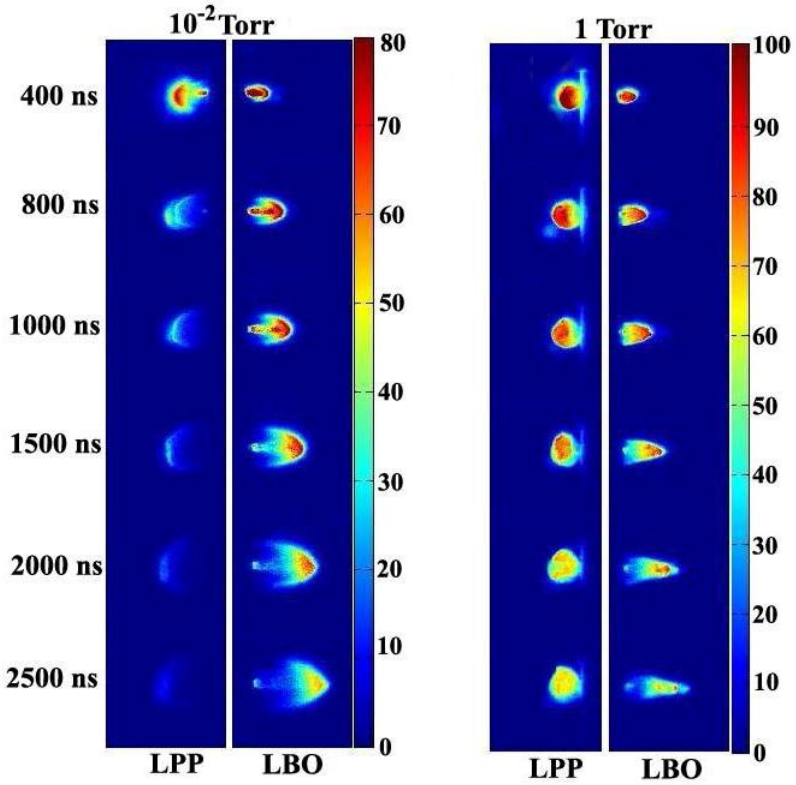

Figure 6.3 *Plume images of Li plasma recorded using ICCD at an argon pressure of 10^{-2} Tor and 1 Torr, at different time delays after the onset of plasma formation. Colorbar shows the normalized intensity in arbitrary units.*

At 10^{-2} Torr, LBO plume showed more focusing in the forward direction compared to LPP. Intensity enhancement is also found to be more in the case of LBO plume. At higher-pressure levels, the shape is again modified. Lateral

confinement has resulted in the case of LBO, on the other hand LPP plume has acquired a spherical shape and which was unchanged over time (Fig.6.3). At higher time delays, the lateral confinement becomes more pronounced in the case of LBO plume unlike in the case of LPP plume. Some of the above mentioned results and its interpretations are already discussed in chapter 3. For further understanding, the emission spectra of Li lines are analysed and results are presented below.

6.4.2 Emission spectroscopy of LBO and LPP in ambient medium

In order to explore the effect of background pressures of ambient gas on the dynamics of the LBO and LPP plasma plume, the study has been extended by monitoring the temporal and spatial evolution of its spectral line emission.

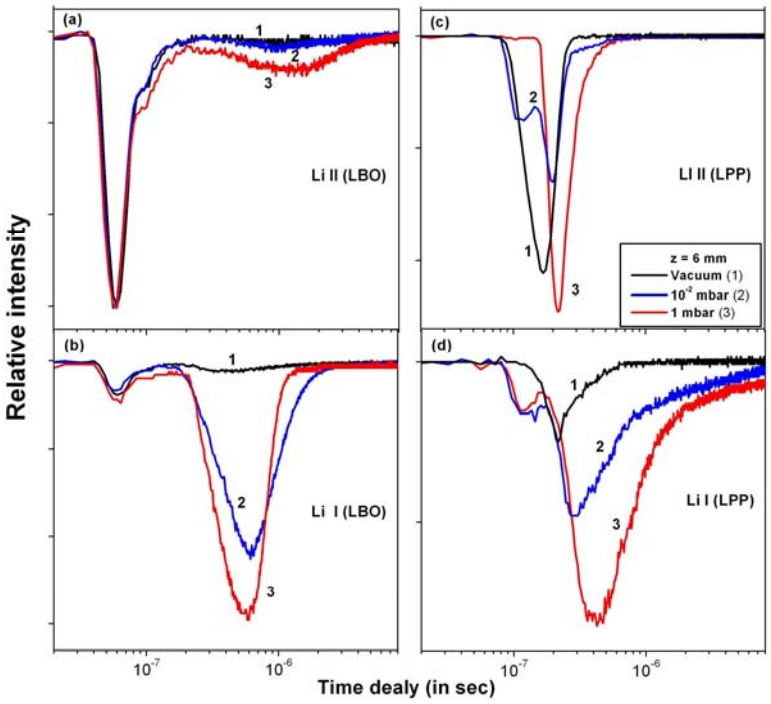

Figure 6.4 *Effect of ambient gas pressure on the temporal profiles of the Li I and Li II observed in the case of LBO and LPP schemes*

For OES studies, the ionic and neutral emission lines are monitored as a function of ambient pressure. Figure 6.4 shows the emission profile recorded at a distance 6 mm from the target.

In the case of LPP, both ions and neutrals show a splitting (fast and slow components) in their profiles under the influence of gas pressure. As already mentioned, no splitting is observed in vacuum environment (Fig.6.2). Therefore, argon gas appears to be responsible for the observed splitting. The physical reason for this behavior is discussed below. When the ambient pressure was 10^{-2} Torr pressure, the profiles split into two components. The comparison of the observed profiles in vacuum and in the presence of ambient gas suggests that a fraction of ions/ neutrals loses its momentum in the presence of ambient gas, whereas the rest of them penetrate into the ambient gas with little interaction.

The ions/neutrals that penetrate into the ambient gas have similar velocities as in vacuum and those that get affected by the ambient gas have lower velocities. The ionic species that have larger velocities form the fast component and the rest of the ions having lower velocities form the slow component. These results can be explained on the basis of a momentum transfer between the plume species and background atoms {38}. In this process, the Li atoms that collide with argon atoms can lose ~27% of their kinetic energy {36}. As the pressure increases, the species may suffer more collisions with argon atoms before reaching the point of observation and hence arrival time is further delayed. This effect is reflected in our results where the time delay of the slow components for both ions and neutrals increased with gas pressure. Further, the intensities of slow components of both ions and neutrals increased with pressure; the effect being more pronounced in the case of neutrals. The increase in electron density due to ionization of ambient gas should be responsible for the observed enhancement of intensity at high pressures {37}. Fast neutrals can also be produced by electron recombination of fast ions. The fast component in neutrals that appeared after the introduction of ambient gas was

unaffected by the increase in pressure, whereas for ions it vanished at 1 Torr pressure. This behavior indicates that most of the fast ions undergo electron recombination at higher pressures.

Another interesting feature that is observed is in the relative broadening of temporal profiles of slow neutrals and slow ions. The temporal profiles became much broader in the case of slow neutrals, whereas there was relatively no broadening in the case of slow ions. It can be understood by the fact that ions having higher energy have less scope for thermalization and hence cannot exhibit broadening, whereas the neutrals may get thermalized resulting in broadened profiles.

In the case of LBO, the profile of fast ions observed at z = 6 mm did not show any change as compared to vacuum when ambient gas was introduced. As the fast ions have larger kinetic energies, the probability of collision with ambient gas molecules is very small for such higher energies. Therefore, these ions transmit through the argon gas without getting affected in any manner. As expected, with increase in gas pressure a small increase in intensity of slow ions has been observed because of collisional ionization. The fast neutrals are also unaffected by the variation in gas pressure, which can also be understood on the basis of their higher energies.

When the pressure is increased from 10^{-5} to 10^{-2} Torr the slow neutrals of LBO also show the same behavior as that of LPP (Fig.6.4). With further increase in argon gas pressure (1 Torr), the profiles became sharper associated with an increase in the peak intensity but with no change in the integrated intensity. As shown in Fig.6.4, with increase in the background pressure, the peak amplitude of the profile increases with a reduction in width. Interestingly, the integrated intensity area under the curve remains constant throughout the chosen pressure range. This observation support the imaging results {Sec.6.4.1} and indicates that in the presence of ambient gas, plume is localized in small volume in space without reduction in total

number density. It is known that the slow ions are produced by electron impact ionization of slow neutrals {39, 40}. The localization of slow neutrals causes an increase in the rate of electron impact ionization and hence results in an increase in the intensity of Li II.

6.5 Conclusions

The evolution dynamics of lithium plasma generated by the LBO of multicomponent LiF–C thin film and LPP from solid lithium have been studied using fast imaging and optical emission spectroscopic technique. The differences between the expansion dynamics with regard to plume splitting, plume confinement and plume expansion were discussed in this chapter. Plume generated in low pressure (10^{-2} Torr) and different argon gas pressure levels were studied. Apart from their similarities, some interesting differences were also noticed in temporal profiles of the plumes generated by LPP and LBO both in vacuum as well as in the presence of the ambient gas.

Imaging studies showed that plume geometry (size, shape etc.) for the plasma generated by LBO and LPP scheme were entirely different. Lifetime of the plume was more for the LPP plume generated in vacuum in comparison with LBO. On the other hand, LBO plume was visible for longer duration in an ambient medium. Nearly, linear expansion of the plume was observed in LBO plasma whereas LPP plume is found to be localized in space with increasing the time delay. A comparative analysis of experimental results indicated that the ablation mechanism and subsequent laser-plume interaction were responsible for the observed differences in LPP and LBO plumes. OES studies of LPP plume in vacuum showed single peak structures for both ions and neutrals, whereas in the case of LBO we observed double peaked structures up to z = 6 mm for ions. In the presence of the ambient gas, both ions and neutrals of LBO and LPP showed an increase in intensity and splitting of plumes.

6.6 References

1. R. K. Singh and J. Narayan., *"Pulsed-laser evaporation technique for deposition of thin films: Physics and theoretical model"*, Phys. Rev. B **41**, 8843 (1990).

2. Ž. Andreić, D. Gracin, V. Henč-Bartolić, H-J Kunze, F. Ruhl and L. Aschke., "*Dynamics of laser-produced carbon plasma*", Physica Scripta **53**, 339 (1996).

3. Kelly, R., Dreyfus, R.W., "*Reconsidering the mechanisms of laser sputtering with Knudsen-layer formation taken into account",* Nuclear Inst. and Methods in Physics Research, B, **32**, 341 (1988).

4. Roger Kelly and R. W. Dreyfus., *"On the effect of Knudsen-layer formation on studies of vaporization, sputtering, and desorption",* Surf. Sci. **198**, 263 (1988).

5. W. Pietsch., *"Effect of Knudsen-layer formation on the initial expansion and angular distribution of a laser-produced copper plasma at reduced pressure of air"*, J. Appl. Phys. **79**, 1250 (1996).

6. F. J. Adrian, J. Bohandy, B. F. Kim, A. N. Jette, and P. Thompson.,"*A study of the mechanism of metal deposition by the laserinduced forward transfer process"*, J. Vac. Sci. Technol. B **5**, 1490 (1987).

7. Robert J. Baseman, Nan M. Froberg, Joseph C. Andreshak, and Zack Schlesinger., *"Minimum fluence for laser blow-off of thin gold films at 248 and 532 nm",* Appl. Phys. Lett. **56**, 1412 (1990).

8. V. Schultze and M. Wagner.,*"Blow-off of aluminium films"*, Appl. Phys. A Solids and Surfaces **53**, 241 (1991).

9. Z. Kántor, Z. Tóth and T. Szörényi., *"Laser induced forward transfer: The effect of support-film interface and film-to-substrate distance on transfer"*, Appl. Phys. A Solids and Surfaces **54**, 170 (1992).

10. R. K. Singh, Ajai Kumar, B. G. Patel, and K. P. Subramanian.,*"Role of ambient gas and laser fluence in governing the dynamics of the plasma plumes produced by laser blow off of LiF–C thin film"*, J. Appl. Phys. **101**, 103301 (2007).

11. Singh, R.K and Kumar, A., *"Flow dynamics of ions generated by laser-blow-off of LiF-C film"*, IEEE Transactions on Plasma Science **35**, 1717 (2007).

12. P. R. Willmott and J. R. Huber.,*"Pulsed laser vaporization and deposition",* Rev. Mod. Phys. **72**, 315 (2000).

13. T. Donnelly, S. Krishnamurthy, K. Carney, N. McEvoy, and J. G. Lunney., *"Pulsed laser deposition of nanoparticle films of Au*", Appl. Surf. Sci. **254**, 1303 (2007).

14. J. N. Leboeuf, K. R. Chen, J. M. Donato, D. B. Geohegan, C. L. Liu, A. A. Puretzky, and R. F. Wood.,*"Modeling of plume dynamics in laser ablation processes for thin film deposition of materials"*, Phys. Plasmas **3**, 2203 (1996).

15. M. Bruchhausen, R. Burhenn, M. Endler, G Kocsis, A. Pospieszczyk, S. Zoletnik and the W7-AS Team2., *"Fluctuation measurements on the Wendelstein 7-AS stellarator by means of repetitive lithium laser blow-off"*, Plasma Phys. Control. Fusion **46**, 489 (2004).

16. A Pospieszczyk and G. G. Ross., *"Density determination in the TEXTOR boundary layer by laser-ablated fast lithium atoms",* Rev. Sci. Instrum. **59**, 605 (1988).

17. S. Sasaki, S. Takamura, Y. Uesugi, Y. Ohkouchi, and K. Kadota., *"Laser blow-off lithium beam probing with high temporal resolution for edge plasma diagnostics"*, Rev. Sci. Instrum. **64**, 2277 (1993).

18. Nieto, M., Allain, J. P., Hassanein, A., et al., *"Plasma-material interaction studies on lithium and lithiated substrates during compact tokamak operation",* Plasma and Fusion Science **875**, 78 (2006).

19. Sony George, Ajai Kumar, R. K. Singh, V. P. N. Nampoori., *"Fast imaging of laser blow off plume: lateral confinement in ambient environment",* Appl. Phys. Lett. **94**, 141501 (2009).

20. Sony George, Ajai Kumar, R. K. Singh, V. P. N. Nampoori.,*"Effect of ambient gas on the expansion dynamics of plasma plume formed by laser blow off of thin film"*, Appl. Phys. A., **98**, 901 (2009).

21. Ajai Kumar, R.K. Singh, Jinto Thomas, S. Sunil., *"Parametric study of expanding plasma plume formed by laser-blow-off of thin film using triple Langmuir probe",* J. Appl. Phys. **10,** 043306 (2009).

22. Joshi, H.C., Prahlad, V., Singh, R.K. and Kumar, A., *"Emission analysis of expanding laser produced lithium plasma plume in presence of ambient gas"*, Phys. Lett. A **373**, 3350 (2009).

23. Ajai Kumar, Sony George, R. K. Singh, V. P. N. Nampoori.,*"Influence of laser beam intensity profile on propagation dynamics of laser-blow- off plasma plume"*, Laser and Part. Beams, **28**, 387 (2010).

24. William Whitty and Jean-Paul Mosnier., *"Diagnostic of an expanding laser-produced lithium plasma using ICCD frame photography and shadowgraphy"*, Appl.Surf. Sci. 127-129, 1035 (1998).

25. Coons R W, Harilal S.S., Polek M, and Hassanein A.,*"Spatial and temporal variations of the electron temperatures and densities of an EUV-emitting lithium plasmas",* Analytical Bioanalytical Chemistry **400**, 3239 (2011).

26. R. K. Thareja, Abhilasha and R.K. Dwivedi.,*"Optical emission spectroscopy of laser-produced carbon plasma at moderate and low irradiance in an ambient atmosphere"*, Laser and Part. Beams **13**, 481 (1995).

27. Y. B. S. R. Prasad, P. A. Naik, A. Kumar, and P. D. Gupta.,*"Simple interferometer for space and time resolved density measurements of laser produced plasmas"*, Rev. Sci. Instrum. **77**, 093106 (2006).

28. M. H. Hong, Y. F. Lu, T. M. Ho, L. W. Lu and T. S. Low., *"Fast ICCD imaging of KrF excimer laser induced titanium plasma plumes for silicon metallization"*, Appl. Surf. Sci., 138-139, 489 (1999).

29. R. A. Lindley, R. M. Gilgenbach, and C. H. Ching., *"Resonant holographic interferometry of laser-ablation plumes"*, Appl. Phys. Lett. **63**, 888 (1993).

30. Brendan Doggett and James G. Lunney., "*Langmuir probe characterization of laser ablation plasmas* ", J. Appl. Phys. **105**, 033306 (2009).

31. Yu Quan-Zhi, Zhang Jie, Li Yu-Tong, Zheng Jun, Yan Fei, Lu Xin, Wang Zhe-Bin, Zheng Jian, Yu Chang-Xuan, Jiang Xiao-Hua, Li Wen-Hong, Liu Shen-Ye and Zheng Zhi-Jian., "*Thomson scattering process in laser-produced plasmas*", Chinese Phys. Lett. **22,** 1717 (2005).

32. S. Amoruso , R. Bruzzese, R. Velotta, N. Spinelli, M. Vitiello and X. Wang., *"Characterization of LaMnO3 laser ablation in oxygen by ion probe and optical emission spectroscopy"*, Appl. Surf. Sci. **248,** 45 (2005).

33. A. Kumar, V. Chaudhari, K. Patel, S. George, S. Sunil, R.K. Singh and R. Singh., "*An experimental setup to study the expansion dynamics of laser blow-off plasma plume in variable transverse magnetic field"*, Rev. Sci. Instrum. **80**, 033503 (2009).

34. N. M. Bulgakova, A. V. Bulgakov, and O. F. Bobrenok., *"Double layer effects in laser-ablation plasma plumes"*, Phys. Rev. E **62**, 5624 (2000).

35. A. V. Gurevich, L. V. Parriskaya, and L. P. Pitaevskii, Sov. Phys. JETP 36, 274 (1973).

36. W. D. Westwood., *"Calculation of deposition rates in diode sputtering systems"*, J. Vac. Sci. Technol. **15**, 1 (1978).

37. R. K. Singh, Ajai Kumar, V. Prahlad, and H. C. Joshi.,*"Generation of fast neutrals in a laser-blow-off of LiF-C film: A formation mechanism"*, Appl. Phys. Lett. **92**, 171502 (2008).

38. R. F. Wood, J. N. Leboeuf, D. B. Geohegan, A. A. Puretzky, and K. R. Chen., *"Dynamics of plume propagation and splitting during pulsed-laser ablation of Si in He and Ar"*, Phys. Rev. B **58**, 1533 (1998).

39. C. Timmer, S. K. Srivastava, T.E. Hall and A. Fucaloro., *"Enhanced line emission from laser-produced plasmas",* J. Appl. Phys.**70**, 1888 (1991).

40. David B. Geohegan and Alexander A. Puretzky.;*"Dynamics of laser ablation plume penetration through low pressure background gases*", Appl. Phys. Lett. **67**, 197 (1995).

Chapter 7

Conclusions and Future Prospects

Abstract

This chapter explains the conclusions brought out from the experimental investigations explained in the previous sections. Suggestions for future work in this field are also provided.

7.1. Conclusions

This thesis has reported the details of results obtained from the studies of the behavior of Laser Produced Plasma (LPP) formed from Li solid and Laser Blow Off (LBO) plasma generated from LiF-C thin film target in the strong and intense laser-matter interaction regimes. The main motive to conduct this study was its usefulness in several applications including neutral beam diagnostics and pulsed beam deposition. Most of these potential applications require improvements in the understanding of the physics of laser-matter interaction in order to enhance design of the application more robust and accurate.

The imaging characterization of LBO plume by exploiting fast photography to follow the plume propagation in various experimental conditions has form the central theme of the thesis. Fast photography adds another aspect to the analysis of the propagation of a laser-induced plasma plume by providing two-dimensional images of the three-dimensional plume expansion.

As a part of the studies reported, we designed and developed an experimental system to perform various diagnostics of plasma plume from both solid (LPP) and thin film (LBO) targets {Chapter 2}. Details of various subcomponents like lasers, ICCD camera, OES etc in the system were included in the present thesis. Generation of variable pulsed magnetic field and synchronization of the above mentioned subcomponents is another major part of the experimental facility.

The effect of ambient gas on the expansion dynamics of the plasma plume is of great interest for several years. We conducted studies in this direction to understand the expansion dynamics of LBO plasma plume, under the influence of various ambient gases such as helium and argon {Chapter 3}. To avoid misinterpretation of the results made using fast imaging, emission spectroscopy also performed simultaneously in every experimental condition. Analysis of recorded data reveals many interesting effects like plume enhancement, geometrical

alterations and instabilities when ambient gas was pressure changed from high vacuum 10^{-5} Torr to 3 Torr. It has been found that the plume geometry and propagation dynamics are highly dependent on the ambient gas nature and composition. Experimental data has been validated with its matching with corresponding theoretical models such as drag, shock wave etc.

In another interesting study, the characteristic expansion of LBO plume was found to depend on the laser beam intensity profile {Chapter 4}. For this we utilized lasers with gaussian (GP) and top hat (THP) intensity profiles. In this work, we succeeded to demonstrate that geometrical shape, velocity and directionality of the plumes formed by the GP and THP laser are significantly different. These observations were interpreted on the basis of the formation mechanism of plasma using two different intensity profiles. The observed results will be of significant importance in shaping laser generated plasma plumes and understanding and controlling the geometrical aspect of the LBO generated atomic/ionic beam.

Low divergence of LBO plume generated in vacuum by the irradiation of GP laser motivated us to conduct similar studies in ambient gas medium also. It has been observed that the LBO plume generated using GP laser expand in ambient gases cause the formation of shock waves. Systematic study has been conducted with different gas pressures, ranging from high vacuum 10^{-5} to 3 Torr of He, O_2 and Ar with fast-gated ICCD camera. Enhancement in emission intensity, structure formation, drag force and confinement effect has been observed to the maximum extent in Ar environment compared to He and O_2 environment. Shock parameters like shock strength, temperature etc were calculated from the images and this also showed that shock parameters are highly dependent on the nature of ambient gas medium to which plasma expands. These studies have given additional information to explore the shock waves in laser plasmas.

Another major work, which we discussed in this thesis, is the research carried out to understand the effect of magnetic field on the dynamics of plasma

created from Li solid as well as LiFC thin film target {Chapter 5}. Imaging as well as OES diagnostics gave better insight into the plume evolution in the presence of magnetic field. Enhancement of the overall emission of the plume and structural modifications were observed as a function of field strength. The observed findings indicated that instead of J × B force, atomic processes got affected by magnetic field in different regions to different extents causing the structure formations. Evidence of instability or collapse of the bubble has not been found to be the cause of these structures.

In continuation of the above studies, we compared plume formed by two different schemes, i.e. LBO and LPP from Li solid and LiF-C thin film target{Chapter 6}. Since the formation mechanism of the above two schemes are different, direct comparison using fast imaging of the plume formed by these two schemes were not much relevant. Due to this constraint, more focus was on the spectroscopic study of the differences between the expansion dynamics with regard to plume splitting, plume confinement, plume composition and plume expansion. Plume generated in low pressure (10^{-5} Torr) and different argon gas pressure levels were studied. Apart from their similarities, some interesting differences were also noticed in the temporal profiles of the plumes generated by LPP and LBO both in vacuum as well as in the presence of ambient gas.

The results obtained from this study has great importance and could be useful for meliorate the hydrodynamic models presently available for simulating the plasma plume expansion dynamics in different gas atmospheres.

7.2. Future prospects

Results and data derived from the above-discussed investigations can be used for further studies in laser-induced plasma from solid as well as thin film targets.

Measurement of different plasma parameters such as temperature, density etc, both temporally and spatially will be the immediate research to be carried out to support the modelling and simulations of LBO plasma. There are many diagnostic techniques available in this regard. Plasma plume images obtained with corresponding interference filters can be utilized.

The physics of the interaction of ultrashort (< 1 ps), intense laser pulses with solid targets considerably differs from the situation with long (nanosecond pulses in many aspects. Undoubtedly, there would be strong interest in extending LBO studies with nanosecond laser pulses to ultra-short regime to explore more insights.

Statistical analysis like single value decomposition (SVD), independent component analysis (ICA) etc are proved to be much better representation than the spectroscopic measurement to show the behavior of expanding plumes, particularly its complex internal structures. Hence, statistical analysis of the image data obtained is another area to be explored.

RESUME OF THE AUTHOR

SONY GEORGE
Research scholar
International School of Photonics
Cochin University of Science and Technology
Cochin-682022
Email: sony@cusat.ac.in
sonytgeorge@gmail.com

Education:

M.Sc. Applied Electronics
National Institute of Technology,
Tiruchirappalli, Tamilnadu, India
Year: 2003-2005

B.Sc. Electronics
M.G. University, Kottayam, India
Year: 1999-2002

Research Experience

Research Fellow (01/2007-09/2011)

International School of Photonics (ISP), Cochin University

Institute for Plasma Research (IPR), Gandhinagar, Gujarat, India

Collaborative Research: Norwegian Colorlab, Faculty of Computer Science and Media Technology, Gjovik University College, Gjovik, Norway

Publications

International Journals: 8

International/National Conferences: 7

Workshops / Training Participation

Winter College on Optics in Imaging Science, held at International Center for Theoretical Physics (ICTP), Italy [24 January to 11 February, 2011]

Summer College on Plasma Physics, held at International Center for Theoretical Physics (ICTP), Italy [9-28 August, 2009]

DST-SERC School on Plasma Diagnostics held at Institute for Plasma Research (IPR), Gandhinagar, Gujarat, India [20-31 July, 2009]

Digital Image Processing Workshop held at National Institute of Technology, Tiruchirappalli, India [7-9 November, 2008]

Awards and Scholarships

Research fellowship for meritorious students (RFSMS), from University Grants Commission (2007 - 2011)

Poster presentation award, DST Summer school held at IPR, Gujarat (2009)

Professional Affiliations

Student member: Optical Society of America

Student member: SPIE-International Society for Optics and Photonics